TRANSPORT PHENOMENA
IN
A FULLY DEVELOPED TURBULENT FLOW REGION
AT
LARGE PRANDTL OR SCHMIDT NUMBERS

FUMIMARU OGINO

TRANSPORT PHENOMENA

IN

A FULLY DEVELOPED TURBULENT FLOW REGION

AT

LARGE PRANDTL OR SCHMIDT NUMBERS

FUMIMARU OGINO

CONTENTS

CHAPTER 1

INTRODUCTION

1-1 Summary of Previous Works

Numerous equations (some of them are listed in Table 1-1) have been proposed for predicting the heat or mass transfer rates between a pipe wall and a fully developed turbulent flow. Most of them are adequate only for Prandtl or Schmidt numbers of unity or less.

In the oldest theory concerning the transport of heat in the turbulent flow, the Reynolds analogy (54), it is simply assumed that there is a complete analogy between transports of momentum and heat. This analogy loses its validity when the Prandtl number differs appreciably from unity.

Table 1-1

Some Expressions for Nusselt or Sherwood Number *)

(a) Analogy equations

Reynolds (54)

$$Nu = (f/2)\,Re$$

Prandtl-Taylor (48,65)

$$Nu = \frac{(f/2)\,Re\,Pr}{1 + (U_\ell/\langle U\rangle)(Pr - 1)} \quad **)$$

von Kármán (27)

$$Nu = \frac{(f/2)\,Re\,Pr}{1 + 5\sqrt{f/2}\,\{(Pr - 1) + \ell n[(5Pr + 1)/6]\}}$$

(b) Empirical correlations

Dittus and Boelter (8)

$$Nu = 0.023\,Re^{0.8}\,Pr^{0.4}$$
$$(Re=10^4\sim10^5\ ,\ Pr=0.7\sim120)$$

Chilton and Colburn (2)

$$Nu = (f/2)\,Re\,Pr^{1/3}$$
$$(Re=10^4\sim10^5\ ,\ Pr=0.7\sim100)$$

Sieder and Tate (61)

$$Nu = 0.026\,Re^{0.8}\,Pr^{1/3}\,(\mu_b/\mu_w)^{0.14}$$
$$(Re=10^4\sim10^5\ ,\ Pr=0.7\sim100)$$

*) For mass transfer Nu and Pr should be replaced by Sh and Sc respectively.

**) U_ℓ denotes the velocity at the outer edge of the laminar sublayer.

Extension of the Reynolds analogy to cases when $Pr \neq 1$ have been formulated by many authors. Prandtl (48) and Taylor (65) extended the Reynolds analogy by taking account of the laminar layer near the wall. In their equation it is still necessary to make a suitable assumption about the ratio of the velocity at the outer edge of the laminar sublayer to the average velocity. Moreover, at large Prandtl numbers the values of the heat transfer coefficient obtained are too small.

In deriving the Prandtl-Taylor equation, it was assumed that the flow could be sharply divided into a turbulent core and a laminar sublayer. In actual fact, one merges into the other in a continuous way and it is possible to discern the existence of an intermediate, or buffer layer. Von Kármán (27) subdivided the flow into three zones and derived a similar formula for the relation between the coefficient of heat transfer and friction factor. Although his equation gives substantial improvement over the Prandtl-Taylor equation, deviations from actual values of the Nusselt number still occur at fairly large Prandtl numbers.

Reichardt (52,53), Lin, Moulton and Putnam (33), Deissler (6,7), Rannie (50) and many other investigators improved on the previous theories by introducing an appropriate amount of turbulence into the laminar sublayer. However, their equations for the heat or mass transfer rates at large Prandtl or Schmidt numbers differ from each other in the predicted effect of the Prandtl or Schmidt number on the transfer rate. For example, the equation of Rannie predicts that at large Prandtl or Schmidt numbers the Nusselt or Sherwood number varies with $Pr^{1/2}$ or $Sc^{1/2}$, while the equations of Lin et al. and Deissler lead to the exponent of $1/3$ and $1/4$, respectively. Some expressions for Nusselt numbers at very large Prandtl numbers are listed in Table 1-2.

Besides these relations based on more or less realistic concepts of the transport processes, there are many purely empirical correlations for the Nusselt number as functions of the Reynolds and Prandtl numbers. Among such correlations, the equation of Dittus and Boelter (8), the analogy of Chilton and Colburn (2), and the equation of Sieder and Tate (61) are well-known. Since the experimental data on which these empirical correlations

Table 1-2

Expressions for Nusselt Number

at Large Prandtl Number *)

Reichardt (53)

$$Nu = 0.0855 \sqrt{f/2}\ Re\ Pr^{1/3}$$

Lin, Moulton and Putnam (33)

$$Nu = 0.0571 \sqrt{f/2}\ Re\ Pr^{1/3}$$

Deissler (7)

$$Nu = 0.112 \sqrt{f/2}\ Re\ Pr^{1/4}$$

Rannie (50)

$$Nu = 0.0438 \sqrt{f/2}\ Re\ Pr^{1/2}$$

Wasan and Wilke (68)

$$Nu = 0.058 \sqrt{f/2}\ Re\ Pr^{0.34}$$

Son and Hanratty (63)

$$Nu = 0.121 \sqrt{f/2}\ Re\ Pr^{1/4}$$

*) For mass transfer Nu and Pr should be replaced by Sh and Sc respectively.

are based were obtained at Prandtl numbers ranging from 0.7 to 120, these empirical equations fail to represent the experimental results at larger Prandtl or Schmidt numbers.

The inadequacy of most of the previous analyses at large Prandtl or Schmidt numbers is principally caused by the expressions used for the eddy diffusivity in the region very close to the wall. This region is important because of the extremely large temperature or concentration gradients in that region at large Prandtl or Schmidt numbers.

However, little is known about the behavior of small eddies very close to the wall because of insufficient theoretical investigations and reliable experimental data. A number of empirical expressions have been proposed for the eddy diffusivities near the wall as listed in Table 1-3. Very few of them are based on experimental data.

Most of expressions in Table 1-3 are those for momentum. To obtain the Nusselt number it is often assumed that the eddy diffusivity for heat is equal to that for

Table 1-3

Various Expressions for Eddy Diffusivity

near the Wall

Reichardt (53)

$$\varepsilon_M/\nu = 0.4 \{y^+ - 11 \tanh(y^+/11)\}$$

$$y^+ \to 0 \quad ; \quad \varepsilon_M/\nu = 0.00110 (y^+)^3$$

Lin, Moulton and Putnam (33)

$$\varepsilon_D/\nu = (y^+/14.5)^3$$

$$y^+ \to 0 \quad ; \quad \varepsilon_D/\nu = (y^+/14.5)^3$$

Deissler (7)

$$\varepsilon_M/\nu = n^2 U^+ y^+ \{1 - \exp(-n^2 U^+ y^+)\}$$

$$n = 0.124$$

$$y^+ \to 0 \quad ; \quad \varepsilon_M/\nu = 0.000236 (y^+)^4$$

Rannie (50)

$$\varepsilon_M/\nu = \sinh^2(0.0688 y^+)$$

$$y^+ \to 0 \quad ; \quad \varepsilon_M/\nu = (0.0688 y^+)^2$$

Table 1-3 (contd.)

van Driest (9)

$$\varepsilon_M = \kappa^2 y^2 \{1 - \exp(-y/A)\}^2 \left| dU/dy \right|$$

$$\kappa = 0.4 \qquad A = 26\nu/u_*$$

$$y^+ \to 0 \quad ; \quad \varepsilon_M = (\kappa/A)^2 y^4$$

Sleicher (62)

$$\varepsilon_M/\nu = 0.00828 (y^+)^2$$

$$y^+ \to 0 \quad ; \quad \varepsilon_M/\nu = 0.00828 (y^+)^2$$

Spalding (64)

$$\varepsilon_M/\nu = AB \{\exp(BU^+) - 1 - BU^+ - (BU^+)^2/2 - (BU^+)^3/6\}$$

$$A = 0.1108 \qquad B = 0.4$$

$$y^+ \to 0 \quad ; \quad \varepsilon_M/\nu = 0.0000473 (y^+)^4$$

Wasan, Tien and Wilke (67)

$$\varepsilon_M/\nu = F(y^+)/ \{1 - F(y^+)\}$$

$$F(y^+) = 0.000416 (y^+)^3 - 0.00001515 (y^+)^4$$

$$y^+ \to 0 \quad ; \quad \varepsilon_M/\nu = 0.000416 (y^+)^3$$

momentum. However, the evidence for this assumption is not affirmative and the ratio $\varepsilon_H/\varepsilon_M$ must be determined experimentally or theoretically.

Various investigators (23,36,39,46) have determined this ratio for the turbulent flow of air or mercury in tubes. It is of the order of unity, values in the literature varying from 0.9 to 1.7. However, no experimental data in the region near the wall had been obtained. On the other hand, when the values of Prandtl and Schmidt number are equal, the eddy diffusivities for heat and mass may also be equal because it is reasonable to assume that the mechanisms of eddy diffusion of heat and mass are analogous.

1-2 Purpose of This Study

The purpose of this study is to investigate the transfer mechanism of heat and mass in the vicinity of the wall to obtain accurate values of the transfer rates at large Prandtl or Schmidt numbers.

The study was started with precise measurements of the eddy diffusivity for heat in the region near the wall, and then a theoretical analysis was made to predict the eddy diffusivity for heat at any value of Prandtl and Reynolds number. Finally, the mass transfer rates at large Schmidt numbers were measured and compared with the calculated values.

Chapter 2 deals with the experimental method used in measuring the eddy diffusivities for heat transfer near the wall. The eddy diffusivities for heat were obtained from the temperature distributions which were measured precisely by means of an interferometric method using a Mach-Zehnder interferometer.

In Chapter 3 an analytical expression for the ratio

of the eddy diffusivities for heat and momentum are presented by modifying the mixing length theory. This analytical expression shows that the eddy diffusivity for heat depends on the Prandtl number and the eddy diffusivity for momentum. Therefore, the expression for the eddy diffusivity for momentum is required to predict the eddy diffusivity for heat.

Simple equations for the eddy diffusivity of momentum which are based on the experimental results available in the literature, and the universal velocity profile which in turn is obtained from the distribution of the eddy diffusivity for momentum, are presented in Chapter 4.

Chapter 5 deals with the comparison between the theoretically and experimentally obtained mass transfer rates at large Schmidt numbers and discusses the effect of the Prandtl and Schmidt numbers on the heat or mass transfer coefficient.

In the concluding chapter, 6, the final results of this study and recommendations for further work are given.

1-3 Basic Equations

For a steady, fully developed rectilinear flow between parallel plates, the time-smoothed equations of motion, temperature and concentration may be written as

$$0 = - \frac{dP}{dx} - \frac{d\tau}{dy} \qquad (1\text{-}1)$$

$$\rho C_p U \frac{\partial T}{\partial x} = - \frac{\partial q}{\partial y} + \mu \Phi^{(\ell)} + \mu \Phi^{(t)} \qquad (1\text{-}2)$$

$$U \frac{\partial C}{\partial x} = - \frac{\partial N}{\partial y} \qquad (1\text{-}3)$$

where $\Phi^{(\ell)}$ and $\Phi^{(t)}$ are the viscous and turbulent energy dissipation functions respectively.

The shear stress τ, heat flux q, and mass flux N, which are associated with the transport of momentum, heat and mass respectively in the direction normal to the wall, are given by

$$\tau = - \mu \frac{dU}{dy} + \rho \overline{uv} \qquad (1\text{-}4)$$

$$q = - k \frac{\partial T}{\partial y} + \rho C_p \overline{tv} \qquad (1\text{-}5)$$

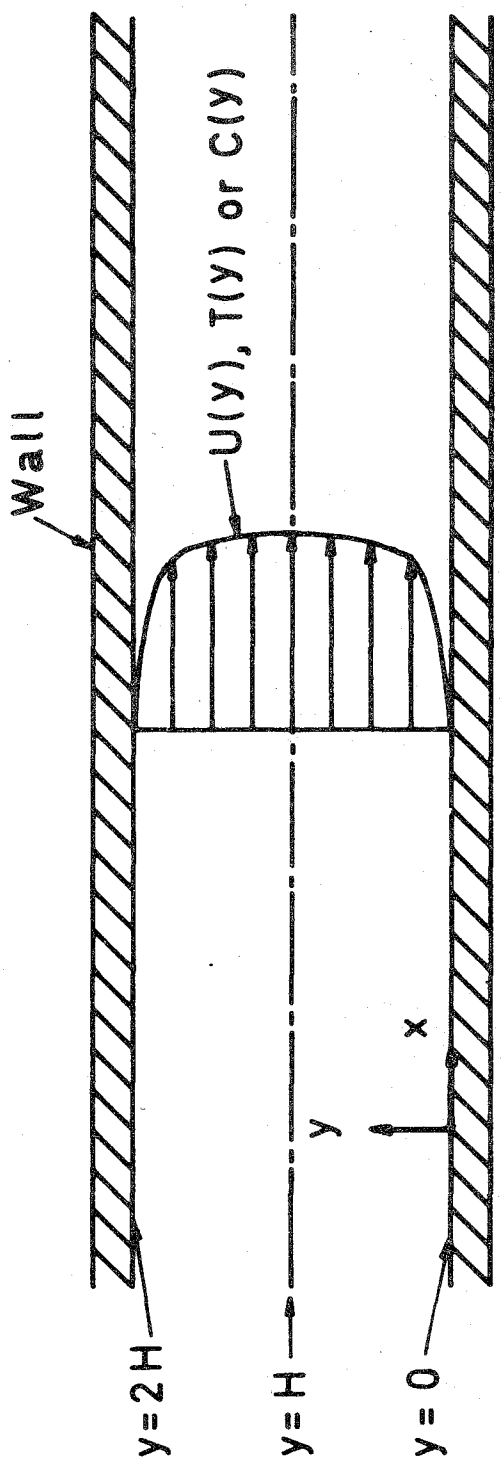

Fig. 1-1 Coordinate system.

$$N = -D \frac{\partial C}{\partial y} + \overline{cv} \qquad (1\text{-}6)$$

where u,v,t and c denote the fluctuating components. These equations are valid if convection occurs only in the x-direction (parallel to the plane surface) and molecular and turbulent transport occur only in the y-direction (perpendicular to the wall surface). The coordinate system is shown in Fig. 1-1.

The definitions of the eddy diffusivities for momentum, heat and mass are as follows,

$$\overline{uv} = - \varepsilon_M \frac{dU}{dy} \qquad (1\text{-}7)$$

$$\overline{tv} = - \varepsilon_H \frac{\partial T}{\partial y} \qquad (1\text{-}8)$$

$$\overline{cv} = - \varepsilon_D \frac{\partial C}{\partial y} \qquad (1\text{-}9)$$

Combining equations (1-4) ∿ (1-6) and (1-7) ∿ (1-9), one obtains

$$\tau = - \rho\nu \left(1 + \varepsilon_M/\nu\right) \frac{dU}{dy} \qquad (1\text{-}10)$$

$$q = - \rho C_p \nu \left(1/Pr + \varepsilon_H/\nu\right) \frac{\partial T}{\partial y} \qquad (1\text{-}11)$$

$$N = - \nu \left(1/Sc + \varepsilon_D/\nu\right) \frac{\partial C}{\partial y} \qquad (1\text{-}12)$$

1-3-1 Velocity distribution and friction factor

Equation (1-1) may be integrated subject to the boundary conditions $\tau = 0$ at $y = H$ and $\tau = \tau_w$ at $y = 0$ to give

$$\tau = \tau_w \left(1 - y/H\right) \qquad (1\text{-}13)$$

in which H is the half width of a two-dimensional channel. Equations (1-10) and (1-13) may be combined to give the dimensionless velocity distribution as

$$U^+ = \int_0^{y^+} \frac{1 - y^+/H^+}{1 + \varepsilon_M/\nu} \, dy^+ \qquad (1\text{-}14)$$

The friction factor is defined as

$$f = \tau_w / \frac{1}{2} \rho \langle U \rangle^2 = 2 (u_*/\langle U \rangle)^2 \qquad (1\text{-}15)$$

The average velocity $\langle U \rangle$ over the cross section of the flow between two parallel plates is given by

$$\langle U \rangle = \frac{1}{H} \int_0^H U \, dy \qquad (1\text{-}16)$$

Substituting equation (1-16) into equation (1-15), one obtains the following expression for the friction factor in terms of the dimensionless quantities.

$$f = 2 \left(H^+ / \int_0^{H^+} U^+ \, dy^+ \right)^2 \qquad (1\text{-}17)$$

If the pipe radius, R, is used instead of the half width of the parallel plates, H, the equations (1-13) ∿ (1-15) may also be used for a circular pipe flow. However, equation (1-16) for the average velocity must be

replaced by the following expression :

$$\langle U \rangle = \frac{2}{R^2} \int_0^R U\,(R - y)\,dy \qquad (1\text{-}18)$$

Hence, the friction factor for a circular pipe flow is given by

$$f = \frac{1}{2} \{ R^+ / \int_0^{R^+} U^+ (1 - y^+/R^+)\, dy^+ \}^2 \qquad (1\text{-}19)$$

1-3-2 Temperature or concentration profile and Nusselt or Sherwood number

In discussing the turbulent heat flow problem under ordinary conditions, it is customary to drop the viscous dissipation terms, $\Phi^{(\ell)}$ and $\Phi^{(t)}$. Moreover, it may be assumed that the convection terms on the left sides of equations (1-2) and (1-3) can be neglected, or in other words, that the heat or mass flux may be assumed constant

at any value of y. This assumption may not cause serious errors at large Prandtl or Schmidt numbers because the resistance of heat or mass transfer is concentrated in the region near the wall.

With these assumptions, equations (1-2) and (1-3) may be rewritten in dimensionless form as

$$0 = \frac{d}{dy^+} \left\{ (1/Pr + \varepsilon_H/\nu) \frac{dT^*}{dy^+} \right\} \qquad (1\text{-}20)$$

$$0 = \frac{d}{dy^+} \left\{ (1/Sc + \varepsilon_D/\nu) \frac{dC^*}{dy^+} \right\} \qquad (1\text{-}21)$$

where $T^* = (T - T_w)/(T_b - T_w)$ and $C^* = (C - C_w)/(C_b - C_w)$. Boundary conditions are

$$T^* = 0 \ , \ C^* = 0 \quad \text{at} \quad y^+ = 0 \qquad (1\text{-}22)$$

$$T^* = 1 \ , \ C^* = 1 \quad \text{at} \quad y^+ = \infty \qquad (1\text{-}23)$$

The values of T^* and C^* at $y^+ = \infty$ are essentially unity

because the temperature and concentration are very nearly constant except in the region very close to the wall, and they are considered to be the bulk temperature or concentration at large Prandtl or Schmidt numbers.

Equations (1-20) and (1-21) are integrated, with the boundary conditions (1-22) and (1-23), to give

$$T^* = \int_0^{y^+} \frac{dy^+}{1/Pr + \varepsilon_H/\nu} \Bigg/ \int_0^{\infty} \frac{dy^+}{1/Pr + \varepsilon_H/\nu} \qquad (1\text{-}24)$$

$$C^* = \int_0^{y^+} \frac{dy^+}{1/Sc + \varepsilon_D/\nu} \Bigg/ \int_0^{\infty} \frac{dy^+}{1/Sc + \varepsilon_D/\nu} \qquad (1\text{-}25)$$

The heat and mass transfer coefficients are defined as

$$q_w = h\,(T_w - T_b) \qquad (1\text{-}26)$$

$$N_w = K\,(C_w - C_b) \qquad (1\text{-}27)$$

It can be shown from these definitions that

$$h^+ = 1 \Big/ \int_0^\infty \frac{dy^+}{1/Pr + \varepsilon_H/\nu} \tag{1-28}$$

$$K^+ = 1 \Big/ \int_0^\infty \frac{dy^+}{1/Sc + \varepsilon_D/\nu} \tag{1-29}$$

where $h^+ = h/\rho C_p u_*$ and $K^+ = K/u_*$. The Nusselt number and Sherwood number are given by

$$Nu = Re\ (f/2)^{1/2}\ Pr\ h^+ \tag{1-30}$$

$$Sh = Re\ (f/2)^{1/2}\ Sc\ K^+ \tag{1-31}$$

where Nu, Sh, and Re are defined as

$$Nu = h\ (4H)/k \tag{1-32}$$

$$Sh = K(4H)/D \tag{1-33}$$

$$Re = (4H)\ \langle U \rangle/\nu \tag{1-34}$$

Equations (1-20) ∿ (1-31) are also valid for a flow in a circular pipe, since the thermal or concentration boundary layer is thin enough that the curvature of the wall can be ignored at large Prandtl or Schmidt numbers. However, the expressions of Nu, Sh, and Re must be replaced by the following equations.

$$Nu = h(2R)/k \tag{1-35}$$

$$Sh = K(2R)/D \tag{1-36}$$

$$Re = (2R) \langle U \rangle / \nu \tag{1-37}$$

Thus, to evaluate the Nusselt and Sherwood numbers, the eddy diffusivities ε_H and ε_D must be evaluated as functions of position and flow conditions.

1-3-3 Eddy diffusivity in the region very close to the wall

Near the wall, the fluctuating and the time-smoothed

velocities, temperatures and concentrations can be expressed by Taylor series about $y = 0$ as

$$u = \left.\frac{\partial u}{\partial y}\right|_w y + \frac{1}{2}\left.\frac{\partial^2 u}{\partial y^2}\right|_w y^2 + \ldots\ldots \qquad (1\text{-}38)$$

$$v = \left.\frac{\partial v}{\partial y}\right|_w y + \frac{1}{2}\left.\frac{\partial^2 v}{\partial y^2}\right|_w y^2 + \ldots\ldots \qquad (1\text{-}39)$$

$$t = \left.\frac{\partial t}{\partial y}\right|_w y + \frac{1}{2}\left.\frac{\partial^2 t}{\partial y^2}\right|_w y^2 + \ldots\ldots \qquad (1\text{-}40)$$

$$c = \left.\frac{\partial c}{\partial y}\right|_w y + \frac{1}{2}\left.\frac{\partial^2 c}{\partial y^2}\right|_w y^2 + \ldots\ldots \qquad (1\text{-}41)$$

$$U = \left.\frac{\partial U}{\partial y}\right|_w y + \frac{1}{2}\left.\frac{\partial^2 U}{\partial y^2}\right|_w y^2 + \ldots\ldots \qquad (1\text{-}42)$$

$$T = \left.\frac{\partial T}{\partial y}\right|_w y + \frac{1}{2}\left.\frac{\partial^2 T}{\partial y^2}\right|_w y^2 + \ldots\ldots \qquad (1\text{-}43)$$

$$C = \left.\frac{\partial C}{\partial y}\right|_w y + \frac{1}{2}\left.\frac{\partial^2 C}{\partial y^2}\right|_w y^2 + \ldots\ldots \qquad (1\text{-}44)$$

The equation of continuity for the fluctuating velocities is written as

$$\partial u/\partial x + \partial v/\partial y = 0 \qquad (1\text{-}45)$$

Equation (1-45) requires that $\partial v/\partial y\big|_w = 0$. Combination of equations (1-38) and (1-39) gives

$$\overline{uv} = \frac{1}{2}\overline{\frac{\partial u}{\partial y}\Big|_w \frac{\partial^2 v}{\partial y^2}\Big|_w}\, y^3 + \left(\frac{1}{4}\overline{\frac{\partial^2 u}{\partial y^2}\Big|_w \frac{\partial^2 v}{\partial y^2}\Big|_w}\right.$$

$$\left. + \frac{1}{6}\overline{\frac{\partial u}{\partial y}\Big|_w \frac{\partial^3 v}{\partial y^3}\Big|_w}\right) y^4 + \ldots\ldots \qquad (1\text{-}46)$$

Similarly,

$$\overline{tv} = \frac{1}{2}\overline{\frac{\partial t}{\partial y}\Big|_w \frac{\partial^2 v}{\partial y^2}\Big|_w}\, y^3 + \left(\frac{1}{4}\overline{\frac{\partial^2 t}{\partial y^2}\Big|_w \frac{\partial^2 v}{\partial y^2}\Big|_w}\right.$$

$$\left. + \frac{1}{6}\overline{\frac{\partial t}{\partial y}\Big|_w \frac{\partial^3 v}{\partial y^3}\Big|_w}\right) y^4 + \ldots\ldots \qquad (1\text{-}47)$$

$$\overline{cv} = \frac{1}{2}\overline{\frac{\partial c}{\partial y}\Big|_w \frac{\partial^2 v}{\partial y^2}\Big|_w}\, y^3 + \left(\frac{1}{4}\overline{\frac{\partial^2 c}{\partial y^2}\Big|_w \frac{\partial^2 v}{\partial y^2}\Big|_w}\right.$$

$$\left. + \frac{1}{6}\overline{\frac{\partial c}{\partial y}\Big|_w \frac{\partial^3 v}{\partial y^3}\Big|_w}\right) y^4 + \ldots\ldots \qquad (1\text{-}48)$$

On the other hand, combining equations (1- 4), (1-13) and (1-42), one obtains the expression for the turbulent shear stress as

$$\overline{uv} = \left(\nu \frac{\partial^2 U}{\partial y^2}\Big|_w - \frac{\tau_w}{\rho H}\right) y + \frac{\nu}{2}\frac{\partial^3 U}{\partial y^3}\Big|_w y^2$$

$$+ \frac{\nu}{6} \left.\frac{\partial^4 U}{\partial y^4}\right|_w y^3 + \cdots\cdots \qquad (1\text{-}49)$$

Comparing equation (1-49) with (1-46), one obtains

$$\left.\frac{\partial^2 U}{\partial y^2}\right|_w = \frac{\tau_w}{\mu H} \quad , \quad \left.\frac{\partial^3 U}{\partial y^3}\right|_w = 0 \quad , \quad \text{etc.}$$

Therefore, the time-smoothed velocity and the turbulent shear stress near the wall can be expressed in dimensionless form as

$$U^+ = y^+ - \frac{1}{2H^+}(y^+)^2 + \frac{1}{4!}\left.\frac{\partial^4 U^+}{\partial y^{+4}}\right|_w (y^+)^4 + \cdots\cdots \qquad (1\text{-}50)$$

$$\overline{u^+ v^+} = -\frac{1}{3!}\left.\frac{\partial^4 U^+}{\partial y^{+4}}\right|_w (y^+)^3 - \frac{1}{4!}\left.\frac{\partial^5 U^+}{\partial y^{+5}}\right|_w (y^+)^4 - \cdots \qquad (1\text{-}51)$$

By definition (1-7), the expression for the eddy diffusivity for momentum is obtained as follows,

$$\varepsilon_M/\nu = -\frac{1}{3!}\left.\frac{\partial^4 U^+}{\partial y^{+4}}\right|_w (y^+)^3 - \frac{1}{4!}\left.\frac{\partial^5 U^+}{\partial y^{+5}}\right|_w (y^+)^4$$

$$- \cdots\cdots \qquad (1\text{-}52)$$

Following a similar procedure, one obtains the power series expressions for the eddy diffusivities for heat and mass as

$$\varepsilon_H/\nu = -\frac{1}{3!}\left.\frac{\partial^4 T^+}{\partial y^{+4}}\right|_w (y^+)^3 - \frac{1}{4!}\left.\frac{\partial^5 T^+}{\partial y^{+5}}\right|_w (y^+)^4 - \cdots\cdots \qquad (1\text{-}53)$$

$$\varepsilon_D/\nu = -\frac{1}{3!}\left.\frac{\partial^4 C^+}{\partial y^{+4}}\right|_w (y^+)^3 - \frac{1}{4!}\left.\frac{\partial^5 C^+}{\partial y^{+5}}\right|_w (y^+)^4 - \cdots\cdots \qquad (1\text{-}54)$$

where $T^+ = \rho C_p u_* (T - T_w)/q_w$, $C^+ = u_*(C - C_w)/N_w$. The above results demonstrate that the eddy diffusivities for momentum, heat and mass vary near the wall with a power of the distance y, not less than three.

For a small range of y^+, ε_M/ν, ε_H/ν and ε_D/ν are usually expressed as follows,

$$\varepsilon_M/\nu = A\,(y^+)^a \tag{1-55}$$

$$\varepsilon_H/\nu = B\,(y^+)^b \tag{1-56}$$

$$\varepsilon_D/\nu = C\,(y^+)^c \tag{1-57}$$

where A and a are constants and B (or C) and b (or c) may be functions of the Prandtl (or Schmidt) number.

A controversy (11,20,41,44,53,63) has existed over the question of whether the eddy diffusivities near the wall vary with the third or fourth power of the distance from the wall.

In the region $8 < y^+ < 40$, calculations of ε_M from the velocity profiles indicate that ε_M is roughly quadratic in y (19). This value, $a \doteq 2$, is lower than the value of 3 or higher predicted by the above discussion. Accordingly, this region $8 < y^+ < 40$ cannot be considered to be sufficiently close to the wall, where the above results are valid. Closer to the wall than this it is difficult to calculate ε_M accurately from the veloci-

ty profiles because the eddy diffusion rate of momentum near the wall is extremely small compared with that of the molecular diffusion (see equation (1-10)).

Son and Hanratty (63) presented an empirical correlation in which ε_D varied with the fourth power of y. Their work was criticized by Hughmark (22) and by Hubbard (21) on the grounds that Son and Hanratty had not used the best available data, and they concluded that ε_D varies with the cube of y.

However, there seems to be no accurate data from which one might draw a definite conclusion to this problem. One of the purposes of this study is to determine the values of b and c experimentally.

CHAPTER 2

EDDY DIFFUSIVITY FOR HEAT TRANSFER

2-1 Introduction

The eddy diffusivity for heat, ε_H, is calculated by equation (1-8) from the temperature profile and the turbulent heat flux distribution, or by equation (1-11) from the temperature profile and the total heat flux distribution.

No experimental and theoretical studies are available on the turbulence quantities of the temperature fluctuations or their correlations with the velocity fluctuations, e.g. the turbulent heat flux. Most of the measurements made refer to the temperature distributions in an air flow and were restricted mainly to the region of the

turbulent core (25, 43, 45), that is, the data for the eddy diffusivity of heat available are restricted mainly to air, which has a Prantdl number of the order of unity, and to the turbulent core.

As seen from equations (1-11) and (1-12), it seems impossible to obtain the eddy diffusivity for heat or mass near the wall from the measurements of temperature or concentration profiles at the Prandtl or Schmidt number of about unity because the molecular diffusion rate of heat or mass has the same order of magnitude as that of momentum which is extremely large in comparison with the eddy diffusion rate of momentum, heat or mass near the wall.

However, the measurements of the temperature or concentration profiles near the wall in a highly viscous liquid stream are recommended, since the molecular diffusion rate of heat or mass is lower than that of momentum, and the effect of small eddies in the layer near the wall becomes appreciable and can be quantitatively detected from temperature or concentration distribution measurements.

Along these lines, Lin, Moulton and Putnam (34) measured the concentration profiles at large Schmidt numbers with a Mach-Zehnder interferometer. However, the rectangular duct used by them had a very small aspect ratio of 1.67 ; hence the flow in their duct can not be regarded as two-dimensional. In addition, most of their experimental runs were made at the Reynolds number less than 10,000 and the Schmidt number of 900 ; and the entry length seems to be too short to develop the concentration profile fully.

The purpose of the present work is to measure precisely the temperature distributions near the wall in fully developed turbulent liquid streams to obtain accurate distributions of the eddy diffusivity for heat in the region close to the wall.

2-2 Experimental Method

The temperature distribution near the wall was measured by means of a Mach-Zehnder interferometer. The optical method is superior to the ordinary traversing method, since the former avoids disturbing the flow.

2-2-1 Mach-Zehnder interferometer

Two-beam interferometers, among which Mach-Zehnder type is the best known one, are convenient for the precise measurement of the temperature. In this instrument, the phase difference between a test beam and a reference beam is determined. This phase difference is caused by the inhomogeneity of the refractive index or by a difference in the geometrical path length of the light beams.

A number of studies have been made on the precision and adjustment of the Mach-Zehnder interferometer, such as done by Hansen (14), Schardin (55), and Kinder (28). Mach-Zehnder interferometers have also been utilized by many investigators in the study of thermal boundary

layers (13) and supersonic air jet (70), etc.

The Mach-Zehnder instrument used in these experiments was a vertical type made by Mizojiri Optical Industry Co. Ltd., Tokyo. Figure 2-1 is a schematic diagram of the interferometer and associated optical equipment.

The light from source H, passing through an aperture S, is rendered parallel by the lens L_2 and is divided by the beam-splitter, plate 1. The transmitted beam A proceeds to the plane mirror 2 and the reflected beam B to the plane mirror 3. The two beams are recombined by the plate 4, and produce interference fringes which are focussed on the screen P by the lens L_3.

Plates 1 and 4, plane mirrors 2 and 3 are circular, 100 mm in diameter. Aluminum coatings on the plates providing for half transmission and half reflection were made by evaporating aluminum metal in a vacuum. The light source is a high pressure, 75 watt, Toshiba SHL-100 UV type mercury arc lamp, producing monochromatic light of wave length 5461 Å.

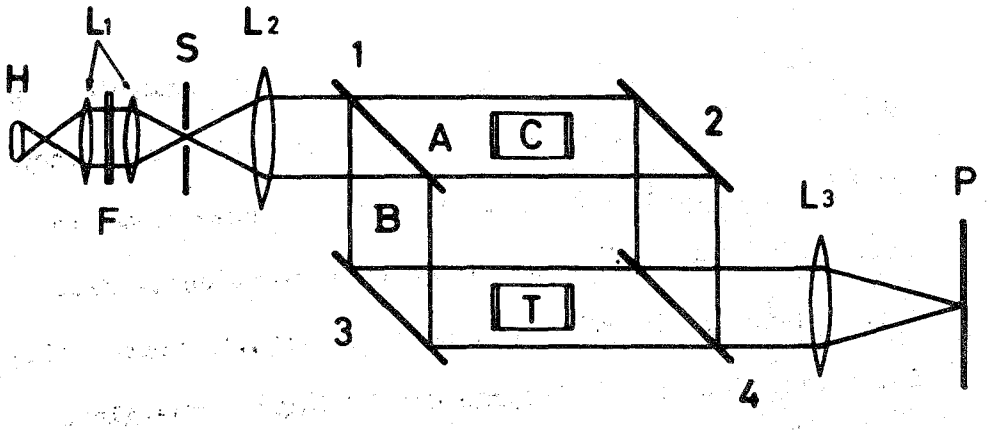

H Light Source

L_1 Condenser Lens

F Filter

S Slit

L_2 Collimating Lens

1,4 Splitter Plate

2,3 Plane Mirror

L_3 Focusing Lens

P Screen

A Transmitted Beam

B Reflected Beam

C Compensating Cell

T Test Section

Fig. 2-1 Schematic diagram of the Mach-Zehnder interferometer and associated optical apparatus.

2-2-2 Experimental apparatus and procedure

(a) Apparatus

The fluid flows in a rectangular duct 10 mm high and 100 mm wide, so the effects of the side walls may be neglected. The test section is made of brass as shown in Fig. 2-2. The windows are high quality optically flat glass plates of uniform thickness (10 mm), thereby avoiding distortion of the interference fringes. The glass plates are mounted parallel to each other.

The test section is placed in path B of the interferometer as shown in Fig. 2-1. To equalize the light beam paths, a compensating chamber having the same width as that of the test section and glass windows similar in both thickness and quality to those in the test section, is placed in path A.

The rectangular ducts, one 220 cm long and the other 70 cm long, are made of brass and have the same inside dimensions as the test section. They are connected to the test section, the longer one at the upstream end and the shorter one at the downstream end, to form calming

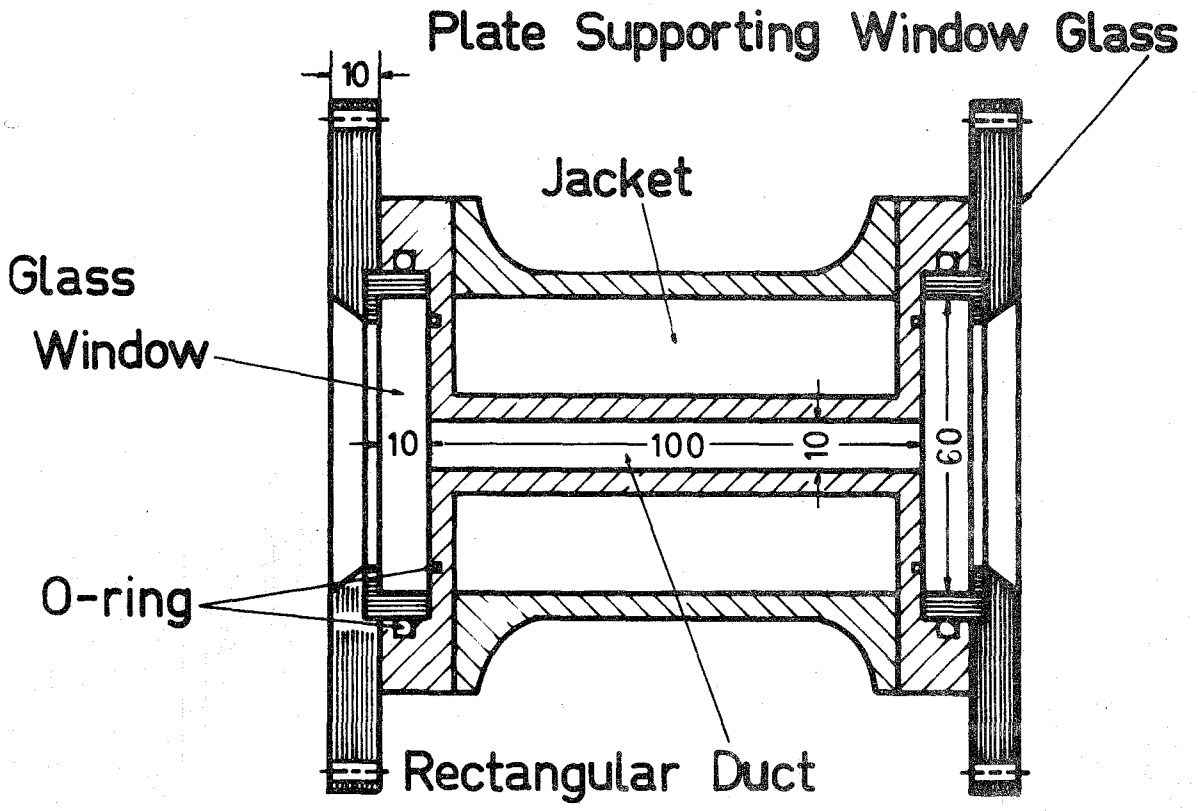

Fig. 2-2 Cross section of the testing duct.

sections. The upstream length is about 120 equivalent diameters of the duct; hence the flow in the test section may be considered to be thermally fully developed.

As shown in Fig. 2-3, the fluid is circulated by means of a polyvinyl chloride pump 2, through a 0.2 m^3 stainless steel storage tank 1. A head tank 4, is used to provide a constant head for uniform flow and the temperature regulating tank 3, in which a thermostat is provided to keep the temperature of the fluid constant. The fluid from the head tank is introduced into a stainless steel mixing tank 5, to make the temperature of the fluid uniform, and then it is divided into two flows. One flow is introduced directly into the jacket 12, and the other, after being heated slightly by an electric heater 6, passes through a tank 8, to achieve a uniform temperature, and then enters the rectangular duct 9. The latter fluid is cooled by the colder fluid in the jacket. The fluids in the duct and jacket flow counter-currently.

To prevent the circulating fluid from contamination, vinyl chloride plastic valves and pipes are used throughout the system. The flow rates are measured with the

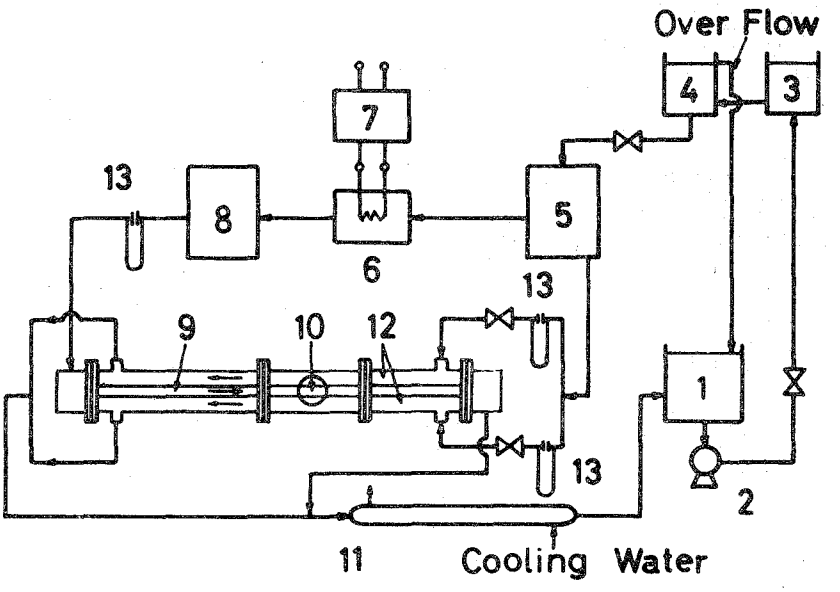

1 Storage Tank
2 Pump
3 Temperature Regulating Tank
4 Head Tank
5 Temperature Uniforming Tank
6 Heater
7 Voltage Stabilizer
8 Temperature Uniforming Tank
9 Rectangular Duct
10 Test Section
11 Heat Exchanger
12 Jacket
13 Manometer

Fig. 2-3 Diagram of the flow system.

calibrated orifices 13.

(b) Procedure

Before measuring the temperature distribution, the interferometer was first adjusted with the aid of a telescope to give fringes of proper width perpendicular to the wall where heat transfer would occur, and the fringes were focussed at the test section.

Next, the temperature gradient was established by heating the fluid flowing in the duct. The telescope was then replaced by a camera to take a picture of the fringes. Kodak TRI-X Pan films with 10 to 20 seconds exposure were found satisfactory for this purpose. Enlarged prints were made from the negatives, the over-all magnification being approximately 60 times. Hence the temperature distributions at distances of the order of 0.01 mm from the wall could be measured.

The fluids used were water and aqueous solutions of glycerol. The temperature of the fluid was varied from 26 to 50 ^{o}C, and the temperature difference between the fluid and the wall was about 0.01 $\sim$ 0.3 ^{o}C. Experiments

were performed at Prandtl numbers from 6 to 40 and Reynolds numbers from 11,700 to 26,400. The Prandtl numbers were varied by altering the temperature and glycerol concentration.

2-2-3 Method of analyzing the interferograms

(a) Calculation of temperature profile from an interferogram

Local temperature variations in the fluid, with resultant changes in the refractive index, cause the displacement of the interference fringes. The measurement of the displacement of the fringes gives an accurate quantitative value of the local temperature at any point in the fluid.

If the refractive index of the fluid in the test section changes from n_0 to n, the interference fringes are shifted and it follows that

$$L\,(n - n_0) = m\lambda \qquad (2\text{-}1)$$

where L denotes the width of the liquid over which the light beam passes, m the number of the fringe shifts, and λ the wave length of the light used respectively; the quantity m need not be an integer.

In the region in which the temperature change is slight, a linear relationship may be assumed, that is,

$$n = n_0 + (dn/dT)(T - T_0) \qquad (2\text{-}2)$$

From equations (2-1) and (2-2), it follows that

$$T - T_0 = m\lambda/L(dn/dT) \qquad (2\text{-}3)$$

The flow in a rectangular duct may be assumed to be two-dimensional and if the temperature distribution exists in a transverse direction to the flow direction, the interference fringes are shifted in the way shown in Fig. 2-4 (b). The x-, y-, and z-axis correspond to the direction of the fluid flow, perpendicular to the wall, and the direction of the light beam respectively. (see Fig. 2-4 (a))

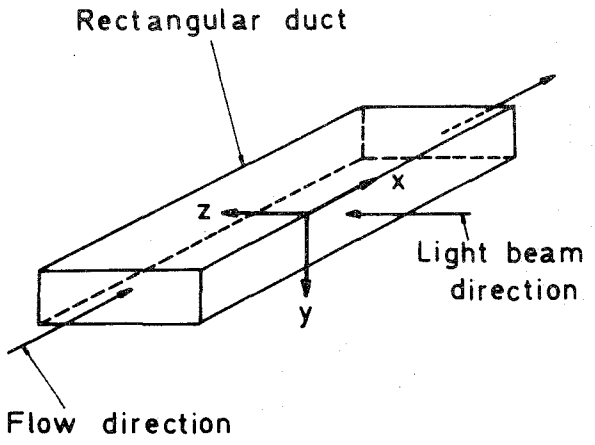

(a) Coordinate system

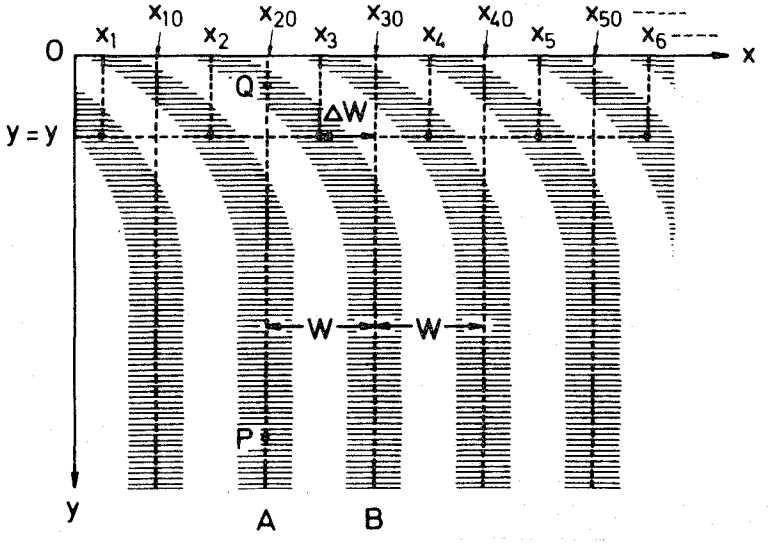

(b) Fringe displacements

Fig. 2-4 Schematic sketch of fringes.

If the temperature were uniform throughout, the center line of fringe A instead of that of B would pass through the point Q. The shift of one fringe at this point indicates that there is one less wave of light in the path through Q than there would be if the temperature at Q were the same as at P , i.e. $m = 1$ at Q . Generally the fringe shift is given by the relation $m = \Delta W/W$, where W denotes the width of the fringes. The Fizeau fringes which are equally spaced were used in this experiment.

(b) Refraction effect

Refraction of the interferometer beam in passing through the region in which the temperature gradient exists, owing to the lens action of this region, cannot be avoided. Since the refractive index obtained from an interferogram is the average value over the entire path length of the refracted light beam, a correcting calculation is needed to obtain the true refractive index profile.

The incident light beam at $y = y_i$, parallel to the wall, refracts as shown in Fig. 2-5 and produces the

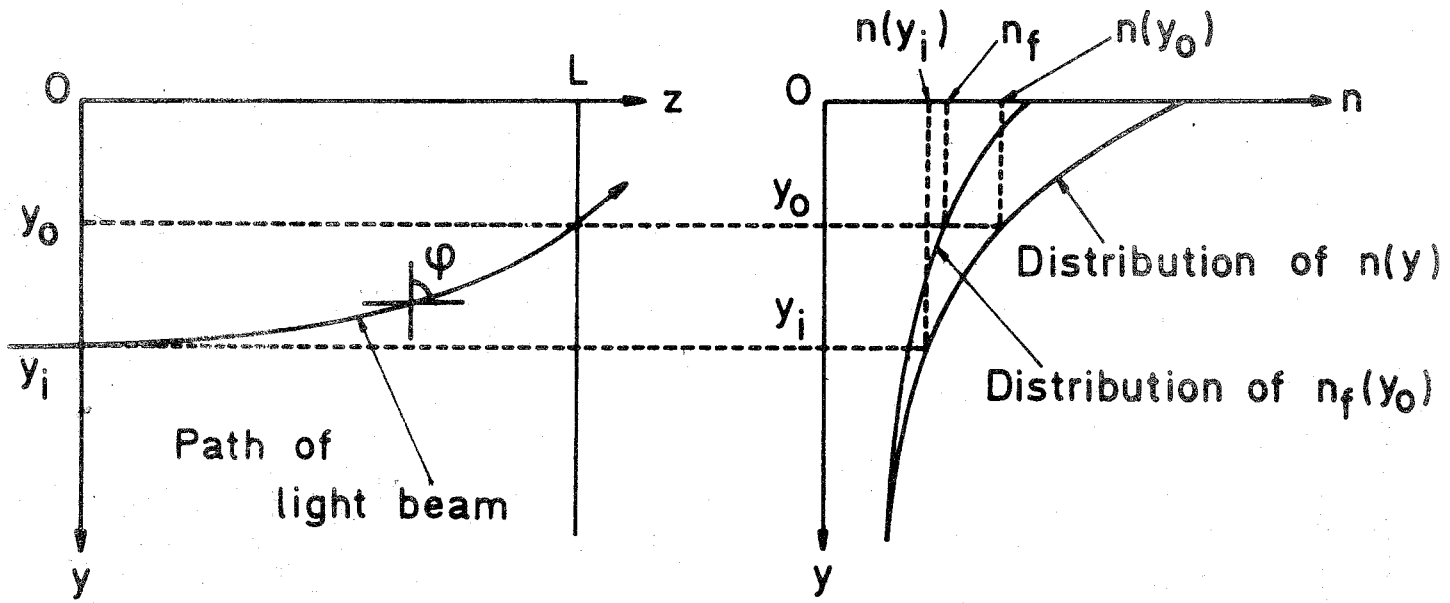

Fig. 2-5 Light beam through a one-dimensional refractive index field $n = n(y)$ and the distributions of $n = n(y)$ and $n_f = n_f(y_o)$.

virtual interference fringes at $z = L$. If the refractive index n is assumed to be a function of y only, the following equation is obtained from the Snell's law.

$$n(y_i) \sin(\pi/2) = n(y) \sin \varphi \tag{2-4}$$

The equation of the path of the light beam is given by

$$dz/dy = -\tan \varphi \tag{2-5}$$

From equations (2-4) and (2-5), eliminating the angle of refraction φ, one obtains the following equation,

$$\frac{dz}{dy} = -\frac{n(y_i)}{\left(n(y)^2 - n(y_i)^2 \right)^{1/2}} \tag{2-6}$$

Integration of equation (2-6) with the boundary conditions $z = 0$ at $y = y_i$ and $z = L$ at $y = y_0$ leads to

$$L = n(y_i) \int_{y_0}^{y_i} \frac{dy}{\left(n(y)^2 - n(y_i)^2 \right)^{1/2}} \tag{2-7}$$

This equation determines the relation between $n(y_i)$ and $n(y_0)$.

The average refractive index over the entire path length of the refracted light beam is

$$n_{av} = \frac{\int_{y_0}^{y_i} n(y) \left((dz/dy)^2 + 1 \right)^{1/2} dy}{\int_{y_0}^{y_i} \left((dz/dy)^2 + 1 \right)^{1/2} dy}$$

By using equation (2-6) one obtains

$$n_{av} = \frac{1}{L'} \int_{y_0}^{y_i} \frac{n(y)^2}{\left(n(y)^2 - n(y_i)^2 \right)^{1/2}} dy \qquad (2\text{-}8)$$

where L' is the actual path length of the light beam and is given by

$$L' = \int_{y_0}^{y_i} \frac{n(y)}{\left(n(y)^2 - n(y_i)^2 \right)^{1/2}} dy \qquad (2\text{-}9)$$

The average refractive index, n_{av}, may then be obtained by counting the fringe shifts in the interferogram and calculating by the following equation.

$$n_{av}L' - n_0L = m\lambda \qquad (2\text{-}10)$$

However, since the actual path length L' is unknown, the width of liquid L is used instead. Thus the refractive index n_f is given by

$$n_fL - n_0L = m\lambda \qquad (2\text{-}11)$$

From equations (2-8), (2-10) and (2-11) it follows that

$$n_f = \frac{1}{L}\int_{y_0}^{y_i} \frac{n(y)^2}{\{n(y)^2 - n(y_i)^2\}^{1/2}}\,dy \qquad (2\text{-}12)$$

Since n_f is obtained by the interference at $z = L$, n_f is considered to be a function of y_0, i.e. $n_f = n_f(y_0)$ (see Fig. 2-5). Equation (2-12) determines the relation between n_f, $n(y_i)$, and $n(y_0)$, that is, $n_f(y_0) = n_f(n(y_i), n(y_0))$.

Eliminating $n(y_i)$ from the two equations (2-7) and (2-12), one obtains

$$n_f(y_0) = n_f(n(y_0)) \tag{2-13}$$

Since the profile of $n_f(y_0)$ is obtained by equation (2-11) from an interferogram, the functional form of $n(y)$ can be obtained by equation (2-13).

The computation was performed by assuming that $n(y)$ may be approximated by a linear function of y over a small interval and using digital computer KDC-II of Kyoto University.

2-3 Experimental Results

The photographs of the interference fringe displacements of each run were taken. A sample of the photographs is shown in Fig. 2-6.

Table 2-1 shows the experimental conditions for each run. In some runs, the effects of axial transport of heat by convection and energy dissipation cannot be neglected because the heat flux at the wall is very small, i.e. the Brinkman number is large. Hence the values of the eddy diffusivities for heat, ε_H/ν , were calculated from the temperature profiles, which were evaluated from photographs of the interference fringes, taking into account the convection term and dissipation terms in equation (1-2).

The temperature gradient in the x-direction, $\partial T/\partial x$, was calculated from the width of the interference fringes. In the test section, if $\partial T/\partial x$ is a function of y only, the following relation is obtained.

$$\frac{\partial T}{\partial x} = \frac{\lambda}{L\,(dn/dT)} \frac{W - W'}{WW'} \qquad (2\text{-}14)$$

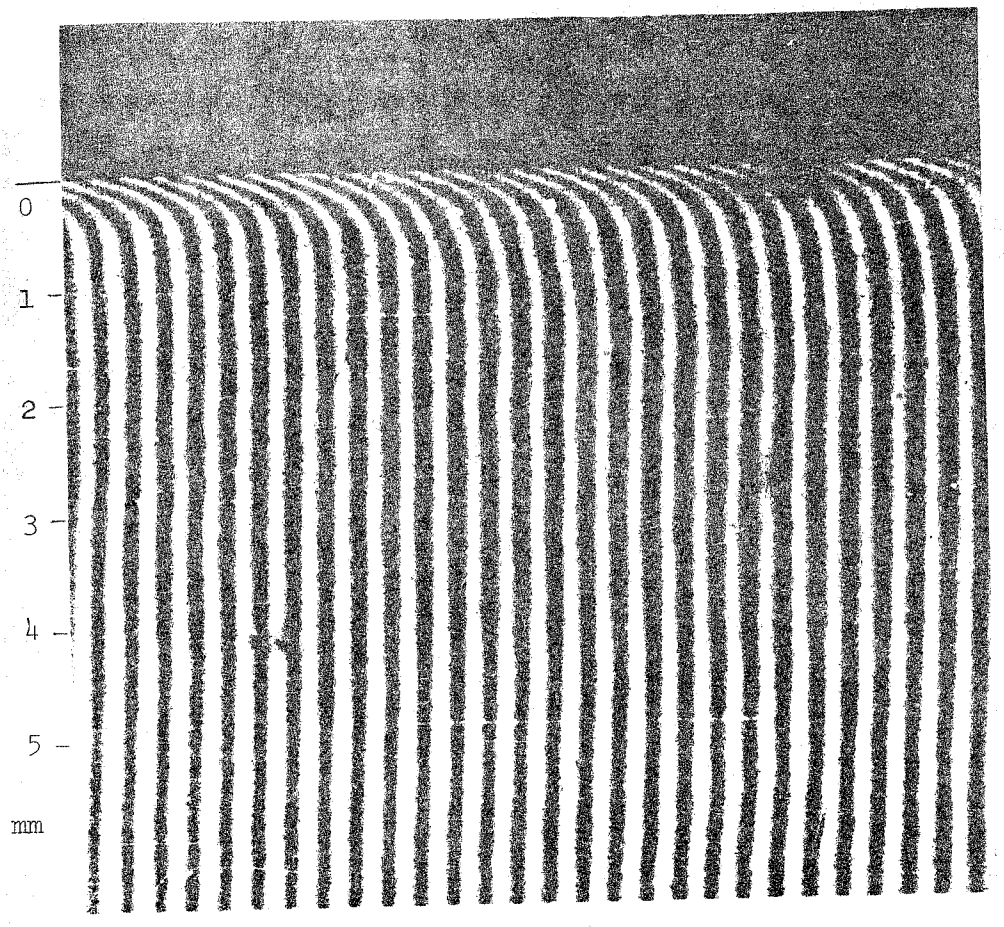

Fig. 2-6 A sample of photographs of fringes.

Table 2-1

Experimental Conditions

Run number		Prandtl number	Reynolds number	Brinkman number *)
1	Glycerol **)	39.5	13,000	8.82
2	"	34.5	14,400	4.61
3	"	34.5	11,700	2.77
4	"	31.0	16,100	3.61
5	"	30.9	13,300	0.708
6	"	25.8	19,400	2.66
7	"	25.6	13,000	0.509
8	"	14.9	22,100	0.482
9	"	14.5	13,400	0.0636
10	"	9.90	22,800	0.0944
11	"	9.66	18,000	0.0327
12	Water	6.01	26,400	0.0141
13	"	6.01	16,700	0.00402
14	"	6.01	14,100	0.00770

*) Brinkman number is defined as

$$Br = \mu \langle U \rangle^2 / k(T_b - T_w)$$

**) "Glycerol" means an aqueous solution of glycerol.

where W and W' are the width of the fringes with no temperature disturbance and with temperature disturbance respectively.

The turbulent energy dissipation function was assumed to be

$$\mu\Phi^{(t)} = \rho\varepsilon_M (dU/dy)^2 \qquad (2\text{-}15)$$

This assumption may be applied to the buffer region (17), but may not be applied to the region very close to the wall. However, in the region very close to the wall, $\mu\Phi^{(t)}$ is very small in comparison with $\mu\Phi^{(\ell)}$, so the assumption (2-15) may not cause the serious errors.

The distributions of the eddy diffusivity for momentum ε_M and the velocity U used are given in Chapter 4. The heat flux at the wall was computed from the temperature gradient at the wall.

The data of ε_H/ν are listed in Table 2-2 and plotted in Fig. 2-7. The experimental results are somewhat scattered and no dependence of ε_H/ν on the Prandtl

Table 2-2

Experimental Results of Eddy Diffusivities for Heat

Run 1 Pr = 39.5 Re = 13,000

y^+	ε_H/ν	y^+	ε_H/ν
4.86	0.0110	6.23	0.0393
7.10	0.0411	7.96	0.0833
8.83	0.0958	9.31	0.150
9.69	0.153	10.6	0.196
11.4	0.252	12.3	0.299
13.6	0.450	15.3	0.602
17.5	1.16	19.7	1.39
25.3	2.89	28.2	5.01
29.6	5.30	33.7	6.35
38.2	8.67	42.2	9.83
47.3	13.4	49.0	16.8
57.5	17.2	66.1	20.0
76.3	24.5	86.7	28.2

Run 2 Pr = 34.5 Re = 14,400

y^+	ε_H/ν	y^+	ε_H/ν
6.56	0.00638	6.90	0.00920

Table 2-2 (contd.)

7.60	0.0102	8.13	0.0111
8.67	0.0151	8.97	0.0247
9.40	0.0390	10.0	0.0582
10.6	0.0745	11.0	0.0920
11.6	0.121	12.1	0.160
14.1	0.250	15.7	0.337
16.1	0.435	18.3	0.670
20.1	1.02	22.2	1.30
28.5	4.59	32.7	10.0
34.9	11.9	38.0	12.6
49.0	19.4	59.9	20.3

Run 3 Pr = 34.5 Re = 11,700

y^+	ε_H/ν	y^+	ε_H/ν
13.8	0.118	14.5	0.234
15.3	0.398	16.1	0.632
16.9	0.952	17.7	1.37
18.5	1.94	19.3	2.78
45.6	10.5	59.2	14.8

Run 4 Pr = 31.0 Re = 16,100

Table 2-2 (contd.)

y^+	ε_H/ν	y^+	ε_H/ν
4.73	0.00292	5.07	0.0137
6.80	0.0398	7.84	0.0412
8.88	0.0702	9.92	0.133
12.0	0.214	12.6	0.244
34.7	13.9	36.9	16.4

Run 5 Pr = 30.9 Re = 13,300

y^+	ε_H/ν	y^+	ε_H/ν
5.82	0.0130	6.20	0.0182
7.97	0.0429	10.2	0.199
11.5	0.361	12.8	0.500
14.6	0.949	16.8	1.84
21.2	4.05	26.5	4.41
30.1	6.18		

Run 6 Pr = 25.8 Re = 19,400

y^+	ε_H/ν	y^+	ε_H/ν
4.42	0.00596	6.69	0.0399

Table 2-2 (contd.)

8.04	0.0541	9.12	0.0564
10.3	0.0937	10.8	0.150
11.6	0.202	12.8	0.399
14.0	0.627	15.2	0.872
16.4	0.974	17.6	1.00
18.7	1.09	19.5	1.10
23.1	2.74	24.9	3.86
27.4	5.81	29.8	6.44
32.8	9.20	35.3	10.8
43.7	17.8	50.1	21.4

Run 7 Pr = 25.6 Re = 13,000

y^+	ε_H/ν	y^+	ε_H/ν
2.17	0.00173	5.63	0.0100
6.49	0.0691	7.36	0.0912
9.09	0.109	9.95	0.137
11.3	0.240	12.2	0.322
13.4	0.470	14.7	0.587
16.0	0.687	17.3	0.864
18.6	1.11		

Run 8 Pr = 14.9 Re = 22,100

Table 2-2 (cont'd.)

y^+	ε_H/ν	y^+	ε_H/ν
4.19	0.00832	4.82	0.0154
5.96	0.0184	6.73	0.0196
7.13	0.0488	9.12	0.124
10.7	0.244	12.8	0.280
13.1	0.327	14.4	0.364
16.4	1.03	17.3	1.61
18.5	1.67	20.5	2.31
22.6	3.04	24.6	3.72
26.7	4.14	32.8	4.87
35.5	8.23	39.6	12.2
42.7	14.7	58.9	24.7
68.8	29.6	77.6	36.7
89.1	42.2		

Run 9 Pr = 14.5 Re = 13,400

y^+	ε_H/ν	y^+	ε_H/ν
4.95	0.00266	6.20	0.0319
7.76	0.0661	8.42	0.152
11.5	0.294	12.4	0.297
16.4	0.580	18.2	1.12
20.4	2.08	22.2	2.58
24.8	3.87	28.4	6.13
31.9	10.2	34.6	12.6

Table 2-2 (contd.)

37.2	13.8

Run 10 Pr = 9.90 Re = 22,800

y^+	ε_H/ν	y^+	ε_H/ν
4.25	0.0123	6.41	0.0243
6.99	0.0343	9.09	0.114
11.2	0.346	13.3	0.429
17.5	0.458	19.6	0.617
21.7	0.983	23.8	1.43
26.6	2.13	30.1	3.68
32.9	5.13	35.0	6.95
39.1	11.3	100.0	27.9

Run 11 Pr = 9.66 Re = 18,000

y^+	ε_H/ν	y^+	ε_H/ν
10.3	0.0678	12.0	0.166
14.0	0.190	18.5	0.435
20.0	1.20	22.4	1.31
24.7	1.78	32.6	3.77
36.0	5.17	40.6	7.02

Table 2-2 (contd.)

90.8	30.1	106.0	38.2

Run 12 Pr = 6.01 Re = 26,400

y^+	ε_H/ν	y^+	ε_H/ν
6.6	0.100	8.1	0.142
9.6	0.187	13.9	0.220
15.9	0.450	17.1	0.600
21.0	0.830	24.1	1.57
26.7	2.76	29.4	3.35
31.3	4.30	35.0	7.10
45.9	15.1		

Run 13 Pr = 6.01 Re = 16,700

y^+	ε_H/ν	y^+	ε_H/ν
6.31	0.0396	6.7	0.0735
7.8	0.103	8.8	0.154
10.0	0.212	11.8	0.325
15.0	0.580	17.0	0.820
19.9	1.40	21.7	2.03
23.9	2.90	27.8	4.18

Table 2-2 (contd.)

39.5	10.3

Run 14 Pr = 6.01 Re = 14,100

y^+	ε_H/ν	y^+	ε_H/ν
5.9	0.0680	6.8	0.0820
8.6	0.124	10.3	0.175
13.1	0.415	14.6	0.351
17.6	0.945	20.6	1.59
25.9	3.15	28.9	4.55
32.5	5.90	37.5	8.50
43.0	13.0		

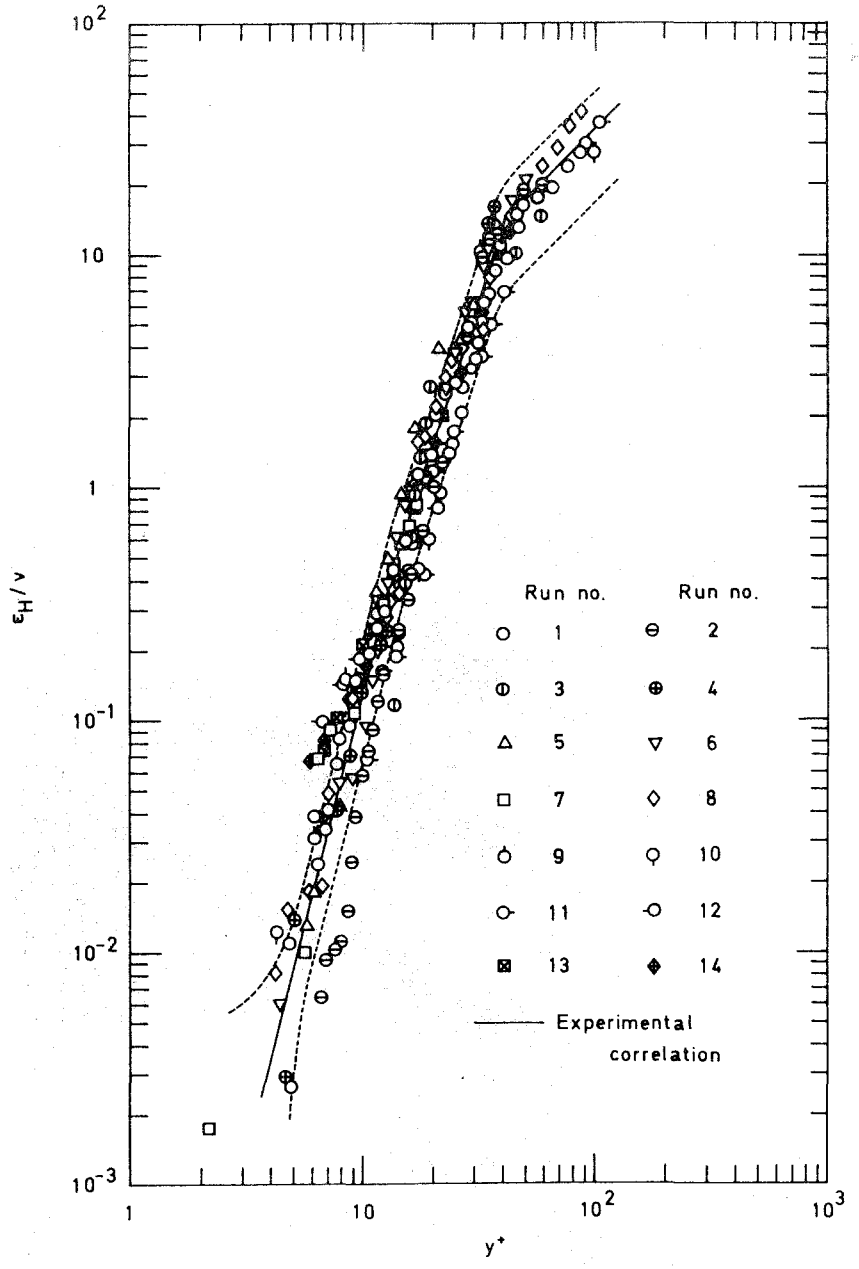

Fig. 2-7 Experimental results of eddy diffusivities for heat

number could be detected within the accuracy of the data. The accuracies of the measured values were estimated as follows.

The accuracy of the distance from the wall was 10^{-3} cm, which was estimated by considering the degree of parallelism between the light beam and the wall surface, the error in reading the fringe shifts in an enlarged photograph, and the degree of flatness of the wall surface.

The temperature is calculated from equation (2-3). By the law of propagation of error the probable error of the measurement of the temperature is given by

$$E_T = \frac{m\lambda}{L(dn/dT)} \{(E_m/m)^2 + (E_\lambda/\lambda)^2 + (E_L/L)^2 + (E_{dn/dT}/(dn/dT))^2\}^{1/2} \qquad (2\text{-}16)$$

The accuracies of the used values of λ , L , and dn/dT were 2×10^{-3} , 10^{-2} and 10^{-2} respectively. The value of m was calculated by the relation $m = \Delta W/W$ and ΔW was calculated as follows (see Fig. 2-4).

$$\Delta W = \frac{x_1+(x_2-W)+(x_3-2W)+(x_4-3W)+\cdots\cdots+(x_j-(j-1)W)}{j}$$

$$- \frac{x_{10}+(x_{20}-W)+(x_{30}-2W)+\cdots\cdots+(x_{j0}-(j-1)W)}{j}$$

$$= \frac{x_1+x_2+x_3+\cdots\cdots+x_j}{j} - \frac{x_{10}+x_{20}+\cdots\cdots+x_{j0}}{j} \qquad (2\text{-}17)$$

Therefore, the probable error of ΔW is given by

$$E_{\Delta W} = E_x/(j)^{1/2} \qquad (2\text{-}18)$$

Since the value of W was nearly 10 mm on an enlarged photograph, the maximum errors in reading of x_1, x_2, ... etc. were considered to be about 1 mm. And the number of fringes, j, was nearly 50 in this experiment. Thus the probable error of the fringe shifts was estimated as

$$E_m = E_{\Delta W}/W \simeq (1/(50)^{1/2}/10 \simeq 10^{-2}$$

From the fact that the value of m was smaller than the order of magnitude of unity and the estimated accuracy of m was 1 % in this experiment, one can obtain the probable error of the measurement of temperature from equation (2-16) as follows.

$$E_T \simeq 10^{-4}\ ^{o}C$$

To obtain the eddy diffusivity for heat, the value of $\partial T/\partial y$ must be known. Since the graphical or numerical differentiation lower the precision of the differentiated values, an approximated polynomial of the temperature distribution which was obtained by the least square method was differentiated analytically with y in this study. Hence one can obtain the probable error of the temperature gradient from the estimation of the probable errors of the coefficients of the polynomial and the following result was obtained in this experiment;

in the region near the wall ($y^+ < 5 \sim 6$)

$$E_{\partial T/\partial y}/(\partial T/\partial y) \simeq (0.5 \sim 1) \times 10^{-1}$$

in the region far from the wall ($y^+ > 5 \sim 6$)

$$E_{\partial T/\partial y}/(\partial T/\partial y) \simeq (0.5 \sim 5) \times 10^{-1}$$

The heat flux is calculated by integrating equation (1-2). The temperature gradient in the x-direction, $\partial T/\partial y$, and the turbulent energy dissipation function were calculated from equations (2-14) and (2-15) respectively. The probable error of the heat flux is given by

$$E_q = (dq/dy)\, E_y \qquad (2\text{-}19)$$

From equations (1-2) and (2-19) the following value was obtained in the whole region of the flow.

$$E_q/q \lesssim 2 \times 10^{-2}$$

The eddy diffusivity for heat is calculated from equation (1-11) and the probable error of ε_H/ν is given by

$$E_{\varepsilon_H/\nu} = \{(\frac{\varepsilon_H}{\nu} \frac{E_{Cp}}{C_p})^2 + (\frac{\varepsilon_H}{\nu} \frac{E_\mu}{\mu})^2 + (\frac{1}{Pr} \frac{E_k}{k})^2 + (\frac{1}{Pr} \frac{q}{k\partial T/\partial y} \frac{E_q}{q})^2 + (\frac{1}{Pr} \frac{q}{k\partial T/\partial y} \frac{E_{\partial T/\partial y}}{\partial T/\partial y})^2 \}^{1/2} \qquad (2\text{-}20)$$

Taking into account that the accuracies of the physical properties were about 1 % and that the estimated accuracy of q was smaller than that of $\partial T/\partial y$, one can see from equation (2-20) that the main contribution to the precision of ε_H/ν was the accuracy of the temperature gradient, $\partial T/\partial y$, which was difficult to measure accurately, and can obtain the following relation.

$$E_{\varepsilon_H/\nu} \simeq \frac{1}{Pr} \frac{q}{k\partial T/\partial y} \frac{E_{\partial T/\partial y}}{\partial T/\partial y} \qquad (2\text{-}21)$$

It is seen from this equation that the measured values of ε_H/ν for smaller Prandtl numbers are less reliable than those for larger Prandtl numbers. In the region near the wall ($y^+ < 5 \sim 6$) equation (2-21) was reduced to

$$E_{\varepsilon_H/\nu} \simeq (1/20)(1)\left(\frac{E_{\partial T/\partial y}}{\partial T/\partial y}\right) \simeq (0.25 \sim 0.5) \times 10^{-2}$$

where the Prandtl number is taken to be 20. On the other hand, the measured values of ε_H/ν at $y^+ < 4$ were less than 0.5×10^{-2}. Hence these data at $y^+ < 4$ are not reliable. At $y^+ > 30 \sim 40$ equation (2-21) was reduced to

$$E_{\varepsilon_H/\nu} \simeq (\varepsilon_H/\nu)(0.5 \sim 5) \times 10^{-1}$$

that is, the maximum error in that region was 50 %. For the region $5 \sim 6 < y^+ < 30 \sim 40$ the accuracy of ε_H/ν was calculated by making use of equation (2-21) directly.

In Fig. 2-7 the maximum deviation from the most probable values of ε_H/ν at $Pr = 20$ is shown by the dotted lines. It is seen from this figure that the measured values are scattered within the area between the two dotted lines.

Finally it is noted that the all numerical calculation and the correction calculation were made with eight significant figures to neglect the calculation error in comparison with the measurement error.

From Fig. 2-7 the exponent of y^+ seems to change from 3 to 4 gradually as y^+ becomes small, and the data are correlated by the following equations.

$$4 < y^+ \leq 14 \qquad \varepsilon_H/\nu = 1.31 \times 10^{-5} (y^+)^4 \qquad (2\text{-}22)$$

$$14 < y^+ \leq 42 \qquad \varepsilon_H/\nu = 1.93 \times 10^{-4} (y^+)^3 \qquad (2\text{-}23)$$

$$42 < y^+ \qquad \varepsilon_H/\nu = 0.36\, y^+ - 1 \qquad (2\text{-}24)$$

These equations are plotted in Fig. 2-8 with several predictions from other investigators. The experimental results show that in the region near the wall, the values of ε_H/ν are smaller than the predictions of other investigators for ε_M/ν and ε_D/ν.

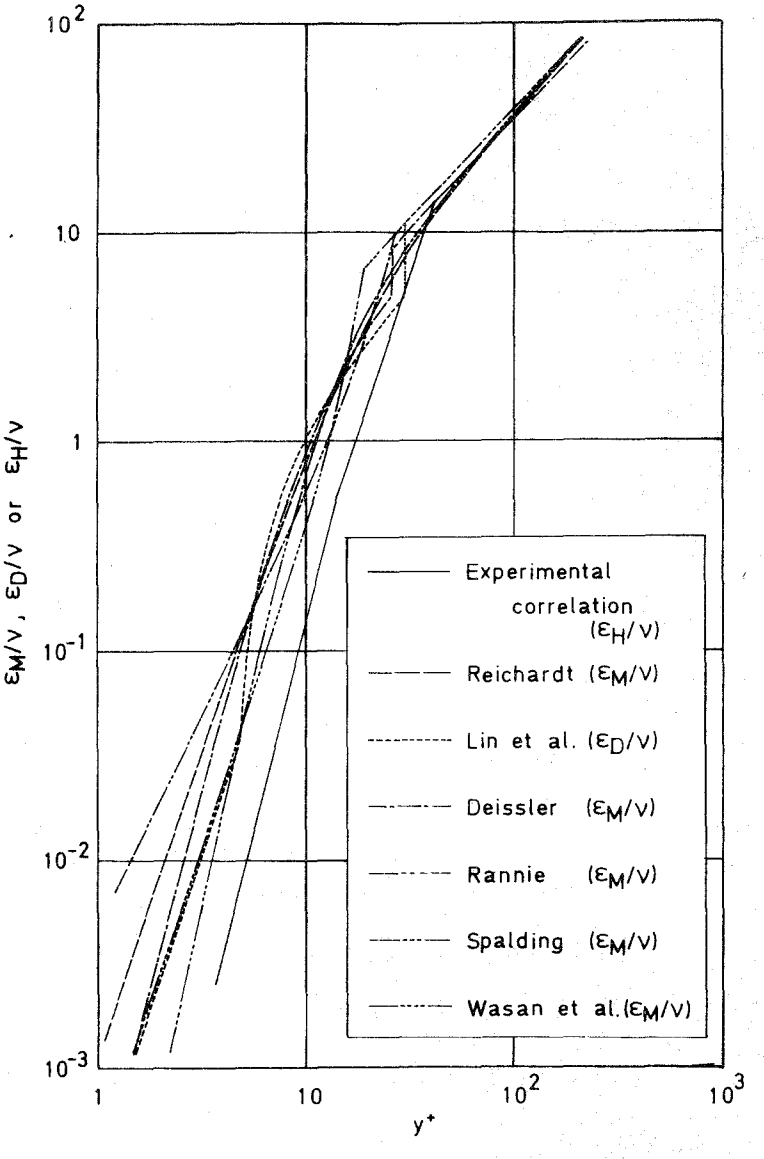

Fig. 2-8 Comparison of experimental result with predictions of other investigators.

2-4 Conclusion

1. The experimental data at $Pr = 6 \sim 40$ and $Re = 11{,}700 \sim 26{,}400$ are correlated by the following equations.

$$4 < y^+ \leq 14 \qquad \varepsilon_H/\nu = 1.31 \times 10^{-5} (y^+)^4$$

$$14 < y^+ \leq 42 \qquad \varepsilon_H/\nu = 1.93 \times 10^{-4} (y^+)^3$$

$$42 < y^+ \qquad \varepsilon_H/\nu = 0.36\, y^+ - 1$$

2. In the region close to the wall the values of ε_H/ν are smaller than the predictions of other investigators for ε_M/ν and ε_D/ν ; no dependence on the Prandtl number could be observed in the range of the experiment.

3. The exponent of y^+ seems to change from 3 to 4 gradually as y^+ becomes small.

CHAPTER 3

RATIO OF THE EDDY DIFFUSIVITIES FOR HEAT AND MOMENTUM

3-1 Introduction

To calculate the Nusselt number it is often assumed that the eddy diffusivity for heat is equal to that for momentum. However, there is no evidence to support this, so the ratio $\varepsilon_H/\varepsilon_M$ must be determined experimentally or theoretically.

Various investigators (23, 36, 39, 46) have determined the ratio $\varepsilon_H/\varepsilon_M$ in pipe flow and in two-dimensional channel flow. From temperature and velocity distributions measured in the air flow through a horizontal duct, Page et al. (46) determined the distribution of the ratio across the duct. They found that the ratio decreased with increasing Reynolds number, approaching unity and increased from the center toward the wall. No data in the region near

the wall were obtained.

Just opposite results were obtained by Isakoff and Drew (23) for mercury flowing upward in a vertical heated pipe. The ratio increased with increasing Reynolds numbers and varied across the pipe in such a way that a maximum value occured at roughly $y/R = 0.2$. It decreased sharply toward the wall region. Here too, no data for the wall region was given.

Jenkins (24), Deissler (5), Azer and Chao (1), Mizushina and Sasano (39) and others (37, 66) have attempted to evaluate the ratio theoretically by modifying the mixing length theory, or by other models. However, the results obtained by these investigators are considerably different from each other and were derived mainly for the eddies in the turbulent core.

This chapter deals with an analytical expression for the ratio of the eddy diffusivities for heat and momentum which is valid in the region near the wall.

3-2 Basic Concept

The basic concept is that a spherical eddy particle loses a part of its heat and momentum as it travels over a distance equal to the mixing length.

It will now be assumed that an eddy particle is displaced from one layer at $y - \ell$ to another at y and has a constant velocity v' in the positive direction of y as shown in Fig. 3-1. The velocity v' is defined as $v' = \overline{|v|}$. The eddy particle loses a part of its original momentum as it travels over the mixing length, the loss of momentum being expressed by following equation of motion.

$$(\frac{\pi}{6}\rho d^3)\{\frac{dU_p}{d(s/v')}\} = c_D\ (\frac{\pi}{4}d^2)\{\frac{\rho}{2}\ (U - U_p)^2\} \qquad (3\text{-}1)$$

where d denotes the diameter of the eddy particle, U_p the velocity of the eddy particle in the x-direction, c_D the drag coefficient and $\{dU_p/d(s/v')\}$ the acceleration term.

The velocity of the flow U is assumed to be linear

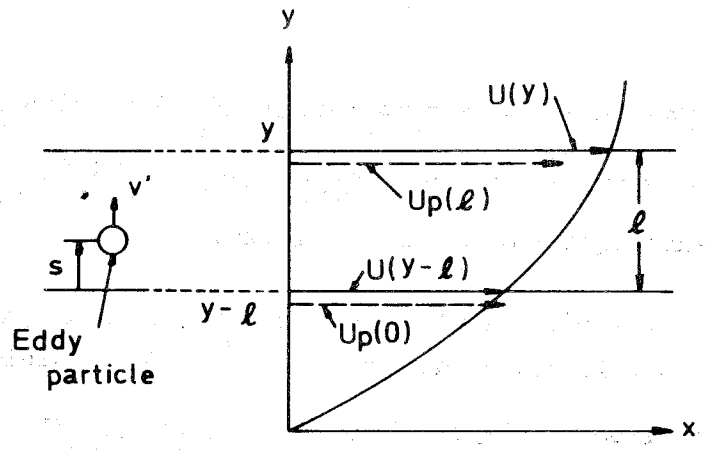

Fig. 3-1 Explanation of the present model for the turbulent exchange of momentum.

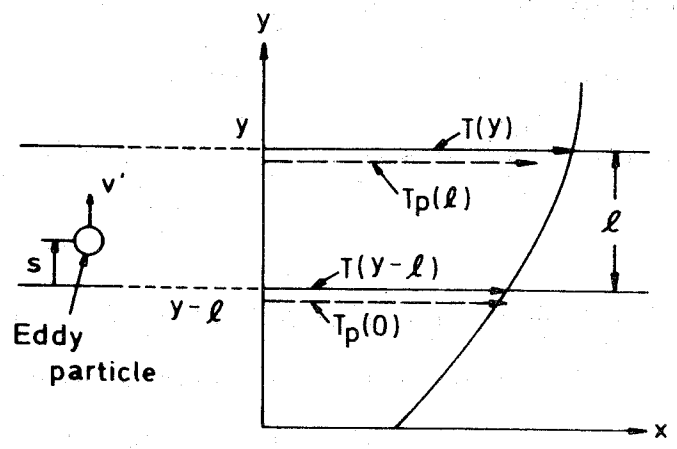

Fig. 3-2 Explanation of the present model for the turbulent exchange of heat.

over the small interval ℓ , i.e.

$$U = U(y - \ell) - \{U(y - \ell) - U(y)\}\ (s/\ell) \qquad (3\text{-}2)$$

The boundary conditions are

$$\begin{aligned} U_p &= U(y - \ell) \quad \text{at} \quad s = 0 \\ U_p &= U_p(\ell) \quad \text{at} \quad s = \ell \end{aligned} \qquad (3\text{-}3)$$

Assuming that the drag coefficient c_D in equation (3-1) is constant over the small interval ℓ and substituting equations (3-2) and (3-3) into equation (3-1), one can integrate the latter to give

$$U_p(\ell) = U(y) - \eta_M \{ U(y) - U(y - \ell)\} \qquad (3\text{-}4)$$

where

$$\eta_M = (\ \tanh\ \phi_M\ ) / \phi_M \qquad (3\text{-}5)$$

$$\phi_M = \left(\frac{k\ell(U(y) - U(y - \ell))}{d\ v'} \right)^{1/2} \qquad (3\text{-}6)$$

and k is a constant.

The difference in the velocities of the eddy particle and the flow at y is then

$$\Delta u_1 = U(y) - U_p(\ell) = \eta_M \{ U(y) - U(y - \ell)\}$$

$$= \eta_M \ell \frac{dU}{dy} \qquad (3\text{-}7)$$

Similarly the eddy particle which arrives at y from the layer at $y + \ell$ posseses a velocity which exceeds that around it, the difference being

$$\Delta u_2 = U_p(\ell) - U(y) = \eta_M \{ U(y + \ell) - U(y)\}$$

$$= \eta_M \ell \frac{dU}{dy} \qquad (3\text{-}8)$$

In this transverse motion, the velocity v' is in the opposite direction to y .

The velocity differences caused by the transverse motion can be regarded as the fluctuating velocity components at y . Hence one can calculate the time-smoothed

absolute value of this fluctuation, i.e.

$$u' = \overline{|u|} = \frac{1}{2} \left(|\Delta u_1| + |\Delta u_2| \right)$$

$$= \eta_M \ell \frac{dU}{dy} \qquad (3\text{-}9)$$

It follows from the preceding representation that the eddy particle which arrives at layer y with a positive value of v (upwards from below in Fig. 3-1) will give rise to a negative value of u, so that their product uv is negative. The eddy particle with a negative value of v (downwards from above in Fig. 3-1) is associated with a positive value of u and the product uv is again negative. Hence one can assume that

$$\overline{uv} = - k \, u'v' \qquad (3\text{-}10)$$

where k is a positive numerical constant.

Combining equations (3-9) and (3-10), one obtains

$$\overline{uv} = - \eta_M \ell v' \frac{dU}{dy} \qquad (3\text{-}11)$$

In this expression the unknown constant k is included with the still unknown mixing length ℓ. Consequently the eddy diffusivity for momentum from equation (1-7) can be written as

$$\varepsilon_M/\nu = \eta_M (\ell v'/\nu) \tag{3-12}$$

where η_M is given by equation (3-5) and ϕ_M is rewritten as

$$\phi_M = \{ k (\ell/d)(u'/v')(1/\eta_M) \}^{1/2} \tag{3-13}$$

Similarly, for the heat transfer from an eddy particle to the surroundings, the following equations are given (see Fig. 3-2).

$$(\frac{\pi}{6} \rho d^3) C_p \{\frac{dT_p}{d(s/v')}\} = h_e(\pi d^2)(T - T_p) \tag{3-14}$$

$$T = T(y - \ell) - \{ T(y - \ell) - T(y) \} (s/\ell) \tag{3-15}$$

B.C. $T_p = T(y - \ell)$ at $s = 0$

$T_p = T_p(\ell)$ at $s = \ell$ (3-16)

where T_p is the temperature of the eddy particle, h_e the heat transfer coefficient and $\{ dT_p/d(s/v') \}$ the differentiation of T_p.

If the relation of Ranz and Marshall (51)

$$\frac{h_e d}{k} = 2 + 0.6 \, (dv'/\nu)^{1/2} \, Pr^{1/3} \qquad (3\text{-}17) \; *)$$

is assumed to be applicable to the heat exchange between an eddy particle and its surroundings, equation (3-14) can be integrated and the following expressions are finally obtained.

$$\varepsilon_H/\nu = \eta_H \, (\ell v'/\nu) \qquad (3\text{-}18)$$

where

$$\eta_H = \phi_H \, \{ 1 - \exp \, (-1/\phi_H) \} \qquad (3\text{-}19)$$

$$\phi_H = \frac{(d/\ell)^2 (1/\eta_M) Pr (\varepsilon_M/\nu)}{12 + 3.6 \, (d/\ell)(1/\eta_M)(\varepsilon_M/\nu)^{1/2} Pr^{1/3}} \qquad (3\text{-}20)$$

From equations (3-12) and (3-18), the ratio of the eddy diffusivities for heat and momentum is given as

$$\sigma = \eta_H/\eta_M = (1/\eta_M)\ \phi_H\ \{\ 1 - \exp\ (-1/\phi_H)\} \qquad (3\text{-}21)$$

---

*) Although the quantity $d\ \{(v')^2 + (U - U_p)^2\}^{1/2}/\nu$ should be used as the Reynolds number, the quantity dv'/ν is adopted instead, i.e. h_e is assumed to be constant over the small interval ℓ. Since the order of magnitude of $U - U_p$ is considered to be smaller than that of v', and to approach the latter at $s = \ell$, dv'/ν is smaller by a factor $\sqrt{2}$ at most than $d\ \{(v')^2 + (U - U_p)^2\}^{1/2}/\nu$. This factor can be included with d/ℓ (see the denominator of equation (3-20)) which has not been still determined, in other words, with the constants α_1 in equation (3-33) and α_2 in equation (3-38) which must be determined to represent the experimental results. Therefore, the error due to this simplification seems to be negligible in the final result of this model.

3-3 Assumptions concerning the Mixing Length and the Diameter of an Eddy Particle

The values of the mixing length are assumed to be determined by the quantities that characterize local turbulence, such as the diameter of the eddy particle d and the local Reynolds number of turbulence dv'/ν. Thus,

$$\ell/d = \text{fn}\,(dv'/\nu) \qquad (3\text{-}22)\ **)$$

If the diameter of the eddy particle is assumed to be the micro scale of turbulence, equation (3-22) represents the same assumption as that of von Kármán (26).

Since fully developed turbulent flow in a two-dimensional channel may be considered to be homogeneous in the x-direction, the diameter of the eddy particle, which may be micro scale of turbulence, is given by

$$2\,(u')^2/d^2 = \overline{(\partial u/\partial x)^2} \qquad (3\text{-}23)$$

Equation (3-23) is a definition of the micro scale of turbulence for the case of homogeneous turbulence (16).

From equation (3-23), one can obtain

$$|\partial u/\partial x| \approx \sqrt{2}\ (u'/d) \qquad (3\text{-}24)$$

On the other hand, the time-smoothed absolute value of the transverse velocity component v' was assumed to be constant over the small interval 2ℓ, as given in Section 3-2. Hence one can assume

$$|\partial v/\partial y| \approx v'/2\ell \qquad (3\text{-}25)$$

From the continuity equation of the fluctuating velocity components (1-45) and equations (3-24) and (3-25), one obtains

$$\ell/d \approx (\sqrt{2}/4)\ (v'/u') \qquad (3\text{-}26)$$

Substitution of equation (3-26) into equation (3-13) gives the result that η_M is a definite value. Therefore, from equations (3-12) and (3-22), the ratio, ℓ/d, may be considered to have the following functionality.

$$\ell/d = Fn(\varepsilon_M/\nu) \tag{3-27}$$

The simplest form is

$$\ell/d = \alpha\ (\varepsilon_M/\nu)^{1/\beta} \tag{3-28}$$

Substitution of equation (3-28) into equation (3-20) gives the result,

$$\phi_H = \frac{(1/\alpha^2\eta_M)\ Pr\ (\varepsilon_M/\nu)^{1-2/\beta}}{12 + 3.6\ (1/\alpha\eta_M)^{1/2}\ Pr^{1/3}\ (\varepsilon_M/\nu)^{(\beta - 1)/2\beta}} \tag{3-29}$$

(a) Determination of the values of η_M and β

In the turbulent core, it may be assumed that $u' \approx v'$, and one obtains $\ell/d \approx$ a constant in the order of unity from equation (3-26), i.e. the power number $1/\beta$ in equation (3-28) is zero. In the turbulent core, equation (3-29) may be rewritten as

$$\phi_H = \frac{(1/\alpha_1^2 \eta_M)\ Pr\ (\varepsilon_M/\nu)}{12 + 3.6\ (1/\alpha_1 \eta_M)^{1/2}\ Pr^{1/3}\ (\varepsilon_M/\nu)^{1/2}} \qquad (3\text{-}30)$$

As seen from equations (3-19) and (3-30), the value of η_H approaches unity when ε_M/ν increases to infinity and η_M is a constant; hence from equation (3-21) one obtains

$$\lim_{\varepsilon_M/\nu \to \infty} \sigma = 1/\eta_M \qquad (3\text{-}31)$$

From the experimental results of Mizushina and Kuriwaki (40) for the ratio of the eddy diffusivities in the turbulent core at large Prandtl numbers, the value of lim σ is supposed to be unity, so the value of η_M is taken as unity. Therefore, the following expression for the ratio of the eddy diffusivities may be obtained from equation (3-21) with $\eta_M = 1$;

$$\sigma = \phi_H \{1 - \exp(-1/\phi_H)\} \qquad (3\text{-}32)$$

and from equation (3-30),

$$\phi_H = \frac{(1/\alpha_1^2)\ Pr\ (\varepsilon_M/\nu)}{12 + 3.6\ (1/\alpha_1)^{1/2}\ Pr^{1/3}\ (\varepsilon_M/\nu)^{1/2}} \qquad (3\text{-}33)$$

In the vicinity of the wall, u' and v' are considered to be proportional to the distance from the wall and to the square of the distance, respectively, as shown in Section 1-3. Hence from equation (3-26), one obtains

$$\ell/d \propto y \qquad (3\text{-}34)$$

By comparing equation (3-34) with equation (3-28), one obtains the following expression for the eddy diffusivity of momentum near the wall.

$$\varepsilon_M/\nu \propto y^{\beta} \qquad (3\text{-}35)$$

In the region very close to the wall, equation (3-32) can be simplified to $\sigma \doteqdot \phi_H$, and using equation (3-35) and the simplified form of equation (3-29), i.e.

$$\phi_H \doteqdot (Pr/12\ \alpha^2)\ (\varepsilon_M/\nu)^{1\ -\ 2/\beta} \qquad (3\text{-}36)$$

one obtains

$$\varepsilon_H/\nu \doteq (Pr/12\,\alpha^2)\,(\varepsilon_M/\nu)^{2\,-\,2/\beta}$$

$$\propto y^{2\beta\,-\,2} \qquad (3\text{-}37)$$

As shown in Chapter 2, the experimental results for the eddy diffusivity of heat in the region very close to the wall show that $\varepsilon_H/\nu \propto y^4$, and hence, by comparing with equation (3-37), one obtains the result that the value of β is 3. Thus, in the region close to the wall,

$$\phi_H = \frac{(1/\alpha_2^{\,2})\,Pr\,(\varepsilon_M/\nu)^{1/3}}{12 + 3.6\,(1/\alpha_2)^{1/2}\,Pr^{1/3}\,(\varepsilon_M/\nu)^{1/3}} \qquad (3\text{-}38)$$

The constants α_1 and α_2 in equations (3-33) and (3-38) are determined by using a suitable expression of ε_M/ν and fitting these equations to the experimental data for ε_H/ν. The expression for ε_M/ν will be given in the next chapter and the final expression for σ is to be

given in Chapter 5.

**) The quantity $d\{(u')^2 + (v')^2\}^{1/2}/\nu$ should be used instead of dv'/ν as the local Reynolds number of turbulence, that is, the equation

$$\ell/d = fn(\, d\{(u')^2 + (v')^2\}^{1/2}/\nu\,) \qquad (3\text{-}22a)$$

should be used instead of equation (3-22). However, it is evident from equations (3-22a) and (3-26) that there is a definite relation between u' and v'. Therefore, the equation (3-22) can be used in place of equation (3-22a) without loss of generality.

3-4 Conclusion

1. The ratio of the eddy diffusivities for heat and momentum have been predicted by a modified mixing length theory. The expression for the ratio is given by

$$\sigma = \phi_H \{ 1 - \exp(-1/\phi_H) \}$$

in the turbulent core;

$$\phi_H = \frac{(1/\alpha_1^2)Pr(\varepsilon_M/\nu)}{12 + 3.6(1/\alpha_1)^{1/2} Pr^{1/3} (\varepsilon_M/\nu)^{1/2}}$$

and near the wall;

$$\phi_H = \frac{(1/\alpha_2^2)Pr(\varepsilon_M/\nu)^{1/3}}{12 + 3.6(1/\alpha_2)^{1/2} Pr^{1/3} (\varepsilon_M/\nu)^{1/3}}$$

2. The ratio σ is a function of the Prandtl number and the eddy diffusivity of momentum, and is smaller than unity, i.e. ε_H/ν is smaller than ε_M/ν, and ε_H/ν

approaches ε_M/ν when the values of Prandtl number and ε_M/ν increase to infinity.

3. Using the present analysis and the experimental results for ε_H/ν, one obtains the result that the eddy diffusivity for momentum close to the wall should be proportional to y^3.

CHAPTER 4

EDDY DIFFUSIVITY FOR MOMENTUM

4-1 Introduction

To predict the eddy diffusivity of heat using the ratio σ, the eddy diffusivity for momentum must be evaluated first. Numerous formulas have been proposed to describe the velocity profile (Table 4-1) and the corresponding expression for the eddy diffusivity of momentum for fluid flow in a tube (see Table 1-3).

Assuming that the eddy diffusivity of momentum is proportional to the distance from the wall,

$$\varepsilon_M/\nu = \kappa y^+ \qquad (4\text{-}1)$$

Table 4-1

Various Expressions for Velocity Distribution

Prandtl-Taylor (49,65)

$$U^+ = \frac{1}{\kappa} \ln y^+ + k \qquad \text{turbulent core}$$

von Kármán (27)

$$U^+ = y^+ \qquad 0 \leq y^+ \leq 5$$

$$U^+ = 5 \ln y^+ - 3.05 \qquad 5 \leq y^+ \leq 30$$

$$U^+ = 2.5 \ln y^+ + 5.5 \qquad 30 \leq y^+$$

Reichardt (53)

$$U^+ = 2.5 \ln (1 + 0.4\, y^+) + 7.8 \{1 - \exp(-y^+/11) - (y^+/11) \exp(-0.33\, y^+)\}$$

whole region

Lin, Moulton and Putnam (33)

$$U^+ = \int_0^{y^+} \frac{dy^+}{1 + (y^+/14.5)^3} \qquad 0 \leq y^+ \leq 5$$

$$U^+ = 5 \ln (y^+ + 0.205) - 3.27$$

$$5 \leq y^+ \leq 30$$

Table 4-1 (contd.)

Deissler (7)

$$U^+ = \int_0^{y^+} \frac{dy^+}{1 + n^2 U^+ y^+ \{1 - \exp(-n^2 U^+ y^+)\}}$$

$0 \leqq y^+ \leqq 26$

$$U^+ = \frac{1}{0.36} \ln y^+ + 3.8 \qquad 26 \leqq y^+$$

Rannie (50)

$$U^+ = \frac{1}{0.0688} \tanh (0.0688\, y^+)$$

laminar sublayer and transition region

van Driest (9)

$$U^+ = 2 \int_0^{y^+} \frac{dy^+}{1+\{1+4\kappa^2 (y^+)^2 (1-\exp(-y^+/A))^2\}^{1/2}}$$

whole region

Sleicher (62)

$$U^+ = \frac{1}{0.091} \tan^{-1}(0.091\, y^+)$$

$y^+ < 45$

and constant shear stress,

$$\tau = \tau_w \text{ (const.)} \qquad (4\text{-}2)$$

Hinze (18) deduced the logarithmic velocity distribution as

$$U^+ = \frac{1}{\kappa} \ln y^+ + k \qquad (4\text{-}3)$$

Similar velocity profiles have been deduced from different assumptions by Prandtl (49, 56), von Kármán (27) and others. Thus different values of κ and k are used by different investigators (4, 29, 42, 69), but $\kappa = 0.4$ and $k = 5.5$ are the generally accepted values.

However, this logarithmic velocity distribution law does not hold for the region close to the wall, i.e. $y^+ < 30$, and fails to predict a zero velocity gradient at the axis. In addition, the experimental data are slightly higher than the logarithmic velocity curve near the axis (42, 47).

For the region near the wall, the eddy diffusivity for momentum becomes very small and hence the velocity profile approaches asymptotically to $U^+ = y^+$, that of the laminar flow. Since this equation does not hold for the whole range of $y^+ < 30$, it was desirable to obtain a formula which could connect the laminar sublayer velocity distribution $U^+ = y^+$ continuously and smoothly to the logarithmic velocity distribution, equation (4-3).

Von Kármán (27) proposed a simplified theory by splitting the tube section into three distinct regions. The drawback of his theory is that the eddy diffusivity for momentum in the region $y^+ < 5$ is zero.

Rannie (50) and Sleicher (62) proposed their velocity distributions and corresponding expressions for the eddy diffusivity for momentum, $\varepsilon_M/\nu \propto (y^+)^2$, in the region near the wall.

On the other hand, from considerations of the behavior of the velocity fluctuations in the immediate vicinity of the wall, it is concluded that the eddy diffusivity for momentum must increase at least as the third power of y^+,

as shown by equation (1-52). Reichardt (53), Deissler (7) and van Driest (9) proposed expressions for the eddy diffusivity for momentum near the wall by choosing a function which satisfies the y^3 or y^4 behavior near the wall and asymptotically approaches to the linear dependence on y for large values of y.

The expressions mentioned above successfully predict the velocity profile, but the functions used are somewhat arbitrary and complicated.

The present analysis gives simple and systematic formulas for the eddy diffusivity for momentum which are based on the experimental results available in the literatures, and the universal velocity distribution which in turn results from the distribution of the eddy diffusivity for momentum. In this analysis, the effect of Reynolds number on the eddy diffusivity for momentum is taken into account.

4-2 Distribution of Eddy Diffusivity for Momentum

4-2-1 Previous experimental results

The eddy diffusivity for momentum ε_M may be calculated by equation (1-14) from the velocity profile, or by equation (1-7) from the velocity profile and the turbulent shear stress distribution.

The eddy diffusivities for momentum computed in both these ways are shown in Fig. 4-1, using the experimental results of Laufer (30), Nunner (43) and Reichardt (53). The data of Reichardt were obtained in a two-dimensional channel flow and those of Laufer and Nunner in a circular pipe flow. In this diagram, the half width of the channel, H, is taken as the length scale and the values of $\varepsilon_M/\nu H^+$ are plotted against y^+/H^+. For the circular pipe flow, the radius of the pipe, R, is taken as the length scale instead of the half width of the channel, H.

As inferred from Fig. 4-1, the eddy diffusivity for momentum increases with y^+/H^+, reaches a maximum at about $y^+/H^+ = 0.3 \sim 0.5$, decreases slightly, and then

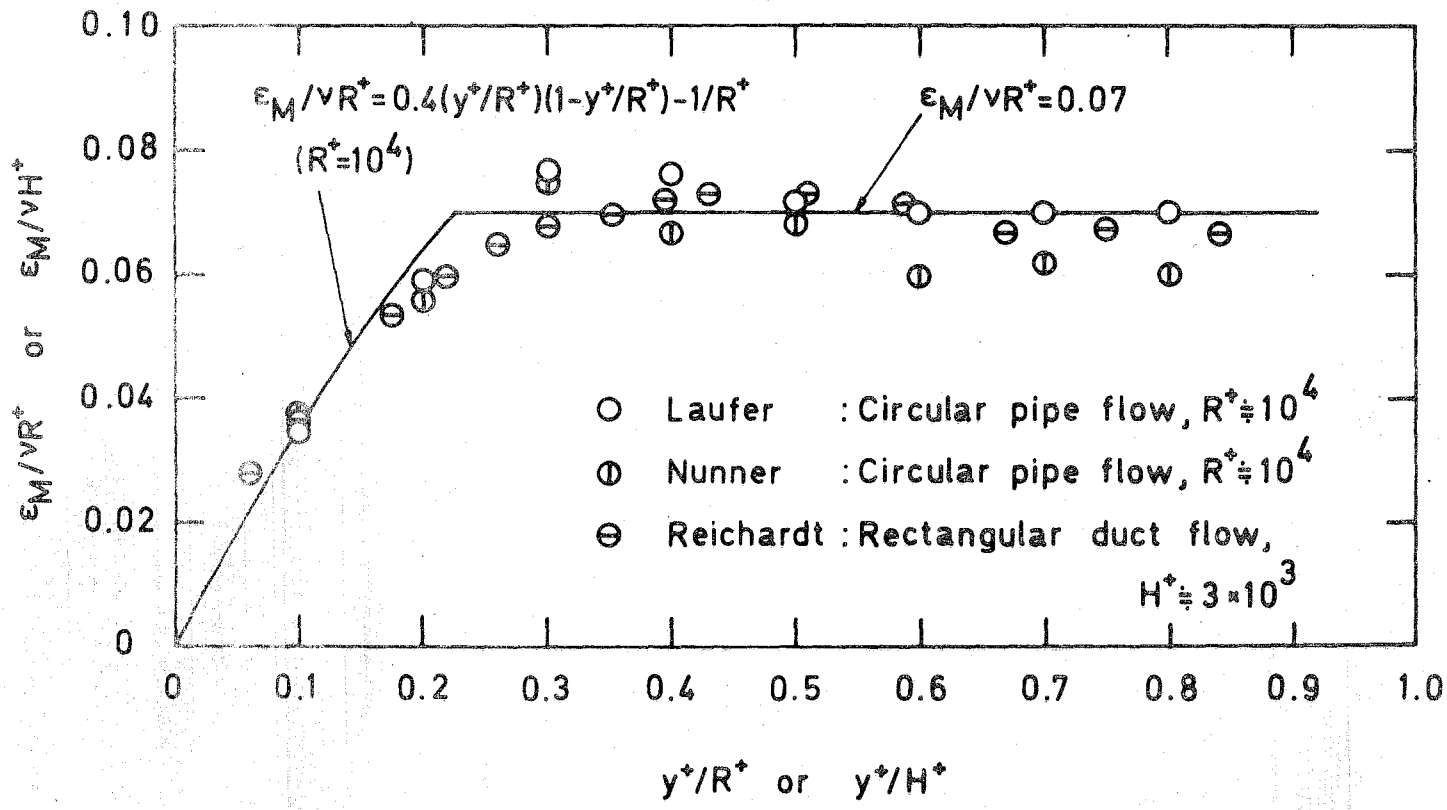

Fig. 4-1 Distributions of eddy diffusivities for momentum in pipe flow and two-dimensional channel flow.

approaches a nearly constant value beyond $y^+/H^+ \doteqdot 0.5$.

The large size of the eddies in the core region, the consequent near-constancy of the integral scale, and the small variation of the turbulence intensity in the central region may explain why the eddy diffusivity for momentum is nearly constant beyond, say, $y^+/H^+ = 0.5$. Therefore, in the present analysis it is assumed that the eddy diffusivity for momentum for the central region is constant, i.e. $\varepsilon_M/\nu H^+ = 0.07$.

Since the flow behavior in the region close to the wall is determined by u_* and ν, the length scale to be used should be ν/u_*. Thus the relation between ε_M/ν and y^+ has to be considered instead of that between $\varepsilon_M/\nu H^+$ and y^+/H^+. For this region, no accurate experimental data are available and it is usually assumed that the eddy diffusivity for momentum is expressed by equation (1-55). According to theory shown in Chapter 1, the value of "a" is three or even higher, but it has not been confirmed experimentally because the measurements were not accurate enough.

However, as shown in Chapter 3, the value of three is obtained for "a" from the experimental results for the eddy diffusivity of heat and the expression for σ. Hence, in the present analysis it is assumed that the exponent of y^+, i.e. "a" in equation (1-55), is 3.

From Fig. 4-1, the variation of the eddy diffusivity for momentum in the region between the constant eddy diffusivity region and y^3-behavior region is expressed by the following equation.

$$\varepsilon_M/\nu = 0.4\, y^+ \left(1 - \frac{y^+}{H^+}\right) - 1 \qquad (4\text{-}4)$$

Substitution of equation (4-4) into equation (1-14) gives exactly the logarithmic velocity distribution, equation (4-3).

4-2-2 Results of the present analysis

From the experimental results mentioned above,

it is assumed that the distribution of the eddy diffusivity for momentum is given by the following equations.

For the region $0 \leqq y^+ \leqq y_1^+$

$$\varepsilon_M/\nu = A\,(y^+)^3 \tag{4-5}$$

For the region $y_1^+ \leqq y^+ \leqq y_2^+$

$$\varepsilon_M/\nu = 0.4\,y^+\left(1 - \frac{y^+}{H^+}\right) - 1 \tag{4-4}$$

For the region $y_2^+ \leqq y^+ \leqq H^+$

$$\varepsilon_M/\nu = 0.07\,H^+ \tag{4-6}$$

To determine the values of A, y_1^+ and y_2^+, the following restrictions are used.

(1) eddy diffusivity for momentum, ε_M/ν, is continuous,

(2) velocity U^+ is continuous,

over the whole range of y^+. These two restrictions may be expressed as follows,

$$A\,(y_1^+)^3 = 0.4\,y_1^+\left(1 - \frac{y_1^+}{H^+}\right) - 1 \qquad (4\text{-}7)$$

$$0.4\,y_2^+\left(1 - \frac{y_2^+}{H^+}\right) - 1 = 0.07\,H^+ \qquad (4\text{-}8)$$

$$\int_0^{y_1^+} \frac{1 - y^+/H^+}{1 + A\,(y^+)^3}\,dy^+ = 2.5 \ln y_1^+ + 5.5 \qquad (4\text{-}9)$$

In equation (4-9) the generally accepted value of the constant for the logarithmic velocity profile, $k = 5.5$, was adopted.

Taking H^+ as a parameter, one can obtain the values of A and y_1^+ simultaneously from equations (4-7) and (4-9). The value of y_2^+ is as follows,

$$y_2^+/H^+ = 0.5\,\{1 - (0.3 - 10/H^+)^{1/2}\} \qquad (4\text{-}10)$$

The results are tabulated in Table 4-2 and plotted in Figs. 4-2 and 4-3 against Reynolds number. The relation

Table 4-2

Values of A , y_1^+ and y_2^+/H^+ or y_2^+/R^+

H^+ or R^+	A x 10^4	y_1^+	y_2^+/H^+ or y_2^+/R^+
100.1	3.674	26.43	0.2763
133.5	4.053	26.42	0.2628
178.0	4.341	26.41	0.2531
237.3	4.560	26.39	0.2461
316.4	4.725	26.38	0.2410
421.9	4.850	26.36	0.2373
562.5	4.943	26.35	0.2343
750.0	5.014	26.34	0.2323
1000	5.067	26.34	0.2307
1519	5.122	26.33	0.2291
2278	5.157	26.33	0.2282
3417	5.180	26.32	0.2275
5126	5.196	26.32	0.2271
7689	5.206	26.32	0.2267
11530	**5.213**	**26.32**	**0.2266**
17300	5.218	26.32	0.2264
25950	5.221	26.32	0.2263
38920	5.223	26.32	0.2263
58390	5.224	26.32	0.2262

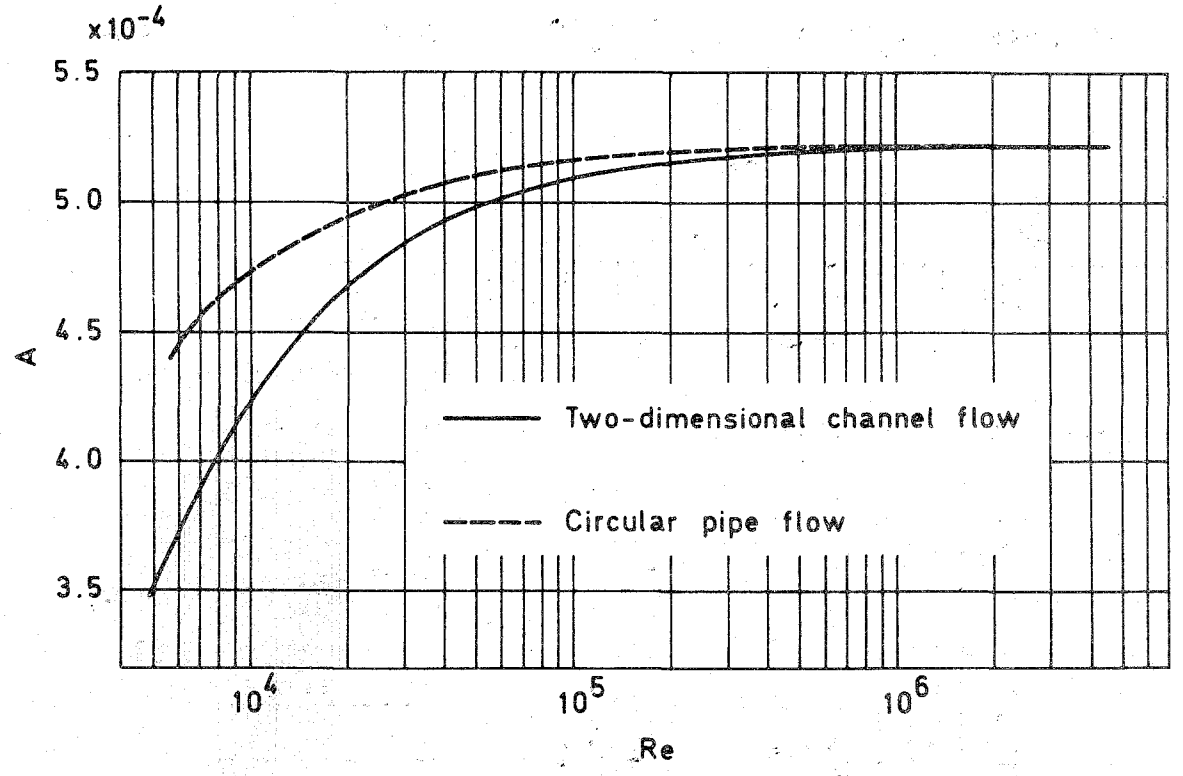

Fig. 4-2 Variation of the coefficient A of the eddy diffusivity for momentum near the wall with Reynolds number.

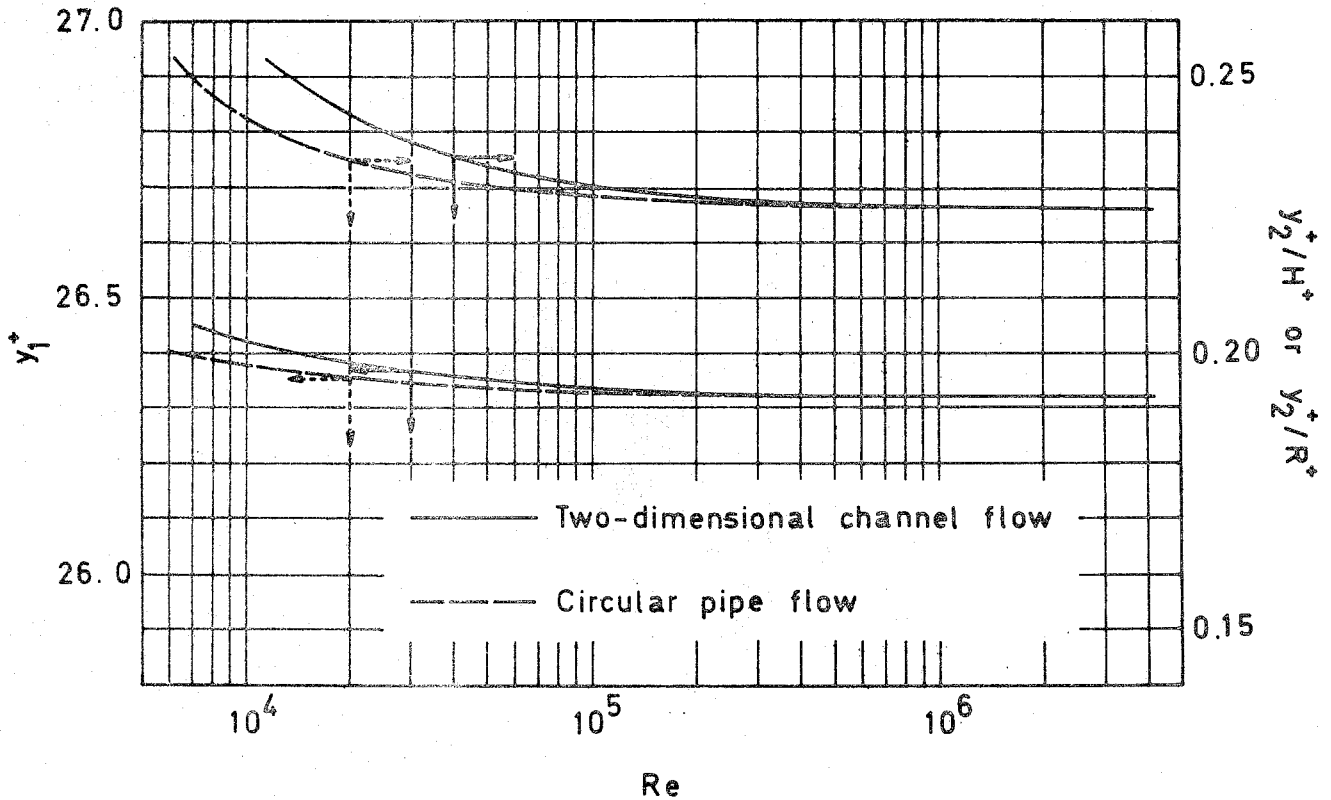

Fig. 4-3 Variation of y_1^+, y_2^+/H^+ or y_2^+/R^+ with Reynolds number.

between H^+ or R^+ and Reynolds number is calculated by equations (4-14) and (4-17) described in a later section. It should be noted that the value of $0.3 - 10/H^+$ is always positive for turbulent flow, i.e. Re > 3,000.

As shown in Fig. 4-2, the value of A and hence the eddy diffusivity for momentum near the wall has a tendency to increase with increasing Reynolds number and attains a constant value 5.22×10^{-4} at very high Reynolds numbers.

As shown in Fig. 4-3, little dependence of the values of y_1^+ and y_2^+/H^+ or y_2^+/R^+ on Reynolds number is observed and their values are about 26.3 and 0.23 respectively.

The variation of the eddy diffusivity for momentum is shown in Fig. 4-4. A similarly shaped distribution curve of the eddy diffusivity for momentum has been observed by Sherwood, Smith and Fowles (60) except in the region close to the wall.

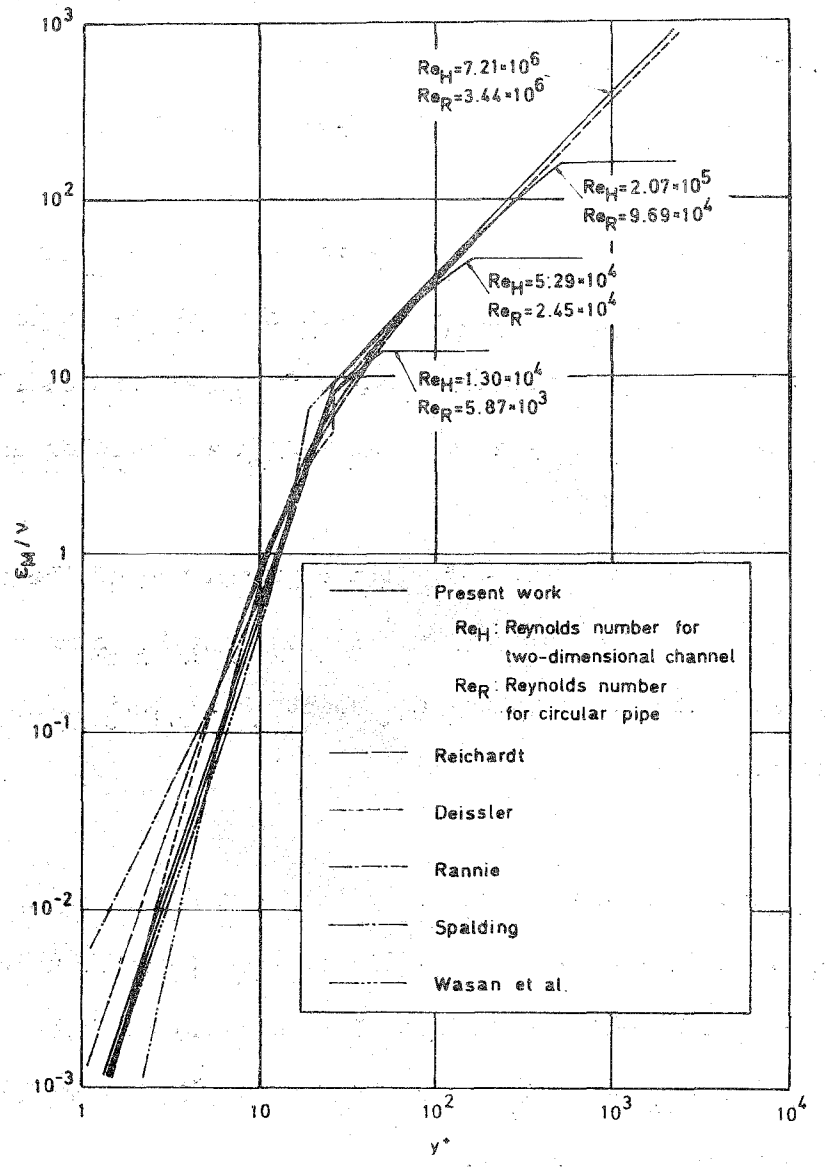

Fig. 4-4 Distribution of the eddy diffusivity for momentum.

4-3 Universal Velocity Profile

Substitution of equations (4-5), (4-4) and (4-6) into equation (1-14) gives the velocity distribution for all parts of the flow, as follows,

$$0 \leq y^+ \leq y_1^+$$

$$U^+ = \frac{A^{-2/3}}{6}\left(A^{1/3} + \frac{1}{H^+}\right) \ln \frac{(y^+ + A^{-1/3})^3}{(y^+)^3 + A^{-1}}$$

$$+ \frac{A^{-2/3}}{(3)^{1/2}}\left(A^{1/3} - \frac{1}{H^+}\right)\left(\tan^{-1} \frac{2\,y^+ - A^{-1/3}}{(3)^{1/2}\,A^{-1/3}}\right.$$

$$\left. + \pi/6\right) \qquad (4\text{-}11)$$

$$y_1^+ \leq y^+ \leq y_2^+$$

$$U^+ = 2.5 \ln y^+ + 5.5 \qquad (4\text{-}12)$$

$$y_2^+ \leq y^+ \leq H^+$$

$$U^+ = \frac{y^+ - y_2^+}{1 + 0.07\ H^+}\left(1 - \frac{y^+ + y_2^+}{2H^+}\right)$$

$$+ 2.5 \ln y_2^+ + 5.5 \qquad (4\text{-}13)$$

The velocity distribution calculated by these equations is shown in Fig. 4-5, which is a similar shape to the distribution curve obtained by Corcoran and Sage (3).

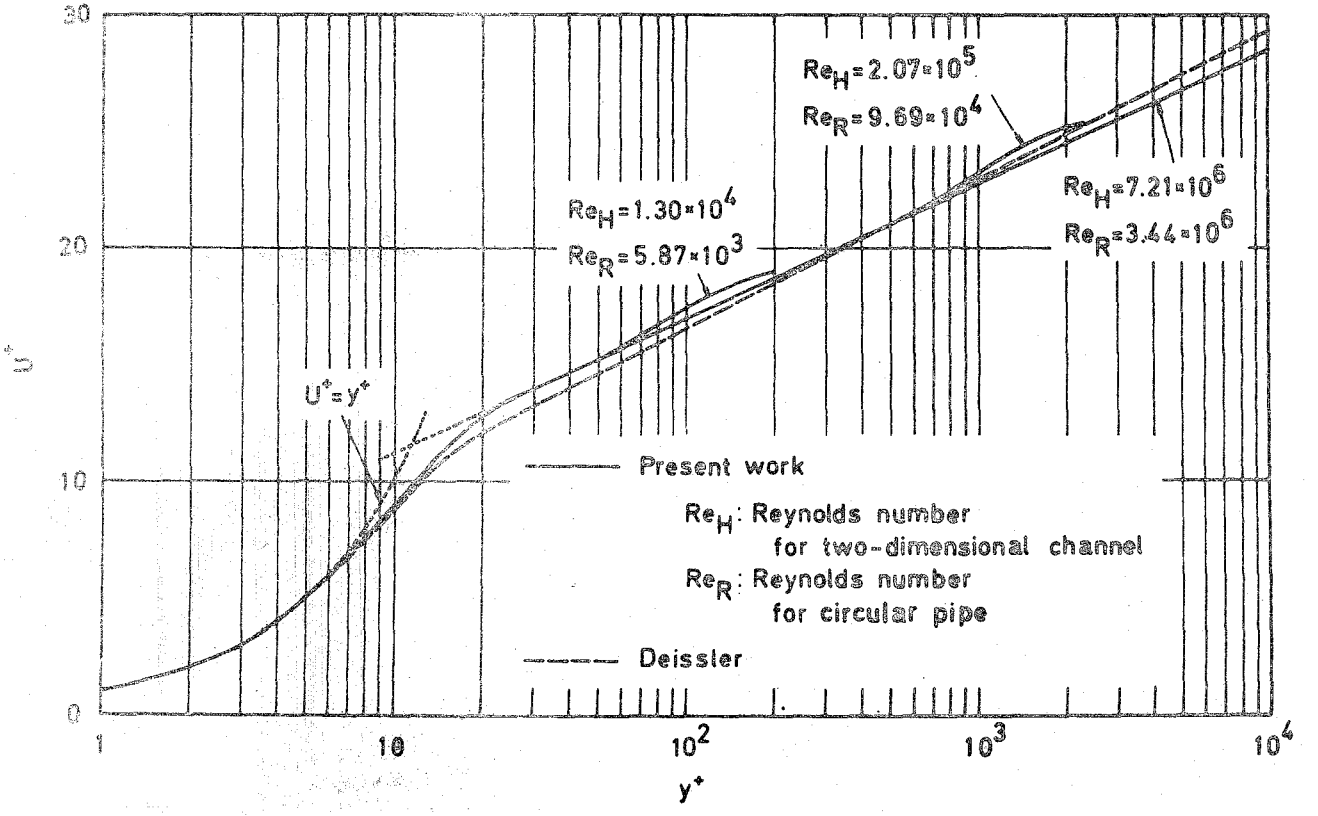

Fig. 4-5 Universal velocity profile.

4-4 Friction Factor

The Reynolds number for a two-dimensional channel flow is usually defined by equation (1-34). From equations (1-16) and (1-34) the relation between H^+ and Reynolds number is given by

$$Re = 4 \int_0^{H^+} U^+ \, dy^+ \qquad (4\text{-}14)$$

The friction factor is calculated by equation (1-17). The calculated relation between H^+, Reynolds number and the friction factor is shown in Table 4-3. The relation between H^+ and Reynolds number is plotted in Fig. 4-6, and the friction factor is plotted against Reynolds number in Fig. 4-7 and compared with the Blasius' formula,

$$f = 0.0791 \, Re^{-1/4} \qquad (4\text{-}15)$$

There is good agreement between analytical relation and Blasius' formula which is derived from the (1/7) - power law of the velocity distribution.

Moreover, the analytical value of the friction factor

Table 4-3

Relation between H^+ (R^+) , Reynolds number and Friction Factor

(A) For Two-Dimensional Channel Flow

H^+	Re	$f \times 10^3$
100.1	5675	9.958
133.5	8050	8.798
178.0	11350	7.873
237.3	15910	7.115
316.4	22230	6.481
421.9	30960	5.941
562.5	43010	5.475
750.0	59600	5.067
1000	82460	4.707
1519	131700	4.253
2278	207000	3.875
3417	324500	3.548
5126	507700	3.261
7689	793000	3.009
11530	1236000	2.785
17300	1925000	2.585
25950	2993000	2.406
38920	4647000	2.245
58390	7207000	2.100

Table 4-3 (contd.)

(B) For Circular Pipe Flow

R^+	Re	$f \times 10^3$
100.1	2484	13.00
133.5	3575	11.15
178.0	5095	9.762
237.3	7209	8.669
316.4	10140	7.787
421.9	14200	7.056
562.5	19830	6.440
750.0	27590	5.912
1000	38300	5.453
1519	61460	4.885
2278	96930	4.419
3417	152400	4.020
5126	239200	3.675
7689	374500	3.373
11530	585200	3.107
17300	913000	2.872
25950	1422000	2.663
38920	2212000	2.477
58390	3437000	2.309

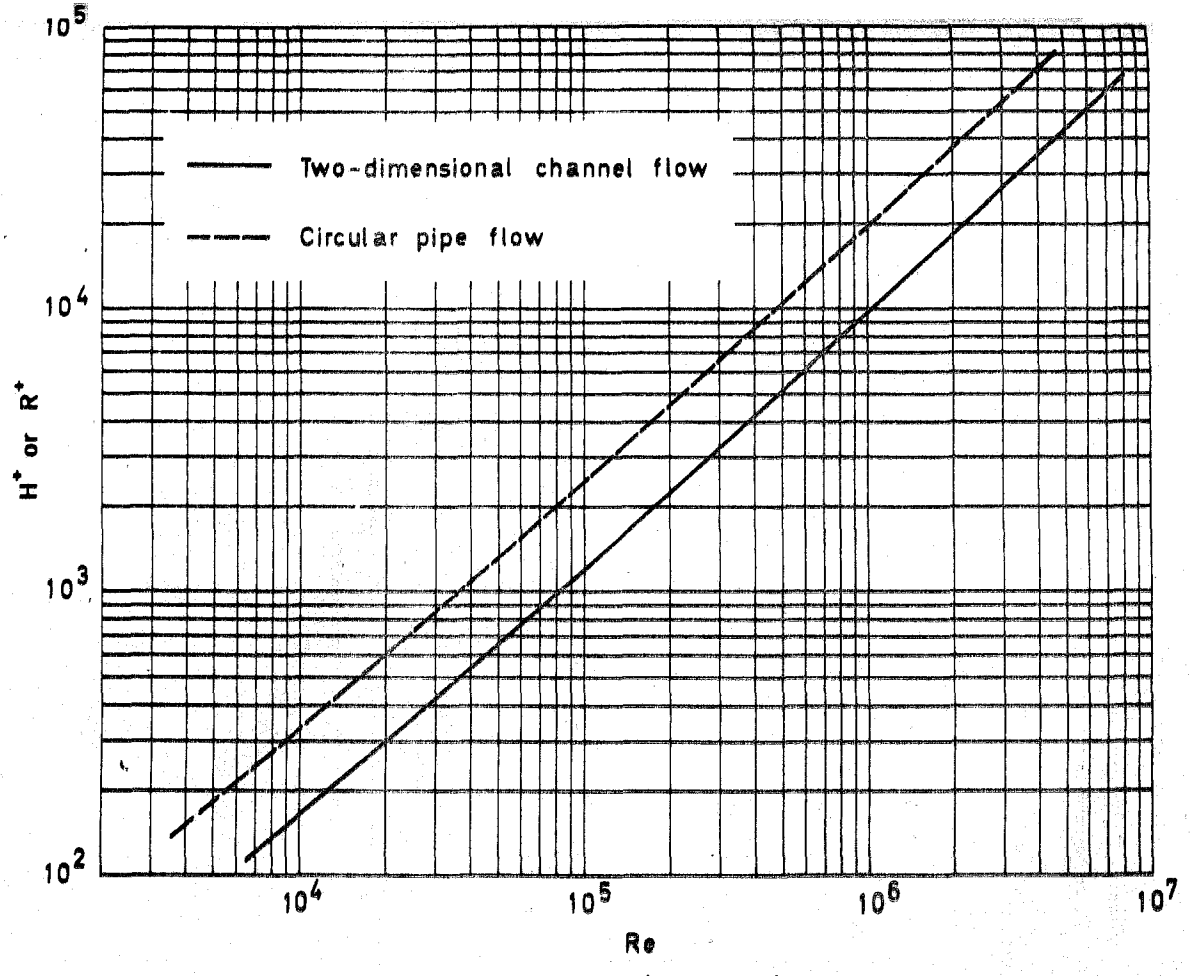

Fig. 4-6 Relation between H^+ or R^+ and Reynolds number.

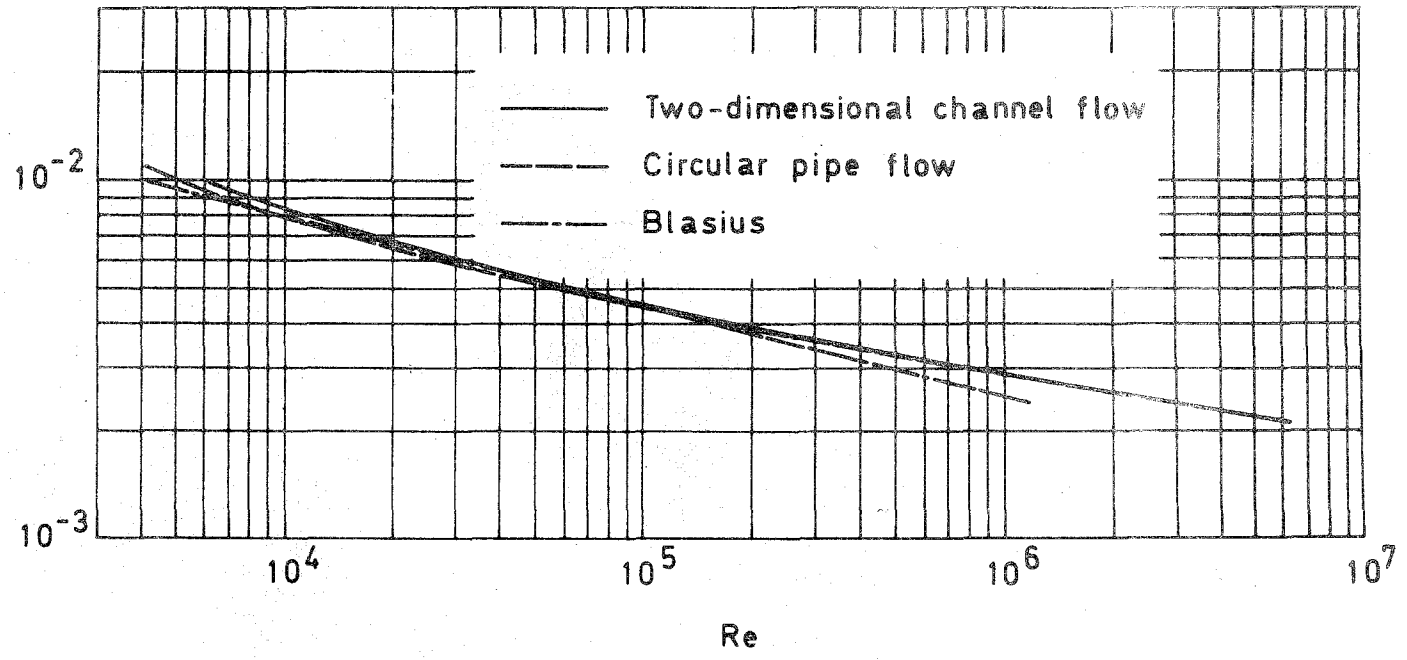

Fig. 4-7 Variation of friction factor with Reynolds number.

is represented precisely by the following equation of Prandtl's universal law of friction (57).

$$1/(f)^{1/2} = 4.0 \log (Re\ (f)^{1/2}) - 0.4 \qquad (4\text{-}16)$$

This equation is derived from the logarithmic velocity distribution law in equation (4-12), adjusting the numerical constants to fit the experimental results.

If the radius of the circular pipe, R , is used instead of the half width of the parallel plates, H , the eddy diffusivity for momentum expressed by equations (4-5), (4-4) and (4-6) may also be used for a circular pipe flow. However, the relation between R^+ and Reynolds number, and hence the relation between friction factor and Reynolds number, are different from the previous expressions (4-14) and (1-17).

The Reynolds number for circular pipe flow is defined by equation (1-37). Hence the relation between R^+ and Reynolds number is given by

$$Re = 4 \int_0^{R^+} U^+ \left(1 - \frac{y^+}{R^+}\right) dy^+ \qquad (4\text{-}17)$$

The friction factor is expressed by equation (1-19). The calculated results of R^+ and the friction factor vs. Reynolds numbers are also plotted in Figs. 4-6 and 4-7 respectively, along with those for the two-dimensional channel flow. Although there is a slight difference between the friction factors for the two-dimensional channel flow and for the circular pipe flow, good agreement between the theoretical results and Blasius' formula is observed.

4-5 Conclusion

1. Simple and systematic formulas for the eddy diffusivity for momentum in a two-dimensional channel flow are as follows

$$0 \leqq y^+ \leqq y_1^+$$

$$\varepsilon_M/\nu = A\,(y^+)^3$$

$$y_1^+ \leqq y^+ \leqq y_2^+$$

$$\varepsilon_M/\nu = 0.4\, y^+ \left(1 - \frac{y^+}{H^+}\right) - 1$$

$$y_2^+ \leqq y^+ \leqq H^+$$

$$\varepsilon_M/\nu = 0.07\, H^+$$

For a circular pipe flow H^+ must be replaced by R^+.

2. The eddy diffusivity for momentum expressed by these formulas depends not only on y^+, but also on Reynolds number.

3. The universal velocity distribution was obtained from the eddy diffusivity distribution for all parts of the flow (see equation (4-11), (4-12) and (4-13)).

4. The friction factor based on the universal velocity profile is in good agreement with Blasius' formula which is derived from the (1/7) - power law of the velocity distribution, not only for the circular pipe but also for the two-dimensional channel flow. Moreover, the analytical value of the friction factor is represented precisely by Prandtl's universal law of friction.

CHAPTER 5

HEAT OR MASS TRANSFER RATE AT LARGE PRANDTL OR SCHMIDT NUMBERS

In Chapter 1, the previous theoretical attempts to obtain expressions for the Nusselt number were reviewed briefly. However, experimental data on heat or mass transfer to fluids at large Prandtl or Schmidt numbers indicate that transfer rates are higher than those predicted by these theories. Discrepancies between the experimental results and the predictions at large Prandtl or Schmidt numbers are principally caused by the expressions used for the eddy diffusivity in the region close to the wall.

The distribution of the eddy diffusivity for heat or mass can now be evaluated by using the expressions for σ and the eddy diffusivity for momentum given in Chapter 3

and 4 respectively. The Nusselt and Sherwood numbers may then be calculated by substitution of these values of the eddy diffusivities for heat or mass into equations (1-28) and (1-29).

5-1 Comparison between the Calculated and Measured Values of Eddy Diffusivities for Heat and Mass

Using the expressions for the eddy diffusivity for momentum, i.e. equations (4-5), (4-4) and (4-6), the numerical values of α_1 and α_2 in equations (3-33) and (3-38) were computed to fit the experimental results of ε_H/ν given in Chapter 2. Thus, finally, the following equations were obtained.

$$\varepsilon_H/\nu = (\varepsilon_M/\nu)\ \phi_H\ \{1 - \exp(-1/\phi_H)\} \qquad (5\text{-}1)$$

$$y^+ \leqq y_\phi^+$$

$$\phi_H = \frac{0.0279\ Pr\ (\varepsilon_M/\nu)^{1/3}}{1 + 0.228\ Pr^{1/3}\ (\varepsilon_M/\nu)^{1/3}} \qquad (5\text{-}2)$$

$$y^+ \geqq y_\phi^+$$

$$\phi_H = \frac{0.00681\ Pr\ (\varepsilon_M/\nu)}{1 + 0.160\ Pr^{1/3}\ (\varepsilon_M/\nu)^{1/2}} \qquad (5\text{-}3)$$

The values of y_ϕ^+ at which the values of ϕ_H calculated

by equations (5-2) and (5-3) are equal each other are nearly constant at about 25 at large Prandtl and Reynolds numbers.

It should be noted that the eddy diffusivity for heat in the region close to the wall is a function of the Reynolds number because the eddy diffusivity for momentum in this region is a function of the Reynolds number as shown in Fig. 4-2.

If the mechanisms for eddy diffusion of heat and mass are assumed to be analogous, equations (5-1), (5-2) and (5-3) are applicable to mass transfer by using ε_D and Sc instead of ε_H and Pr.

The predictions of equations (5-1), (5-2) and (5-3), the experimental correlations (2-22), (2-23) and (2-24) for ε_H/ν, and ε_D/ν by Lin, Moulton and Putnam (33) and Son and Hanratty (63) are plotted in Fig. 5-1.

There is fairly good agreement between the predictions and experimental results not only for ε_H/ν but also for ε_D/ν. Though there should be a difference between

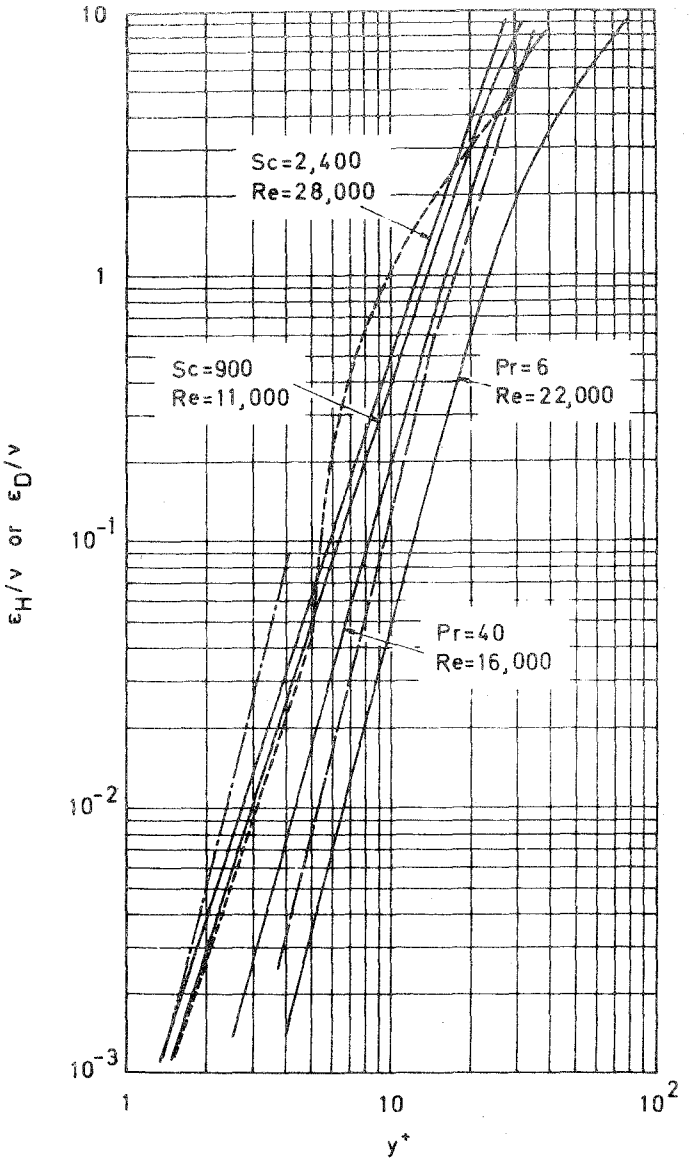

Fig. 5-1 Comparison of experimental data with predictions of eddy diffusivity for heat and mass.

——— Predictions , ——— Experimental correlation (ε_H/ν) , --------- Lin et al. (ε_D/ν, Sc=900) , ——— Son et al. (ε_D/ν, Sc=2,400).

Pr = 6 and 40 in the predictions of ε_H/ν, no dependence of the experimental values of ε_H/ν on Prandtl number could be observed. This may be due to experimental errors as described in Chapter 2.

5-2 Predicted Nusselt and Sherwood Number

Temperature and concentration distributions calculated from equations (1-24) and (1-25) are presented in Fig. 5-2. The curves indicate that the temperature and concentration distributions are flat over most of the tube section at large Prandtl or Schmidt numbers.

The relation between Nusselt, Reynolds and Prandtl numbers or Sherwood, Reynolds and Schmidt numbers can be obtained from equations (1-30) and (1-31). Predicted Nusselt or Sherwood numbers are plotted against Reynolds number for various values of Prandtl or Schmidt numbers in Fig. 5-3. From these calculations, no difference was found between the Nusselt or Sherwood numbers for a two-dimensional channel flow and for a circular pipe flow if the Reynolds numbers defined by equations (1-34) and (1-37) respectively are used.

A comparison of various analyses is given in Fig. 5-4. At large Prandtl or Schmidt numbers, the present analysis and the analysis of Lin et al. are in fair agreement, whereas other analyses diverge considerably. As inferred

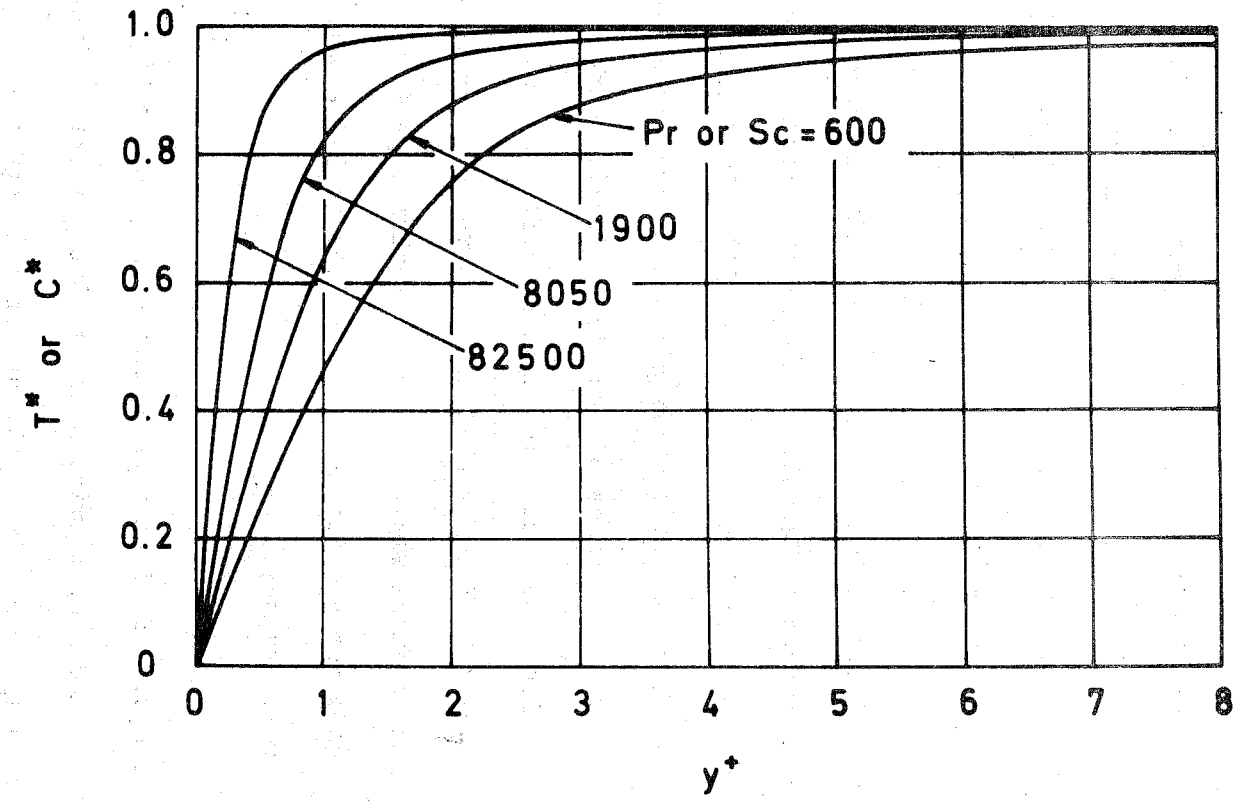

Fig. 5-2 Temperature or concentration distributions at large Prandtl or Schmidt numbers and at $Re = 10^4$.

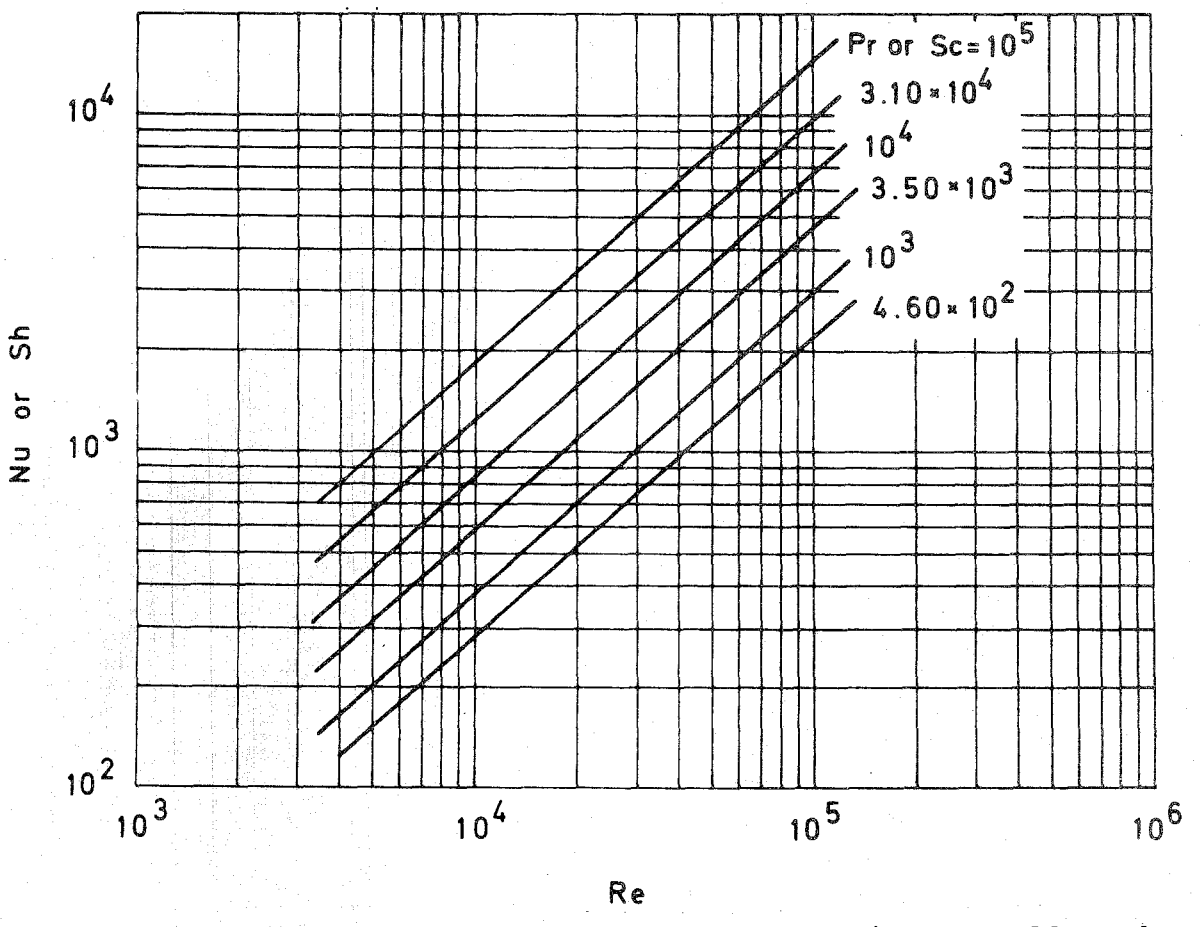

Fig. 5-3 Fully developed Nusselt or Sherwood number against Reynolds number for various Prandtl or Schmidt numbers.

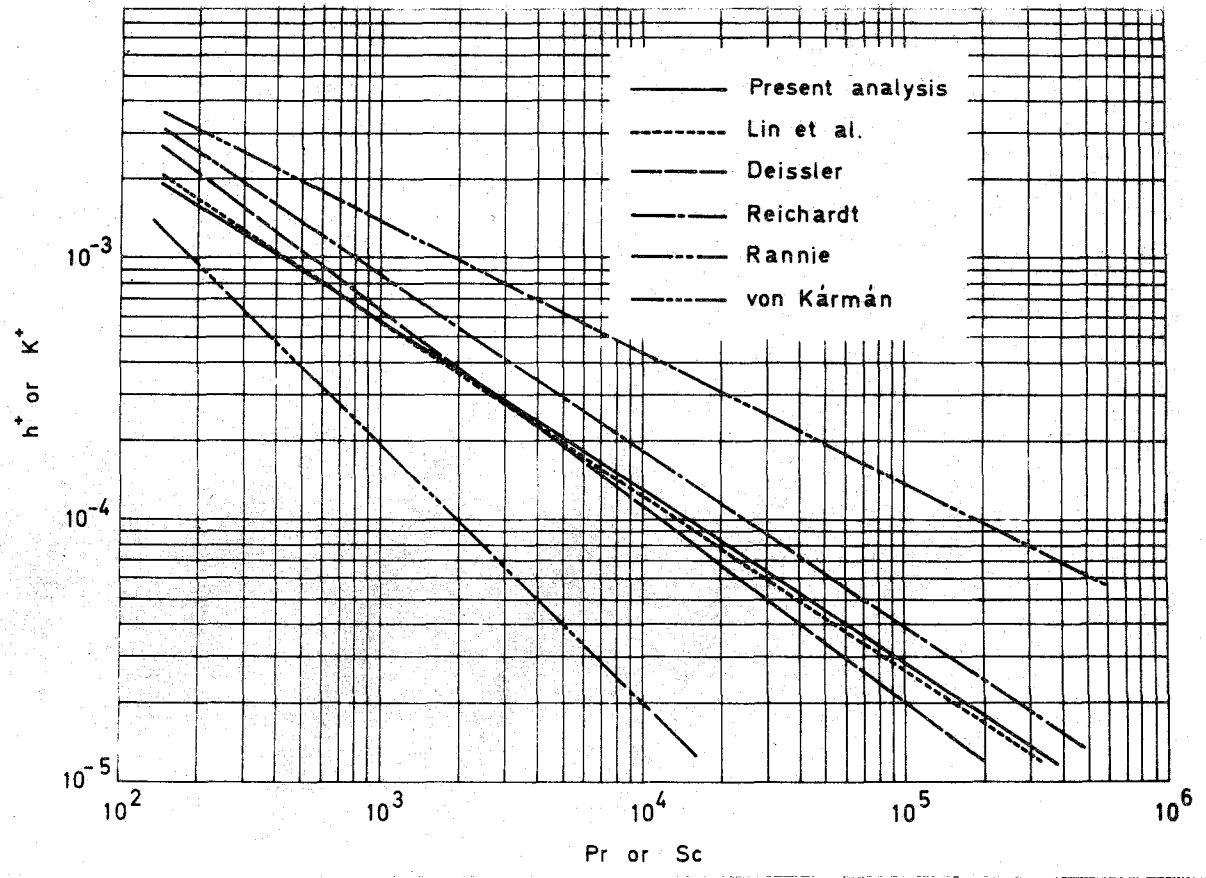

Fig. 5-4 Comparison of various analyses at Re = 10^4

from Fig. 5-4, the calculated value of h^+ varies with $Pr^{-2/3}$, i.e. $Nu \propto Pr^{1/3}$ at large Prandtl numbers.

Experimental data on heat or mass transfer rates at large Prandtl or Schmidt numbers are particularly scarce and fragmentary.

Friend and Metzner (12) performed their heat transfer experiments in the range of $Pr = 50 \sim 600$. Linton and Sherwood (35), Meyerink and Friedlander (38) and Harriott and Hamilton (15) measured the mass transfer rates of a substance which dissolves from the wall of a pipe into turbulently flowing fluid. Linton et al. performed their experiments at Schmidt numbers from 1,000 to 3,000, Meyerink et al. at $Sc = 300$ and 900, and Harriott et al. at $Sc = 900 \sim 10^5$. Recently Hubbard and Lightfoot (20) used an electrochemical method to obtain the mass transfer rates at Schmidt numbers from 1,700 to 30,000.

However, most of these experimental results are too scattered and different from each other to determine the effect of the Prandtl or Schmidt number on the transfer rates. Since the differences in Nusselt or Sherwood

numbers predicted by the various analyses are not so large, as shown in Fig. 5-4, highly accurate measurements are required to determine the relationship between Nu, Re and Pr or Sh, Re and Sc.

In the following sections, the experimental study performed to compare the experimental data with the present analysis will be given. The technique chosen was measurement of the limiting current at a completely polarized electrode.

5-3 Experimental Method

The process chosen for this study was reduction of ferricyanide ions at a nickel cathode in the presence of a large excess of sodium or potassium hydroxide,

$$Fe(CN)_6^{3-} + e^- \rightarrow Fe(CN)_6^{4-}$$

This system has been used with good results by many previous investigators (10,32) and offers a number of important advantages.

First, the electrochemical reaction, involving only an electron transfer, is very rapid and so nearly complete concentration polarization is obtained, even at high mass transfer rates. This is evidenced by the shape of the polarization curves, of which Fig. 5-5 is a representative sample.

Second, competing reactions can be almost completely avoided. The only important competing reaction that may be encountered here is reduction of the dissolved oxygen,

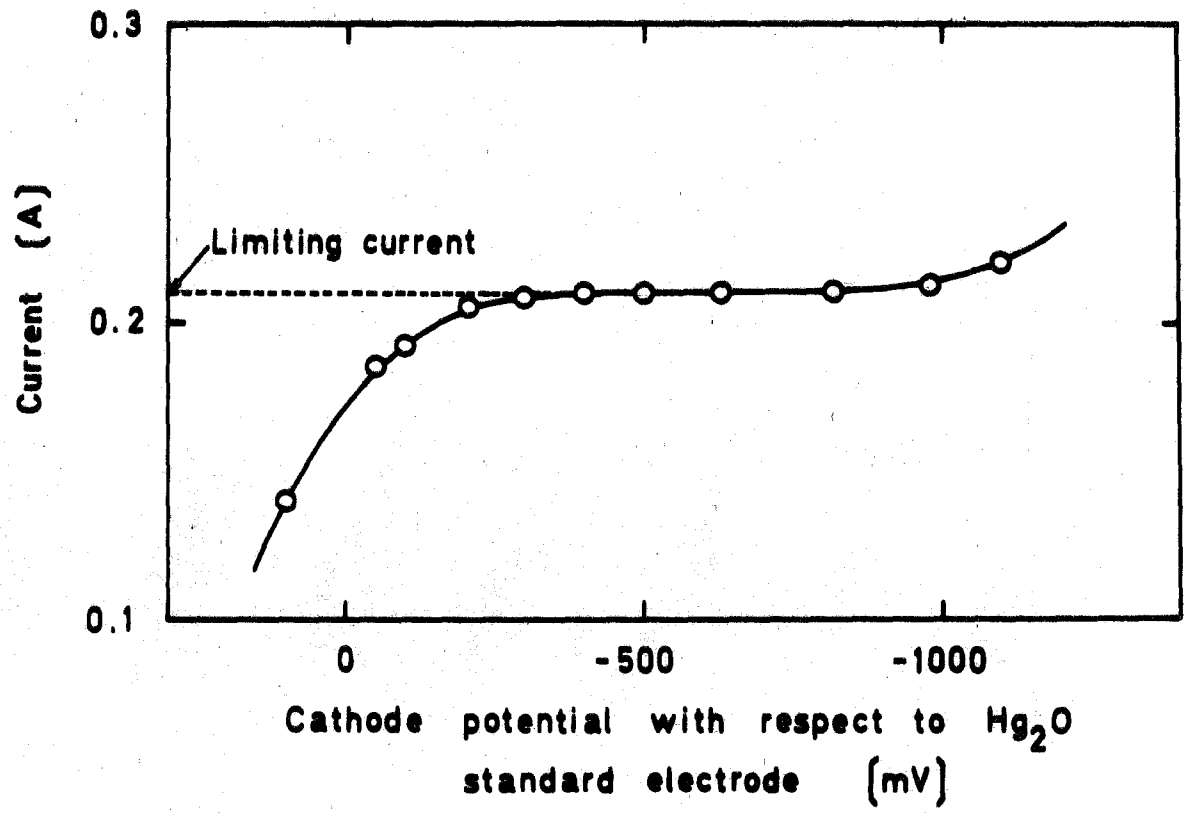

Fig. 5-5 Typical polarization curve.

but this is easily avoided by continuous purging with nitrogen gas.

Finally, the most significant advantage is that surface roughness can be kept very small compared with the dissolving wall method. This is particularly important at large Schmidt numbers because the surface roughness influences the mass transfer rate significantly in that case.

The experiments were performed in a rectangular duct of polyvinyl chloride, 5 mm by 50 mm cross section and 2 m long. The three nickel cathodes, 398, 201 and 52 mm long and 20 mm wide, were mounted in series, flush with the upper surface in the center of the duct. The anode, 2 m long and 50 mm wide, was mounted on the lower surface of the duct.

The cathodes were made narrower than the anode to ensure that the limiting current occured at the cathode rather than at the anode, and to eliminate any effects of flow disturbance in the corners of the duct. The cross section of the duct is shown in Fig. 5-6.

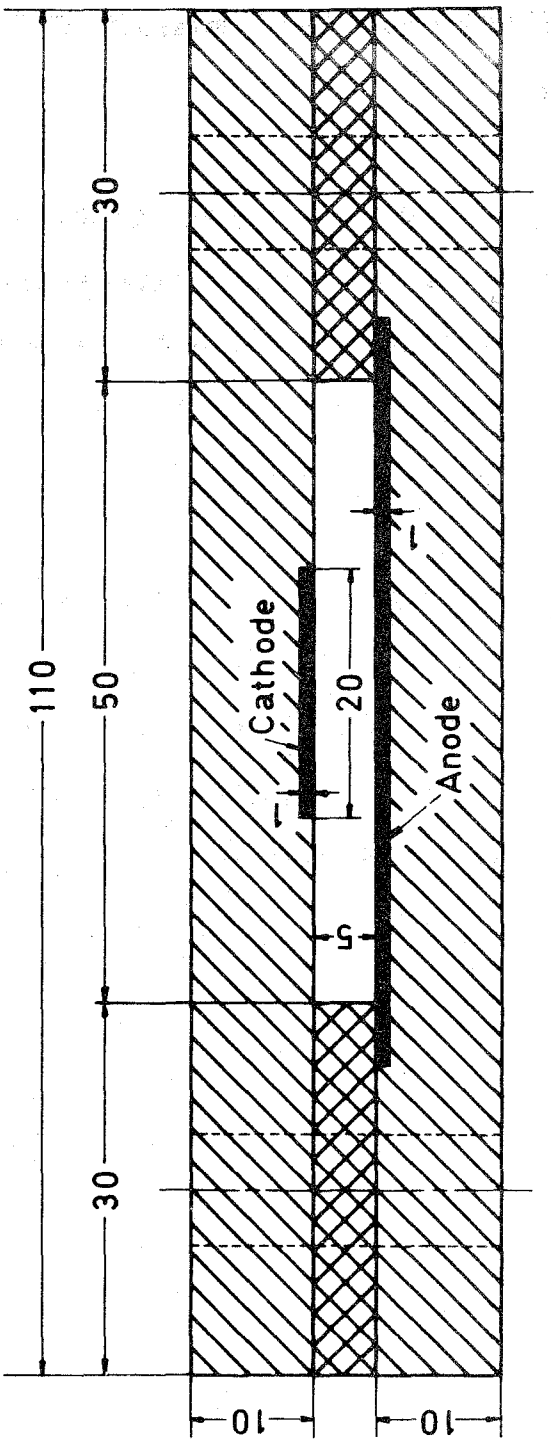

Fig. 5-6 Cross section of the duct.

The inlet length required to achieve a fully developed velocity profile at the cathode (mass transfer section) was about 100 times the equivalent diameter of the duct.

When a fluid in a fully developed velocity profile enters a mass transfer section, the local value of the mass transfer coefficient decreases from infinity at the inlet to a minimum value, which is the fully developed value, downstream.

Schütz (58) measured the local transfer rate in the mass tranfer entry region at Sc = 2,170. In Fig. 5-7, his results are plotted and compared with the curve of prediction calculated numerically using equations (1-3), (1-6) and (1-9) and the eddy diffusivity of the present analysis.

As may be seen from Fig. 5-7, the entry length required to obtain the fully developed mass transfer coefficient is about $x^+ \approx 10^4$ at Sc = 2,170. This value decreases with increasing Schmidt number.

Therefore, in this experiment the measurement of mass

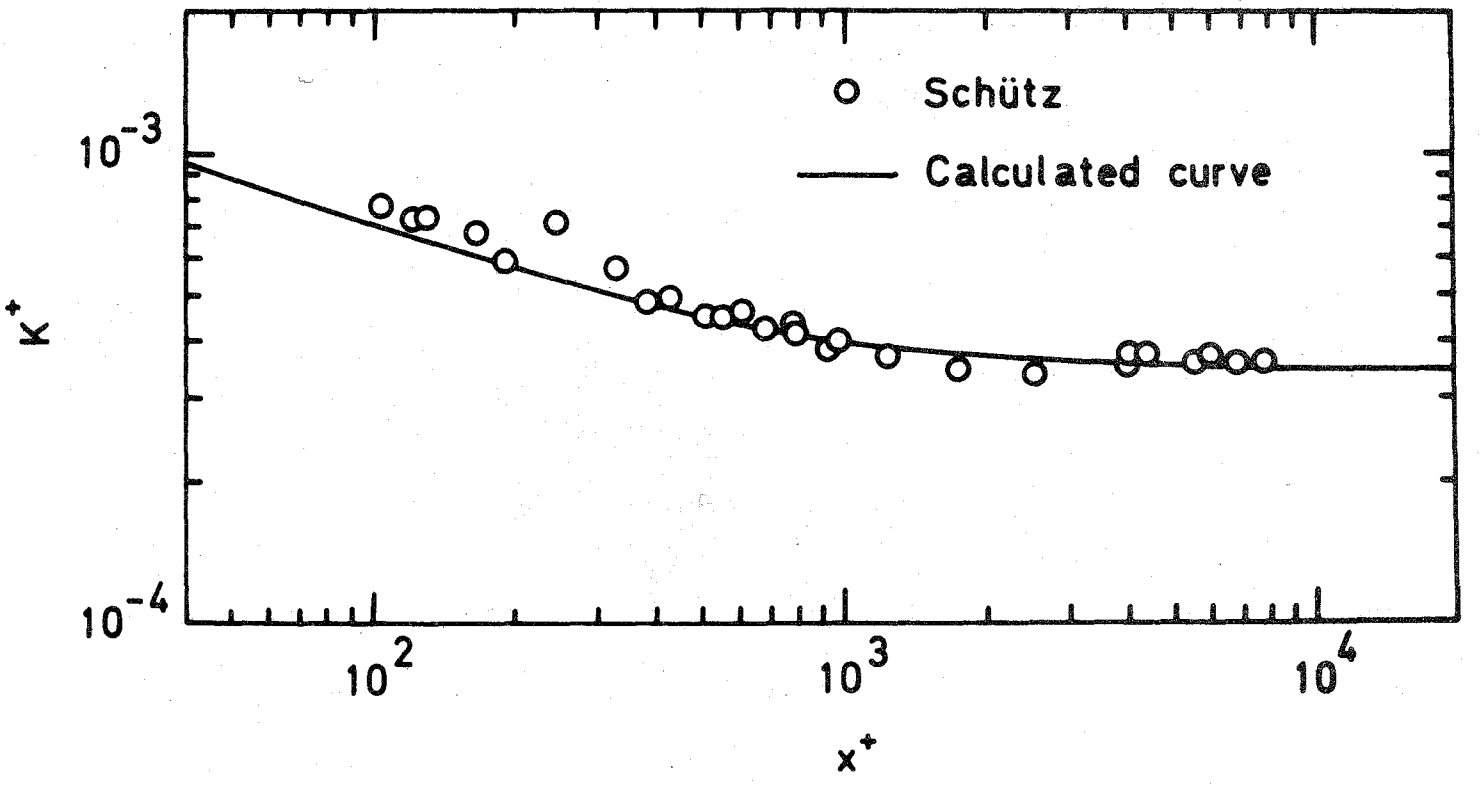

Fig. 5-7 Variation of the local mass transfer rate in the mass transfer entry region at Sc = 2,170.

transfer rates was made by a cathode 201 mm long, located downstream of a 398 mm long cathode. Thus the entry length for developing the concentration profile was $x^+ > 10^4$ in the range of the experiment, so the measured mass transfer coefficient may be considered to be a fully developed one.

The electrolyte solution was recirculated through the duct by means of a polyvinyl chloride pump. To prevent the circulating fluid from becoming contaminated, vinyl chloride plastic valves and pipes were used throughout the system. The experimental apparatus is shown schematically in Fig. 5-8.

The solution used contained $0.001 \sim 0.01$ mole of $K_3Fe(CN)_6$ and $K_4Fe(CN)_6$ and $0.1 \sim 5.0$ moles of KOH or NaOH per liter. The concentration of ferricyanide ions at the cathode surface can be assumed to be zero at the limiting current and the bulk concentration was measured with an iodometric titration.

The mass transfer coefficient is calculated by the following equation.

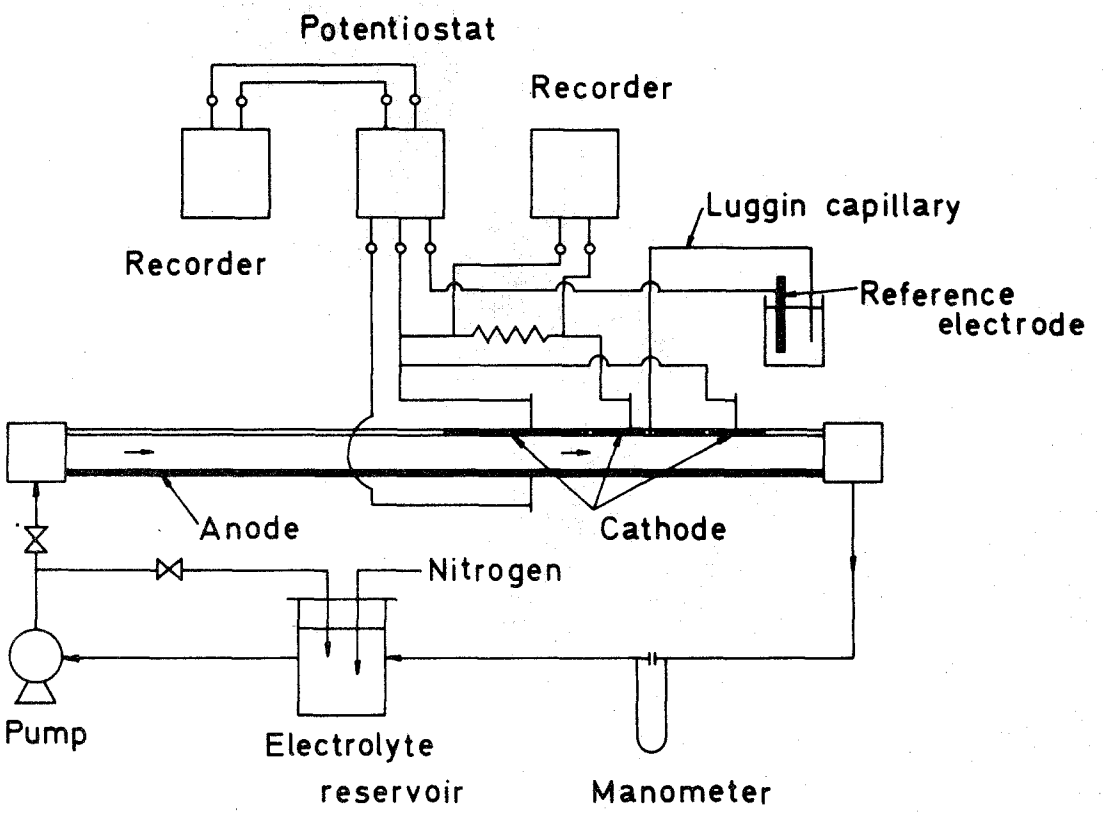

Fig. 5-8 Schematic diagram of the apparatus.

$$K = i/FC_b \qquad (5\text{-}4)$$

where i is the limiting current density and F the Faraday constant. Several assumptions are implicit in this equation;

(1) Concentration polarization is complete. This was confirmed by the shapes of the experimental polarization curves.

(2) The current is due solely to reduction of ferricyanide ions. This was assured by purging with nitrogen before each run and keeping the electrolyte under a nitrogen atmosphere during the runs.

(3) Mass transfer occurs only by molecular and eddy diffusion. This was ensured by the very high concentration of the indifferent electrolyte relative to that of the ferricyanide.

The Reynolds and Schmidt numbers were varied from 3,000 to 80,000 and 800 to 15,000 , respectively. The flow rates were measured with a calibrated orifice.

5-4 Experimental Results

The experimental results are summarized in Table 5-1. The variation of K^+ with Re are plotted in Fig. 5-9 for various values of Sc , and compared with the predicted values. The predicted values of K^+ have a tendency to decrease with decresing Reynolds numbers because of the dependence of ε_M/ν on Re , and are in reasonable agreement with the measured values. This tendency of K^+ vs. Re has been suggested also by Lawn (31). On the other hand, experimental data for K^+ at Sc = 2,400 by Shaw and Hanratty (59) shows that K^+ is independent of the Reynolds number. This is probably due to the inaccuracy of their measurements.

The variations of K^+ with Re are so small that the averaged values of the measured K^+ at various Reynolds numbers are plotted against Schmidt number in Fig. 5-10. For comparison with the predictions of the present analysis, that of Deissler (7), and of Lin et al. (33), the experimental data of Harriott and Hamilton (15) and Hubbard and Lightfoot (20) are also plotted in Fig. 5-10.

Table 5-1

Experimental Results of Mass Transfer Coefficients

Sc = 631

Re	Sh	$K^+ \times 10^4$
32,500	638	7.40

Sc = 782

Re	Sh	$K^+ \times 10^4$
14,600	465	6.77
17,500	552	6.85
20,800	681	7.26
24,900	810	7.39
30,400	960	7.35
36,800	1,130	7.31
44,200	1,310	7.23
49,900	1,450	7.25
54,900	1,550	7.09
60,600	1,700	7.16
66,200	1,850	7.15
82,400	2,230	7.14

Table 5-1 (contd.)

Sc = 981

Re	Sh	$K^+ \times 10^4$
36,000	891	6.27

Sc = 1,200

Re	Sh	$K^+ \times 10^4$
22,000	669	5.08

Sc = 1,500

Re	Sh	$K^+ \times 10^4$
9,310	399	4.49
10,100	456	4.77
11,400	490	4.65
12,600	538	4.68
14,300	594	4.62
17,300	709	4.66
19,300	770	4.61
22,000	850	4.52
25,400	960	4.56

Table 5-1 (contd.)

Sc = 2,390

Re	Sh	$K^+ \times 10^4$
5,630	310	3.42
6,080	317	3.27
7,320	374	3.28
8,600	444	3.38
10,200	506	3.31
13,200	631	3.30
14,500	685	3.30
15,900	748	3.33
20,200	919	3.32
26,800	1,170	3.28
35,600	1,500	3.22
41,000	1,790	3.48
44,800	1,820	3.17
57,400	2,180	3.16

Table 5-1 (contd.)

Sc = 3,600

Re	Sh	$K^+ \times 10^4$
5,760	359	2.52
6,090	387	2.56
6,760	426	2.67
8,830	523	2.60
10,200	623	2.68
12,400	730	2.68
15,000	859	2.68
17,600	984	2.67
20,200	1,110	2.68
23,200	1,270	2.70
27,500	1,470	2.70
36,000	1,860	2.64
44,000	2,210	2.65

Table 5-1 (contd.)

Sc = 5,480

Re	Sh	$K^+ \times 10^4$
4,520	332	1.93
5,500	396	1.93
6,620	459	1.91
7,900	539	1.92
9,420	642	1.96
10,900	728	1.95
12,600	819	1.93
13,400	883	1.99
15,600	1,020	1.99
18,400	1,170	1.98
24,000	1,490	2.00

Table 5-1 (contd.)

Sc = 9,170

Re	Sh	$K^+ \times 10^4$
5,050	411	1.30
5,450	432	1.27
6,460	514	1.31
7,470	613	1.37
8,440	683	1.37
10,400	848	1.42
12,700	1,030	1.44
14,700	1,160	1.44
17,700	1,370	1.44
22,500	1,720	1.46

Table 5-1 (contd.)

Sc = 15,100

Re	Sh	$K^+ \times 10^4$
3,570	377	0.980
3,800	403	0.990
4,600	478	0.994
5,280	535	0.988
6,200	616	0.987
7,200	723	1.02
7,950	785	1.01
8,960	884	1.03
10,100	993	1.04
12,300	1,170	1.02
14,000	1,320	1.04
15,500	1,470	1.05

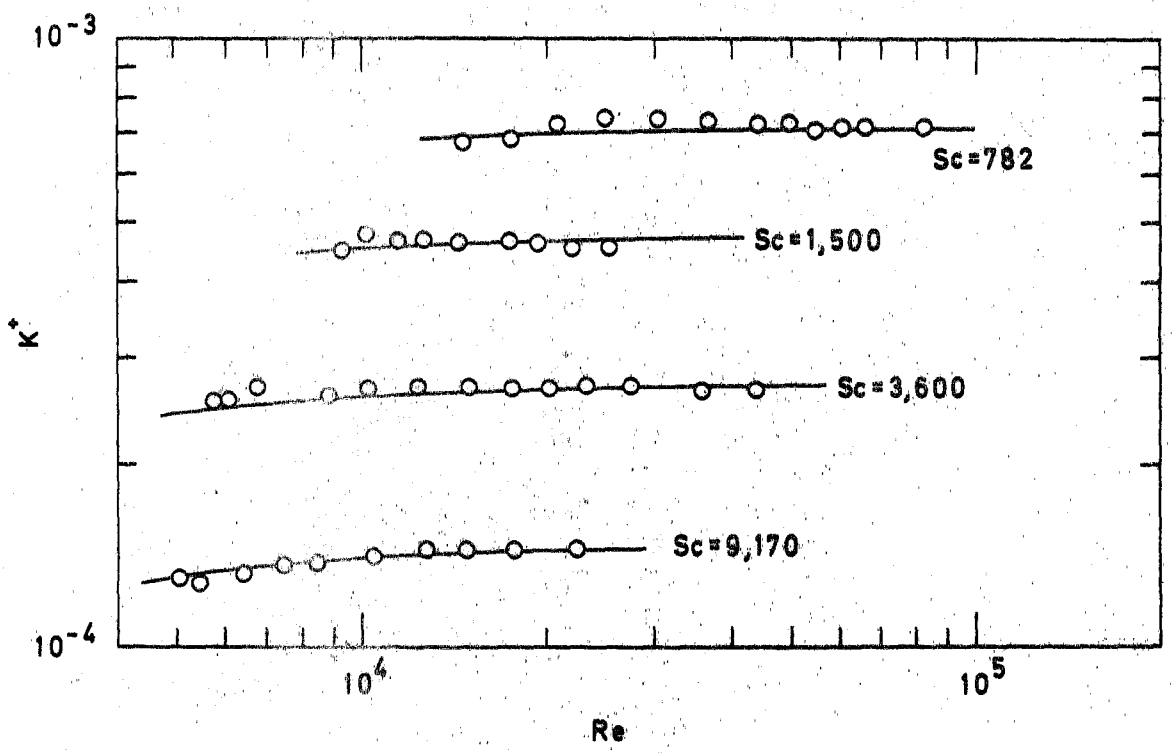

Fig. 5-9 Variation of K^+ with Reynolds number.

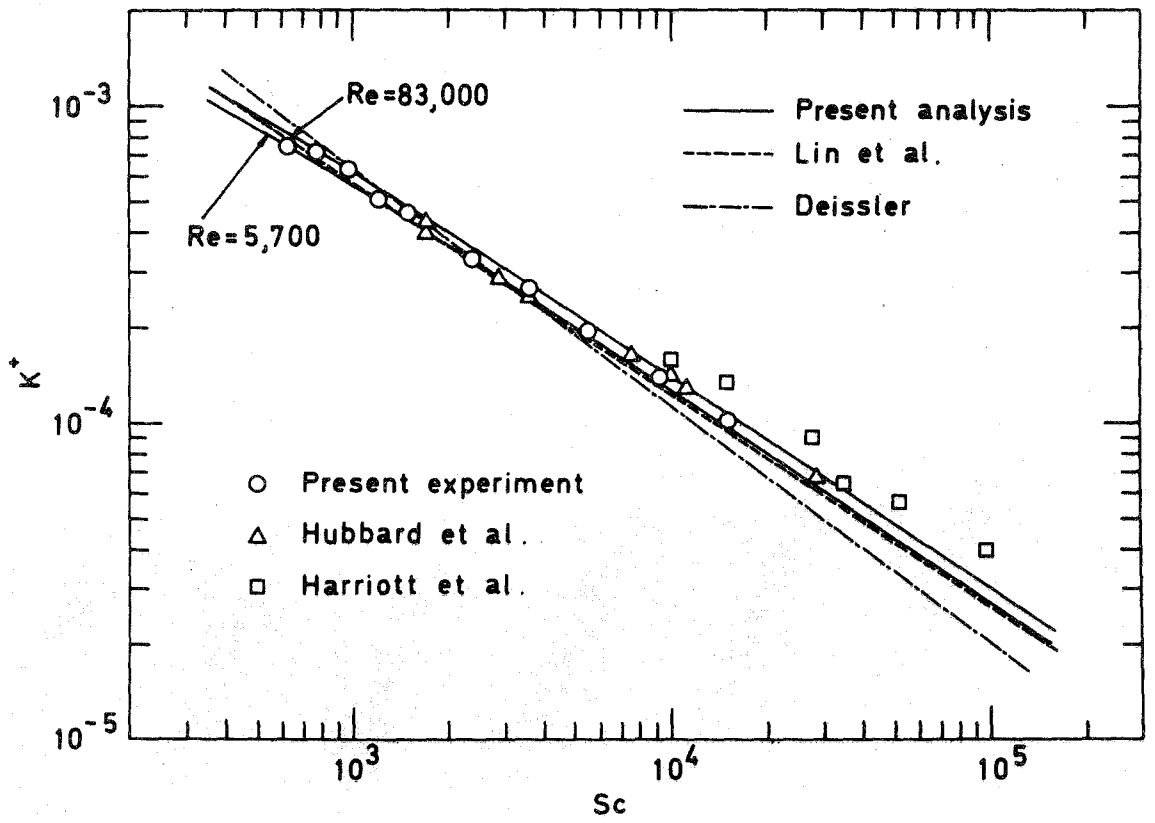

Fig. 5-10 Variation of K^+ with Schmidt number.

The predictions of the author represent the experimental results of the author and Hubbard et al. quite well and are in good agreement with the prediction of Lin et al., but in poor agreement with that of Deissler. The experimental results of Harriott et al. are slightly greater than the present prediction, probably because of the effect of the surface roughness.

The experimental results at Schmidt numbers of 15,100 and 782 are plotted as the Sherwood number versus the Reynolds number in Fig. 5-11, and compared with the present prediction, the equation of Sieder and Tate (61), the analogy of Chilton and Colburn (2), and the prediction of Deissler.

The experimental data shows that the Sherwood number varies with about the 0.9 power of the Reynolds number at large Schmidt numbers, in reasonable agreement with the present prediction. It also appears from Fig. 5-11 that the other three predictions apparently fail to represent the experimental results.

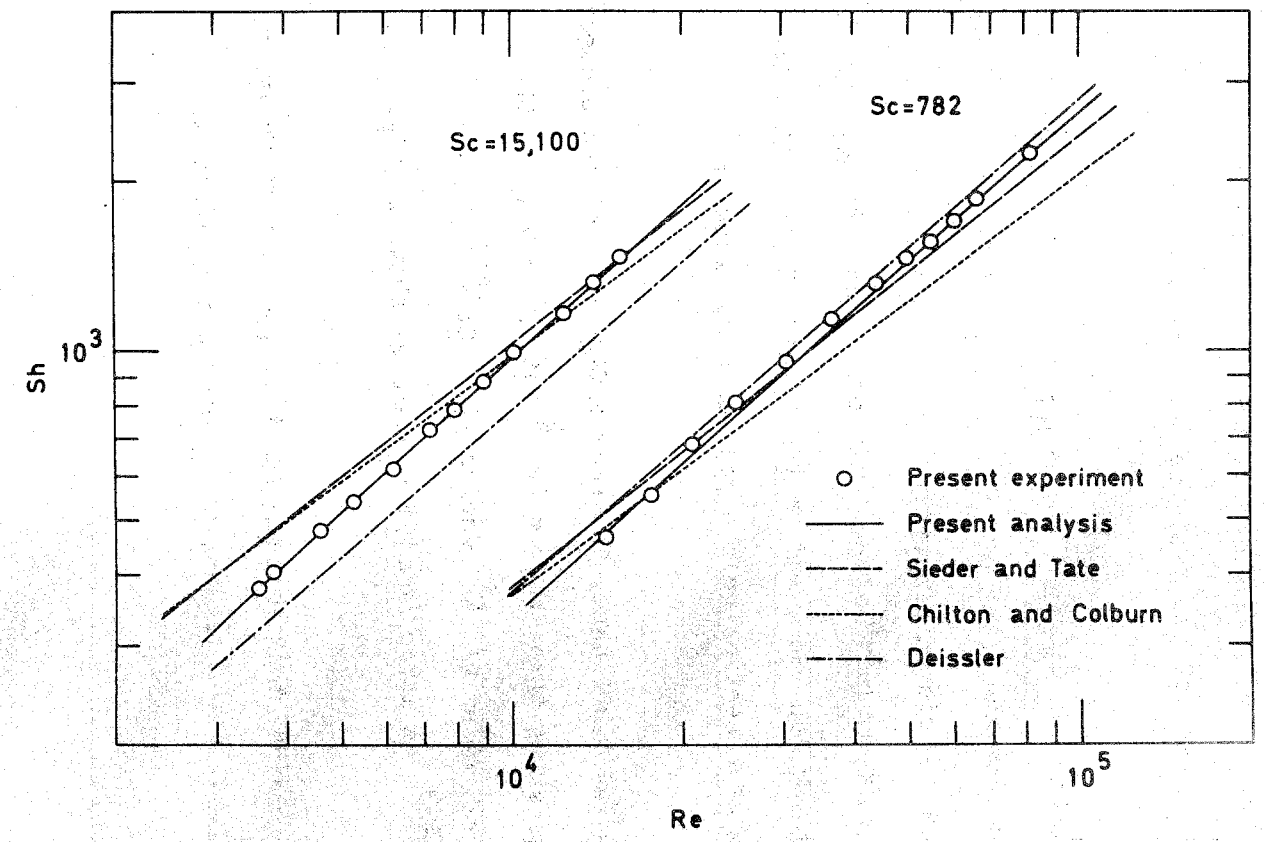

Fig. 5-11 Variation of Sherwood number with Reynolds number.

5-5 Discussion

It is generally accepted that the exponent $1/n$ in the relation $Nu \propto Pr^{1/n}$ or $Sh \propto Sc^{1/n}$ follows from the fact that the eddy diffusivity near the wall varies with the n-th power of the distance from the wall.

Hubbard et al. (20) concluded from their experimental results that the value of n was 3, but Son et al. (63) obtained the eddy diffusivity expression at $y^+ \to 0$ as $\varepsilon_D/\nu = 0.00032\ (y^+)^4$ from their experiments on the dependence of Sc on Sh, and on the effect of the length of the transfer section on the rate of mass transfer.

On the other hand, the eddy diffusivity of the present analysis shows that $\varepsilon_D/\nu \propto (y^+)^4$ at $y^+ \to 0$, but the calculated value of K^+ varies with $Sc^{-2/3}$, i.e. $Sh \propto Sc^{1/3}$ at large Schmidt numbers as shown in Fig. 5-9.

To discuss this problem further, the eddy diffusivity expressions of the present study may be simplified as follows.

Since the case considered is at large Prandtl or Schmidt numbers, only the equations (5-2) and (4-5) which are valid in the vicinity of the wall, will be discussed here.

In the immediate vicinity of the wall, ε_M/ν is very small. Hence, from equations (5-1) and (5-2), the expressions of the eddy diffusivity for heat is given by the following simple equation.

$$y^+ \leq y_B^+$$

$$\varepsilon_H/\nu = 0.0279\ A^{4/3}\ Pr\ (y^+)^4 \qquad (5\text{-}5)$$

In the region where the magnitude of the product of Pr and ε_M/ν is very large compared with unity, ε_H/ν is given by

$$y^+ \geq y_B^+$$

$$\varepsilon_H/\nu = A\ (y^+)^3 \qquad (5\text{-}6)$$

y_B^+ is located at a boundary of two regions, where

equations (5-4) and (5-5) are valid respectively, and is obtained by equating these two equations as follows,

$$y_B^+ = 1/(0.0279\ A^{1/3}\ Pr) \qquad (5\text{-}7)$$

The value of y_B^+ is proportional to Pr^{-1}, and depends slightly on the Reynolds number because of the dependence of A on Re as shown in Fig. 4-2.

The thickness δ^+ of the thermal boundary layer is defined simply as that which satisfies the following condition :

$$\varepsilon_H/\nu\Big|_{at\ \ y^+=\delta^+} = 10^2/Pr \qquad (5\text{-}8)$$

When equation (5-8) is applied to equation (1-24), the value of the integrand of equation (1-24), i.e. $1/(1/Pr + \varepsilon_H/\nu)$, becomes $Pr/(1 + 10^2) \fallingdotseq 0.01\ Pr$ at $y^+ = \delta^+$, which is only 1 per cent of the value at $y^+ = 0$, i.e. Pr.

Therefore, one can assume that

$$\int_0^{\infty} \frac{dy^+}{1/Pr + \varepsilon_H/\nu} \doteqdot \int_0^{\delta^+} \frac{dy^+}{1/Pr + \varepsilon_H/\nu} \qquad (5\text{-}9)$$

and hence the value of T^* at $y^+ = \delta^+$ becomes nearly unity.

Combining equation (5-8) with equations (5-5) or (5-6), one obtains the thickness of the boundary layer as

$$\delta^+ \leqq y_B^+$$

$$\delta^+ = 7.74\, A^{-1/3}\, Pr^{-1/2} \qquad (5\text{-}10)$$

$$\delta^+ \geqq y_B^+$$

$$\delta^+ = 4.64\, A^{-1/3}\, Pr^{-1/3} \qquad (5\text{-}11)$$

In Fig. 5-12, y_B^+ and δ^+ are plotted against Prandtl number at $Re = 10^4$. As shown in Fig. 5-12, there are two regions where the eddy diffusivity varies with $(y^+)^4$ and $(y^+)^3$ in the thermal boundary layer at large

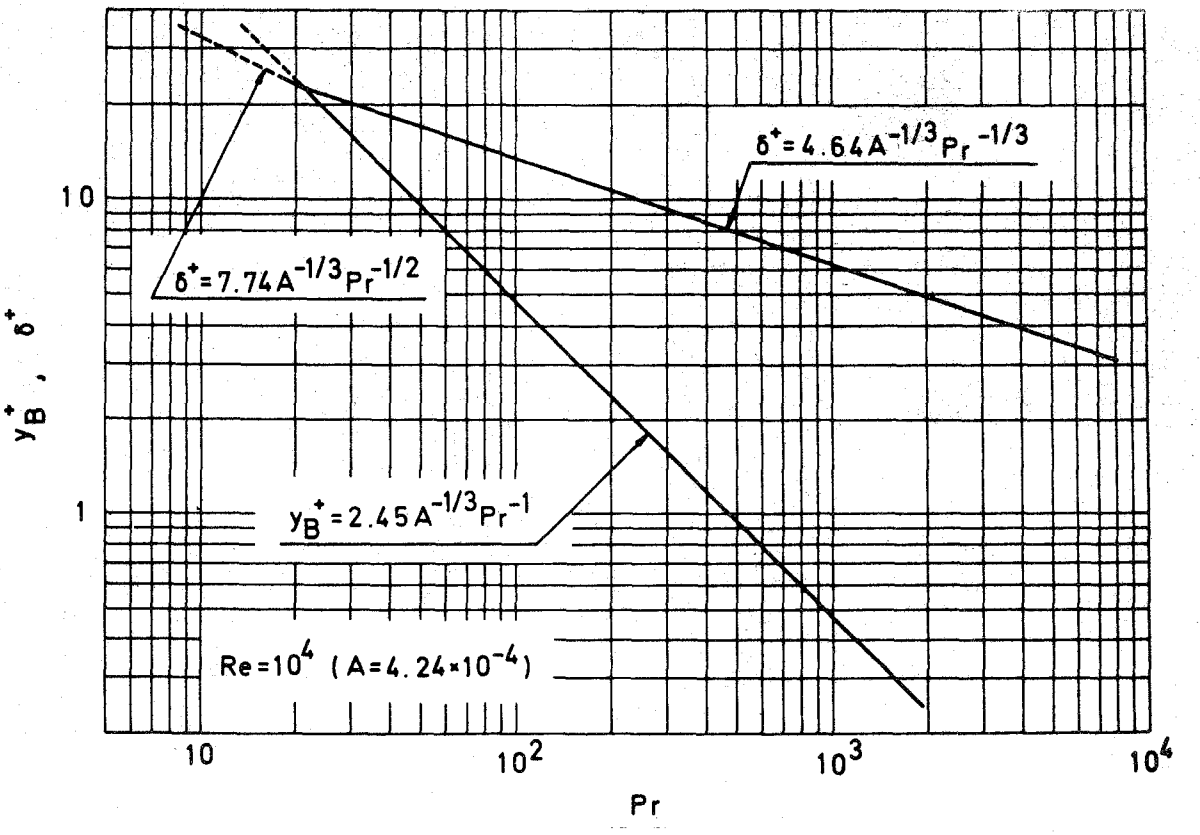

Fig. 5-12 Variation of δ^+ and y_B^+ with Prandtl number at $Re = 10^4$.

Prandtl numbers.

At $Pr > 10^3$ the eddy diffusivity for heat varies with $(y^+)^3$ in almost all parts of the boundary layer. Hence the transfer coefficient may be expressed approximately as

$Pr > 10^3$

$$h^+ = 1/\int_0^\infty \frac{dy^+}{1/Pr + A\,(y^+)^3}$$

$$= 0.827\, A^{1/3}\, Pr^{-2/3} \qquad (5\text{-}12)$$

Similarly, for mass transfer,

$Sc > 10^3$

$$K^+ = 0.827\, A^{1/3}\, Sc^{-2/3} \qquad (5\text{-}13)$$

The result of this discussion is that the relation $K^+ \propto Sc^{-2/3}$ at large Schmidt numbers does not always indicate that $\varepsilon_D/\nu \propto (y^+)^3$ at $y^+ \to 0$, but that the eddy

diffusivity varies with $(y^+)^3$ in almost all parts of the boundary layer.

5-6 Conclusion

1. Good agreement was obtained between the predicted and experimental results of mass transfer at Schmidt numbers between 800 and 15,000.

2. Both the predicted and experimental results show that the Sherwood number varies with the 1/3 power of the Schmidt number and about the 0.9 power of the Reynolds number at large Schmidt numbers, i.e.

$$Sh = 0.827\ A^{1/3}\ (f/2)^{1/2}\ Re\ Sc^{1/3}$$

3. The exponent $1/n$ in the relation $Nu \propto Pr^{1/n}$ or $Sh \propto Sc^{1/n}$ does not always indicate that the eddy diffusivity near the wall varies with the n-th power of the distance from the wall.

CHAPTER 6

CONCLUSIONS AND RECOMMENDATIONS FOR FURTHER WORK

6-1 Conclusions

(1) The experimental data taken at $Pr = 6 \sim 40$ and $Re = 11{,}700 \sim 26{,}400$ were correlated by the following equatios.

$$4 \leq y^+ \leq 14$$

$$\varepsilon_H/\nu = 1.31 \times 10^{-5} (y^+)^4$$

$$14 \leq y^+ \leq 42$$

$$\varepsilon_H/\nu = 1.93 \times 10^{-4} (y^+)^3$$

$$42 \leq y^+$$

$$\varepsilon_H/\nu = 0.36\ y^+ - 1$$

(2) From a modification of the mixing length theory, the expression for the ratio, $\varepsilon_H/\varepsilon_M$, was found to be given by

$$\sigma = \phi_H \{ 1 - \exp(-1/\phi_H) \}$$

$$y^+ \geq y_\phi^+$$

$$\phi_H = \frac{0.00681\ Pr\ (\varepsilon_M/\nu)}{1 + 0.160\ Pr^{1/3}\ (\varepsilon_M/\nu)^{1/2}}$$

$$y^+ \leq y_\phi^+$$

$$\phi_H = \frac{0.0279\ Pr\ (\varepsilon_M/\nu)^{1/3}}{1 + 0.228\ Pr^{1/3}\ (\varepsilon_M/\nu)^{1/3}}$$

where $y_\phi^+ \doteqdot 25$.

(3) From the available experimental data, the eddy

diffusivity for momentum was found to be given by

$$0 \leqq y^+ \leqq y_1^+$$

$$\varepsilon_M/\nu = A\,(y^+)^3$$

$$y_1^+ \leqq y^+ \leqq y_2^+$$

$$\varepsilon_M/\nu = 0.4\,y^+\left(1 - \frac{y^+}{H^+}\right) - 1$$

$$y_2^+ \leqq y^+ \leqq H^+$$

$$\varepsilon_M/\nu = 0.07\,H^+$$

For a circular pipe flow, H^+ must be replaced by the pipe radius R^+.

(4) There was good agreement between the mass transfer rates calculated using the eddy diffusivity for mass and those obtained experimentally at $Sc = 800 \sim 15{,}000$. Both the calculated and experimental results showed that the Sherwood number varies with the $1/3$ power of the Schmidt number and about the 0.9 power of the Reynolds number at

large Schmidt numbers.

At Pr or Sc > 10^3

$$Nu = 0.827\ A^{1/3}\ (f/2)^{1/2}\ Re\ Pr^{1/3}$$

$$Sh = 0.827\ A^{1/3}\ (f/2)^{1/2}\ Re\ Sc^{1/3}$$

6-2 Recommendations for Further Work

(1) The author's experimental data of the eddy diffusivity for heat, upon which the final equations for the eddy diffusivities are based, cover only the range of $y^+ > 4$, $Pr = 6 \sim 40$, and $Re = 11{,}700 \sim 26{,}400$. It is highly recommended that measurements of eddy diffusivity be extended to larger values of Prandtl or Schmidt number and to locations closer to the wall.

(2) Measurements of the eddy diffusivities for heat in the turbulent core, which are important in heat transfer especially at low Prandtl numbers, have been made by many investigators for the flow of air and mercury. However, their experimental results are considerably different from each other, so more accurate and extensive experimental data are also required in the turbulent core region. In this work the author was forced to assume simply that $\sigma = 1$ in the turbulent core, which has still not been confirmed.

(3) The model for the turbulent transfer mechanism of heat and momentum in this study is believed to give a

fairly good insight into the actual situation, which appears, however, much more complicated than that assumed in this model. It would seem then more profitable in the future to study the turbulent transport phenomena from a more fundamental standpoint.

(4) In addition, the experimental data on the turbulence quantities of temperature fluctuations or their correlations with velocity fluctuations would be necessary to reveal the transfer mechanism of heat in the turbulent flow.

NOMENCLATURE

A	: Coefficient in equations (1-55) and (4-5)	-
a	: Exponent in equation (1-55)	-
B	: Coefficient in equation (1-56)	-
Br	: Brinkman number $=\mu \langle U \rangle^2 / k\ (T_b - T_w)$	-
b	: Exponent in equation (1-56)	-
C	: Time-smoothed concentration	g-mole/cm^3
C	: Coefficient in equation (1-57)	-
C^+	: Dimensionless concentration $= u_*(C - C_w)/N_w$	-
C*	: Dimensionless concentration $= (C-C_w)/(C_b-C_w)$	-
C_p	: Heat capacity at constant pressure	cal/g$^\circ$C
c	: Concentration fluctuation	g-mole/cm^3
c	: Exponent in equation (1-57)	-
c_D	: Drag coefficient of an eddy particle	-
D	: Molecular diffusivity for mass	cm^2/sec
d	: Diameter of an eddy particle	cm
E	: Probable error	

F	: Faraday constant = 9.652×10^4	coulomb/g-mole
f	: Fanning friction factor	-
H	: Half width of a two-dimensional channel	cm
H^+	: Dimensionless half width of a two-dimensional channel = Hu_*/ν	-
h	: Heat transfer coefficient	cal/cm^{2}sec$^\circ$C
h^+	: Dimensionless heat transfer coefficient = $h/\rho C_p u_*$	-
h_e	: Heat transfer coefficient of an eddy particle	cal/cm^{2}sec$^\circ$C
i	: Limiting current density	ampere/cm^2
j	: Number of the fringes	-
K	: Mass transfer coefficient	cm/sec
K^+	: Dimensionless mass transfer coefficient = K/u_*	-
k	: Thermal conductivity	cal/cm sec$^\circ$C
k	: Constant	-
L	: Path length of the light beam	cm
L'	: Actual path length of the light beam	cm

ℓ	: Mixing length	cm
m	: Number of the fringe shifts	-
N	: Mass flux	g-mole/cm^{2}sec
Nu	: Nusselt number	-
n	: Refractive index	-
n_o	: Reference refractive index	-
n_{av}	: Averaged refractive index	-
n_f	: Refractive index obtained from an interferogram	-
P	: Time-smoothed pressure	dyne/cm^2
Pr	: Prandtl number = $C_p\mu/k$	-
q	: Heat flux	cal/cm^{2}sec
R	: Radius of a circular pipe	cm
R^+	: Dimensionless radius of a circular pipe = Ru_*/ν	-
Re	: Reynolds number	-
r	: Radial distance in the cylindrical coordinate	cm
Sc	: Schmidt number = ν/D	-

Sh	: Sherwood number	-
s	: Lagrangian coordinate of an eddy particle	cm
T	: Time-smoothed temperature	^{o}C
T^+	: Dimensionless temperature = $\rho C_p u_* (T - T_w)/q_w$	-
T*	: Dimensionless temperature = $(T - T_w)/(T_b - T_w)$	-
T_0	: Reference temperature	^{o}C
T_p	: Temperature of an eddy particle	^{o}C
t	: Temperature fluctuation	^{o}C
U	: Time-smoothed velocity in the x-direction	cm/sec
U^+	: Dimensionless velocity = U/u_*	-
U_ℓ	: Time-smoothed velocity at the outer edge of the laminar sublayer	cm/sec
U_p	: Velocity of an eddy particle	cm/sec
<U>	: Average velocity over a flow cross section	cm/sec
u	: Velocity fluctuation in the x-direction	cm/sec
u^+	: Dimensionless velocity fluctuation = u/u_*	-
u'	: Time-smoothed value of the absolute velocity fluctuation in the x-direction = $\overline{\lvert u \rvert}$	cm/sec

u_* : Friction velocity = $(\tau_w/\rho)^{1/2}$ cm/sec

v : Velocity fluctuation in the y-direction cm/sec

v^+ : Dimensionless velocity fluctuation = v/u_* -

v' : Time-smoothed value of the absolute velocity fluctuation in the y-direction = $\overline{|v|}$ cm/sec

W_o : Fringe width with no temperature disturbance cm

W' : Fringe width with temperature disturbance cm

x : Distance in the flow direction or length of the mass transfer section cm

x^+ : Dimensionless distance = xu_*/ν -

y : Distance perpendicular to the wall cm

y^+ : Dimensionless distance from the wall = yu_*/ν -

y_1^+ : Boundary between the regions where equations (4-5) and (4-4) are valid respectively -

y_2^+ : Boundary between the regions where equations (4-4) and (4-6) are valid respectively -

y_i : Position of the incident light beam cm

y_o : Position of the light beam at $z = L$ cm

y_B^+ : Equation (5-7) -

y_ϕ^+	: Boundary between the regions where equations (5-2) and (5-3) are valid respectively	-
z	: Distance in the light beam direction	cm

Greek symbols

α	: Constant in equation (3-28)	-
α_1	: Constant in equation (3-30)	-
α_2	: Constant in equation (3-38)	-
β	: Exponent in equation (3-28)	-
δ^+	: Dimensionless thickness of the thermal or concentration boundary layer	-
ε_D	: Eddy diffusivity for mass	cm^2/sec
ε_H	: Eddy diffusivity for heat	cm^2/sec
ε_M	: Eddy diffusivity for momentum	cm^2/sec
η_H	: Equation (3-19)	-
η_M	: Equation (3-5)	-
κ	: Constant	-
λ	: Wave length of the light	cm
μ	: Viscosity	g/cm sec

ν	: Kinematic viscosity = μ/ρ	cm^2/sec
ρ	: Density	g/cm^3
σ	: Ratio of the eddy diffusivities for heat and momentum = $\varepsilon_H/\varepsilon_M$	-
τ	: Shear stress	$dyne/cm^2$
$\Phi^{(\ell)}$	: Viscous dissipation function = $\mu\,(dU/dy)^2$	$1/sec^2$
$\Phi^{(t)}$	: Turbulent energy dissipation function	$1/sec^2$
ϕ_H	: Equation (3-20)	-
ϕ_M	: Equation (3-6)	-
φ	: Angle of refraction	-

Overline

-	: Time-smoothed	

Subscripts

b	: Bulk	
W	: Wall	

REFERENCES

(1) Azer, N. Z. and B. T. Chao ; Int. J. Heat Mass Transfer, 1, 121 (1960)

(2) Colburn, A. P. ; Trans. A. I. Ch. E., 29, 174 (1933)

(3) Corcoran, W. H. and B. H. Sage ; A. I. Ch. E. Journal, 2, 251 (1956)

(4) Deissler, R. G. ; NACA Tech. Note 2138 (1950)

(5) Deissler, R. G. : NACA RME52 F05 (1952)

(6) Deissler, R. G. ; NACA Tech. Note 3145 (1954)

(7) Deissler, R. G. ; NACA Report 1210 (1955)

(8) Dittus, F. W. and L. M. K. Boelter ; Univ. Calif., Pubs. Eng., 2, 443 (1930)

(9) Driest, E. R. van ; J. Aeronaut. Sci., 23, 1007 (1056)

(10) Eisenberg, M., C. W. Tobias and C. R. Wilke ; Chem. Eng. Progr. Symp. Ser., 51, 1 (1955)

(11) Elrod, H. G. ; J. Aeronaut. Sci., 24, 468 (1957)

(12) Friend, W. L. and A. B. Metzner ; A. I. Ch. E. Journal, 4, 393 (1958)

(13) Grigull, U. ; Int. J. Heat Mass Transfer, 6, 669 (1963)

(14) Hansen, G. ; Z. tekhn. Physik, 12, 436 (1931)

(15) Harriott, P. and R. M. Hamilton ; Chem. Eng. Sci., 20, 1073 (1965)

(16) Hinze, J. O. ; "Turbulence", McGraw-Hill Book Company, Inc. (1959) p.37

(17) Hinze, J. O. ; ibid. p. 457

(18) Hinze, J. O. ; ibid. p. 467

(19) Hinze, J. O. ; ibid. p. 526

(20) Hubbard, D. W. and E. N. Lightfoot ; I and EC Fundamentals, 5, 370 (1966)

(21) Hubbard, D. W. ; A.I.Ch.E. Journal, 14, 354 (1968)

(22) Hughmark, G. A. ; A.I.Ch.E. Journal, 14, 352 (1968)

(23) Isakoff, S. E. and T. B. Drew ; Proc. General Discussion on Heat Transfer, p. 405, 479, New York (1951)

(24) Jenkins, R. ; Heat Transfer and Fluid Mechanics Institute, Preprints of Stanford University, p. 147 (1951)

(25) Johnk, R. E. and T. J. Hanratty ; Chem. Eng. Sci., 17, 867 (1962)

(26) Kármán, T. von ; J. Aeronaut. Sci., 4, 131 (1937)

(27) Kármán, T. von ; Trans. ASME, 61, 705 (1939)

(28) Kinder, W. ; Optik, 1, 413 (1946)

(29) Laufer, J. ; NACA Tech. Note 2123 (1950)

(30) Laufer, J. ; NACA Tech. Report 1174 (1954)

(31) Lawn, C. J. ; Trans. ASME, 91, 532 (1969)

(32) Lin, C. S., E. B. Denton, H. S. Gaskill and G. L. Putnam ; Ind. Eng. Chem., 43, 2136 (1951)

(33) Lin, C. S., R. W. Moulton and G. L. Putnam ; Ind. Eng. Chem., 45, 636 (1953)

(34) Lin. C. S., R. W. Moulton and G. L. Putnam ; Ind. Eng. Chem., 45, 640 (1953)

(35) Linton, W. H. Jr. and T. K. Sherwood ; Chem. Eng. Progr., 46, 258 (1950)

(36) Ludwieg, H. ; Z. f. Flugwiss., 4, 73 (1956)

(37) Marchello, J. M. and H. L. Toor ; I and EC Fundamentals, 2, 8 (1963)

(38) Meyerink, E. S. C. and S. K. Friedlander ; Chem. Eng. Sci., 17, 121 (1962)

(39) Mizushina, T. and T. Sasano ; International Developments in Heat Transfer, ASME, 662 (1961)

(40) Mizushina, T. and Y. Kuriwaki ; J. Eng. Physics, 12, 152 (1967)

(41) Notter, R. H. and C. A. Sleicher ; A. I. Ch. E. Journal, 15, 936 (1969)

(42) Nikuradse, J. ; Forschungsheft, No. 356 (1932)

(43) Nunner, W. ; VDI - Forschungsheft, No. 455 (1956)

(44) Ohji, M. ; Phys. Fluids, Supplement, 10, 153 (1967)

(45) Page, F. Jr., W. H. Corcoran, W. G. Schlinger and B. H. Sage ; Ind. Eng. Chem., 44, 419 (1952)

(46) Page, F. Jr., W. G. Schlinger, D. K. Breaux and B. H. Sage ; Ind. Eng. Chem., 44, 424 (1952)

(47) Patel, V. C. and M. R. Head ; J. Fluid Mech., 38,

181 (1969)

(48) Prandtl, L. ; Phys. Zeitschr., 11, 1072 (1910)

(49) Prandtl, L. : Z. angew. Math. u. Mech., 5, 136 (1925)

(50) Rannie, W. D. ; J. Aeronaut. Sci., 23, 485 (1956)

(51) Ranz, W. E. and W. R. Marshall ; Chem. Eng. Progr., 48, 141 (1952)

(52) Reichardt, H. ; Z. angew. Math. u. Mech., 20, 297 (1940)

(53) Reichardt, H. : ibid., 31, 208 (1951)

(54) Reynolds, O. ; Proc. Manchester Lit. Phil. Soc., 14, 7 (1874)

(55) Schardin, H. ; Z. Instrumentenk., 53, 396, 424 (1933)

(56) Schlichting, H. ; "Boundary Layer Theory" McGraw-Hill Book Company, Inc., Fourth Edition, p. 477

(57) Schlichting, H. ; ibid. p. 514

(58) Schütz, G. ; Int. J. Heat Mass Transfer, 7, 1077 (1964)

(59) Shaw, P. V. and T. J. Hanratty ; A. I. Ch. E.

Journal, 10, 475 (1964)

(60) Sherwood, T. K., K. A. Smith and P. E. Fowles ; Chem. Eng. Sci., 23, 1225 (1968)

(61) Sieder, E. N. and G. E. Tate ; Ind. Eng. Chem., 28, 1429 (1936)

(62) Sleicher, C. A. ; Trans. ASME, 80, 693 (1958)

(63) Son, T. S. and T. J. Hanratty ; A. I. Ch. E. Journal, 13, 689 (1967)

(64) Spalding, D. B. ; J. Appl. Mech., 28, 455 (1961)

(65) Taylor, G. I. ; ARCR. and M. 272 (1919)

(66) Tyldesley, J. R. and R. C. Silver ; Int. J. Heat Mass Transfer, 11, 1325 (1968)

(67) Wasan, D. T., C. L. Tien and C. R. Wilke ; A. I. Ch. E. Journal, 9, 567 (1963)

(68) Wasan, D. T. and C. R. Wilke ; Int. J. Heat Mass Transfer, 7, 87 (1964)

(69) Wattendorf, F. L. ; Proc. Roy. Soc. (London), A148, 565 (1935)

(70) Winckler, J. ; The Review of Scientific Instruments 19, 307 (1948)

ACKNOWLEDGEMENT

The author expresses his gratitude to Professor Tokuro Mizushina of Department of Chemical Engineering, Kyoto University, to whom the author was greatly indebted for the many valuable suggestions in this study.

Professor Ryuzo Ito, of Department of the Chemical Engineering, Osaka University, deserves many thanks for his continued interest and many important instructive remarks on this study.

Many persons ; Messrs Toshihide Araki, Hiromu Kojima, Akio Yamori, Hiroshi Muramoto, Keizo Masuda, Masakatsu Fujii, Yoichi Oka, and Hideki Fukuda, have contributed directly to this study. The author acknowledges their great help.

Also the author wishes to thank Miss Kumiko Yoshinari for her help in preparing this thesis.

F. OGINO

Kyoto, August 1970